2018-12-07

Controlling Photo Processes Within a Confined Space: Switches, Triggers, and Electron Transfer

Mohan Raj Anthony Raj
University of Miami, m.anthonyraj@umiami.edu

UNIVERSITY OF MIAMI

CONTROLLING PHOTO PROCESSES WITHIN A CONFINED SPACE: SWITCHES, TRIGGERS, AND ELECTRON TRANSFER

By

Mohan Raj Anthony Raj

A DISSERTATION

Submitted to the Faculty
of the University of Miami
in partial fulfillment of the requirements for
the degree of Doctor of Philosophy

Coral Gables, Florida

December 2018

UNIVERSITY OF MIAMI

A dissertation submitted in partial fulfillment of
the requirements for the degree of
Doctor of Philosophy

CONTROLLING PHOTO PROCESSES WITHIN A CONFINED SPACE: SWITCHES, TRIGGERS, AND ELECTRON TRANSFER

Mohan Raj Anthony Raj

Approved:

_____
V. Ramamurthy, Ph.D.
Professor of Chemistry

_____
Francisco Raymo, Ph.D.
Professor of Chemistry

_____
Rajeev Prabhakar, Ph.D.
Professor of Chemistry

_____
Guillermo Prado, Ph.D.
Dean of the Graduate School

_____
Linda S. Shimizu, Ph.D.
Professor of Chemistry
University of South Carolina

ANTHONY RAJ, MOHAN RAJ (Ph.D., Chemistry)
Controlling Photo Processes within a Confined Space: Switches, Triggers and Electron Transfer Process (December 2018)

Abstract of a dissertation at the University of Miami.

Dissertation supervised by Professor V. Ramamurthy
No. of pages in text. (155)

The research work presented in this thesis is a consolidated report on role of confined medium to study the photoactive molecules. The deep cavity cavitand called Octa acid(OA) is used as a host molecule which has the confined space to accommodate guest molecules. The cavitand Octa acid is soluble in water in slightly basic conditions and it forms different type of complexes with various organic guest molecules. Unlike other host molecules, OA self assembles in aqueous environment to form a capsular complex through hydrophobic effect. The polarity of the confined space is non-polar resembles like benzene.

Chapter-1 introduces the concept of supramolecular organic photochemistry with some background information. It discusses the properties of various supramolecular hosts. It also explains the unique behavior of the host OA. A brief overview of molecular switches and their photophysical behavior inside capsule is also given.

Chapter-2 discusses the encapsulation of spiropyran derivatives inside OA capsule. We have demonstrated that the reversible photoisomerization of spiropyran to merocyanine triggers the disassembly/assembly of the OA capsule. We have followed this process by

absorption spectra. OA cavity also provides the stability for the merocyanine isomer and protects from hydrolysis to form by products.

Chapter-3 deals with photoisomerization of azobenzene derivatives inside OA capsule. We show that photoisomerization of azobenzene follows different mechanism than the structural similar stilbene using the confined space of capsule. We also demonstrate that the thermal isomerization of azobenzene derivatives from *cis* to *trans* isomer can be enhanced by electron transfer from gold nanoparticles (AuNP) to the encapsulated azobenzene.

Chapter-4 shows that confined space of OA controls the photobehavior of encapsulated photoactive molecules. We use NMR techniques to show the competitive binding between *cis* and *trans* isomer of stilbene deriviatives with OA. We also show the molecular modeling to confirm our prediction by NMR studies.

Chapter-5 discusses the electron transfer from upper excited state of encapsulated azulene derivatives to the acceptor electrostatically attached to the wall of the OA capsule. We have demonstrated the photoinduced electron transfer from azulene to methylviologen by femto-second transient absorption spectroscopy. We also show that electron transfer from azulene to bound TiO_2 surface.

Chapter-6 explains the phototriggering process of 2-Nitrobenzyl derivatives inside the OA capsule. We show that the photoproducts especially the toxic nitroso derivative can be trapped within OA after the photoreaction by NMR studies. We also show that confirmation of formation of nitroso product by LC-DAD traces, LC-MS and GC-MS studies.

Acknowledgement

Firstly, I would like to thank Prof. V. Ramamurthy for making my dream come true. I am so grateful to Prof. V. Ramamurthy for believing me and in my capability to perform independent research work. His continuous motivation, guidance and support have driven me to pursue my degree. I would also like to express my gratitude to him for teaching me the basics of photochemistry and photophysics, which eventually transformed me into a photochemist from synthetic chemist.

I would also like to thank my committee members Prof. Francisco Raymo and Prof. Rajeev Prabhakar and for their valuable suggestions and support throughout the program. I am also thankful to external committee member Prof. Linda Shimizu for reviewing my thesis and suggestions to improve it.

Good research needs collaboration. The major part of the works demonstrated in this thesis has been done in collaboration with different research groups. I would like to thank Prof. N. Jeyaraman from IISC, Bangalore, India; Prof. Pratik sen form IIT Kanpur, India; Prof. Elena Galoppini from Rutgers University, United States; Prof. Chris Elles from University of Kansas, United States; Prof. Francisco Raymo from University of Miami, United States; Prof. Rajeev Prabhakar from University of Miami, United States; and Prof. Jose P. Da Silva from Universidade do Algarve, Portugal.

I would like to express my sincere gratitude to Prof. K. K. Balasubramaniam (KKB) who encouraged me to pursue my graduate studies and recommended me to Prof. Ramamurthy. I am also thankful to my colleagues worked in Shasun Pharmaceutical, India, for their motivation to expand my knowledge.

I am also grateful to my professors at St. Joseph's College, Trichy. My special thanks to Prof. N. Xavier, Prof. V. Alexramani and Prof. S. R. Bheeter.

I thank all the faculty and staff in the Department of Chemistry, University of Miami, for their assistance and support as needed.

I would like to thank all the current and former members of our lab. Special thanks to Dr. Mintu Porel, Dr. Barnali Mondal, and Dr. Pradeepkumar Jagadesan for teaching me the instruments and correcting my thesis. My sincere thanks to fellow lab mates, Dr. Ashwini Danao, Dr. V. Giribabu, Dr. Nareshbabu Kamatham and Ramkumar for being encouraging colleagues.

My heartfelt thanks must go to my family and friends. I would not have been this position without their prayers and sacrifice. I would like to dedicate this thesis to my wife, Bhuvaneswari and my son, Bhavamanyu. She has been the backbone for me in everything I do in my life.

Table of Contents

List of Figures

Chapter 1

Chapter 2

List of Schemes

List of Tables

Chapter 1. Introduction to supramolecular chemistry

1.1 Background of supramolecular chemistry

The area of supramolecular chemistry research has been explored for over fifty years since 1967. The year 2017 marked the 50th anniversary for supramolecular chemistry and also was the 30th anniversary for Nobel Prize in supramolecular chemistry. In 1967, chemist Charles Pederson accidentally obtained first macrocylic ether dibenzo[18]crown-6 along with other homologues.[1-2] He named these macrocylic ethers as "crown ethers" because of the crown-like appearance of the model of these molecules with alkali metal cations. This serendipitous discovery subsequently led to the development of "host-guest chemistry" by Donald Cram[3] and "supramolecular chemistry" developed by Jean-Marie Lehn.[4] Lehn demonstrated that alkali metal cations could also be encapsulated to three-dimension (3D) receptors, which he called "cryptands".[5-8] He described supramolecular chemistry as "*chemistry beyond the molecule*". Donald J. Cram developed sophisticated molecular containers called "cavitands" and "spherands" with holes and cavities.[9-12] The cavities can bind not only alkali and alkaline earth metals but also encapsulate small organic molecules. Pederson, Lehn, and Cram shared the Nobel Prize in Chemistry in 1987. The pioneering work of these Nobel Laureates inspired lots of scientists to explore supramolecular chemistry area of research.

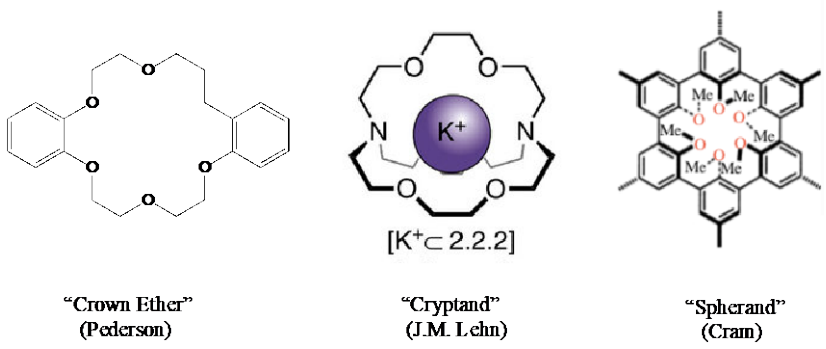

Figure 1.1 Structures of cryptands and cavitands.

1.2 Supramolecular assembly and mode of interactions

Supramolecular assembly is the interaction between two different molecules via weak interactions like electrostatic interactions, cation-π, π- π, CH-π interactions, hydrogen bonding, van der Waals forces or hydrophobic effects. These non-covalent interactions are considered to be weaker than covalent interactions (ca. 150-450 KJ/mol for single bonds). These interactions are summarized in the table below and a few of the interactions are discussed further below.

Interactions	**Directionality**	**Bond energy (KJ/mol)**
Ion-ion	Non directional	100-350
Ion-dipole	Slightly directional	50-200
Dipole-dipole	Slightly directional	5-50
Hydrogen bond	Directional	4-120
π- π	Directional	2-50
van der Waals	Non directional	< 5

Table.1.1 Characteristics of some common supramolecular interactions.[13-14]

1.2.1 Hydrogen bonding

Hydrogen bonding is one of the most important non-covalent interactions. The hydrogen bond is a specific type of dipole-dipole interactions in which a hydrogen atom covalently bonded to a more electronegative atom (typically, O, N, S, F). Formation of hydrogen bonds causes a significant decrease in energy and stabilizes the structure. Hydrogen bond provides overall shape of biological molecules like double helix-structure for DNA, proteins and nucleic acids

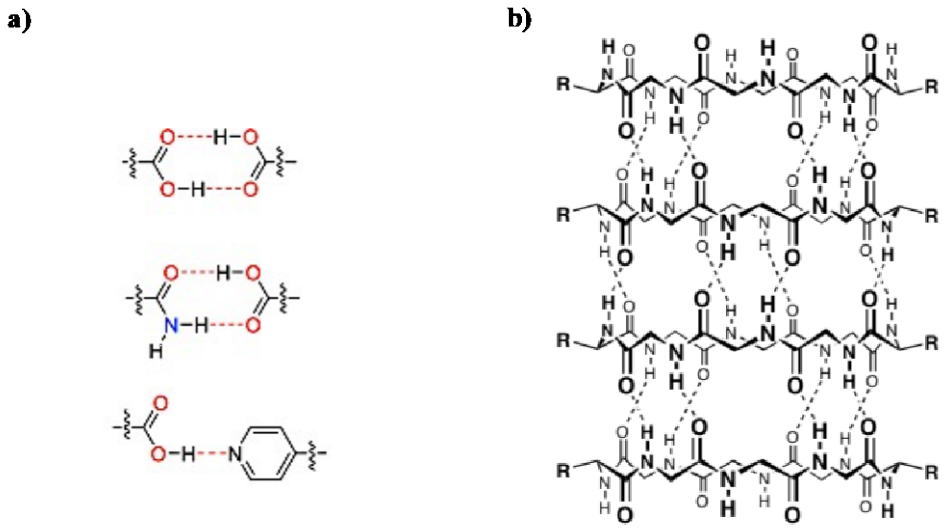

Figure 1.2 a) Representative H-bond patterns in supramolecular chemistry; b) Nanotube assembly from cyclic D,L- peptides through H-bonding.[15]

1.2.2 Weak interactions involving π system

The weak interactions involving π systems are categorized into cation-π, π- π, and CH-π interactions. Cation- π interactions result from interaction of a cation with the face of a simple π system. π- π interactions are the interactions between two aromatic systems. The interactions are favorable based on the geometry of two aromatic molecules. The stacking

could be displaced, edge-to-face or sandwich type. (**Figure-1.3**). Edge-to-face geometry is favorable since it forms between partial positive charge on the face of one aromatic ring and partial negative charge on the edge of another aromatic ring.[16] This type of interactions happens between nucleobase pairs in DNA and helps to stabilize the double helix structure of DNA.

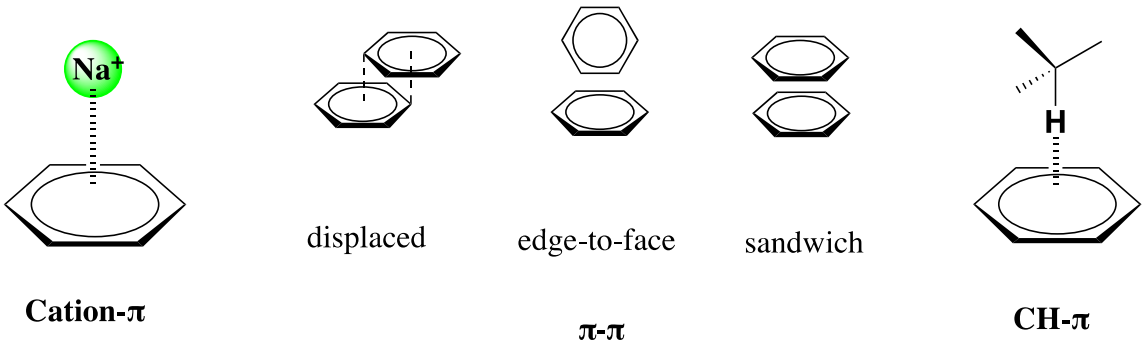

Figure 1.3 Various types of π systems with weak interactions.

1.2.3 The Hydrophobic effect

The hydrophobic effect[17-19] is a water-mediated phenomenon that is not to be considered as a force, even though it results in effective attractions between guest and host molecules in supramolecular assembly. Hydrophobic effect can be classified into two types (i) entropy driven " classical" (ii) enthalpy driven "non classical hydrophobic effects. At ambient temperatures, the hydrophobic effect is mainly entropically driven, but at higher temperatures, enthalpy effects dominate entropy effects. Hydrophobic effect is dependent on the nature of the solute (size, shape, polarity) and the relative strengths of the resulting solute-solvent, solute-solute and solvent-solvent interactions. There are plenty of

molecular host for which binding is controlled by hydrophobic effect, which will be discussed in the following section.

1.3. Water-soluble hosts

During last few decades there has been increasing interest among the researchers to develop synthetic macromolecular host molecules. Most of the synthetic macromolecules are not water- soluble (crown ether, cryptand, resorcinarene etc.). To mimic the nature, water-soluble macromolecules are important. Water-soluble hosts that possess hydrophobic cavity that can bind one or more guest molecules are discussed in this section.

1.3.1 Cyclodextrins

Cyclodextrins (CDs) are family of hosts commonly composed of five or more α-D-glucopyranoside units in a ring linked by α-1-4-glycosidic bonds. The most commonly used CDs contain six, seven, or eight glucopyranoside monomers, namely, α-cyclodextrin (α-CD), β-cyclodextrin (β-CD) and γ-cyclodextrin (γ-CD) respectively. Generally, CDs have a truncated cone structure that has hydrophilic exterior surface and hydrophobic interior cavity.[20] Hydrophobic interior cavities can bind nonpolar guest molecules **(Figure 1.4).** CDs inclusion properties led to various applications include artificial enzymes, biosensors, drug delivery, cosmetics, food technology and textiles.[21]

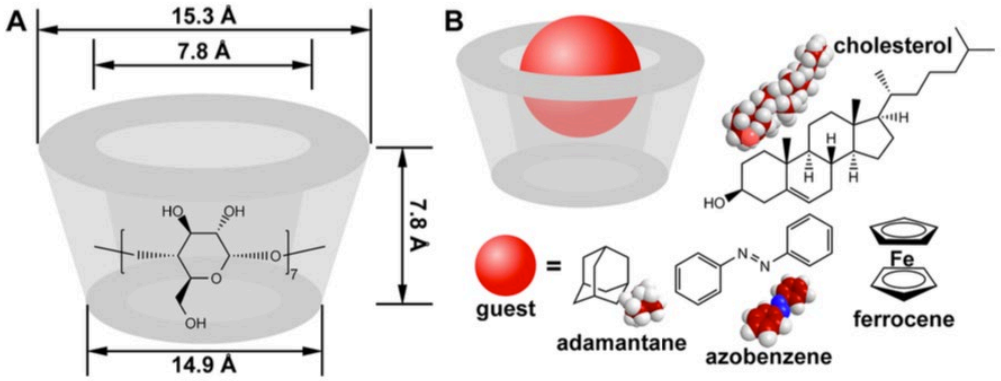

Figure 1.4 A) Structure of β-CD and B) common guest molecules forming inclusion complex with β-CD host.[22]

1.3.2 Cucurbit[*n*]urils

Cucurbiturils are generally represented as CB[*n*]s, where n is the number of glycouril units linked by the methylene bridge to form the macrocycle. CB[6] was first isolated and characterized in 1981.[23] Then their homologues CB[5] , CB[7] , CB[8] CB[5] and CB[14] were synthesized by various research groups. CB[*n*]s possess highly symmetric structure with hydrophilic carbonylated rims at the top and bottom of an inner cavity which is unusually hydrophobic. The hydrophobic cavity can bind hydrophobic neutral guest molecules while hydrophilic rims can bind the cationic guest molecules through ion-dipole and hydrogen bonding. The cavity volume of CB[*n*]s increases as the number of glycouril unit increases (**Figure 1.5**). CB[5]- CB[10] can form different types of host-guest complexes ranging from binary to ternary. Due to this ability, CB[*n*]s have found to be used in various applications like drug delivery, catalysis and nanotechnology.[24]

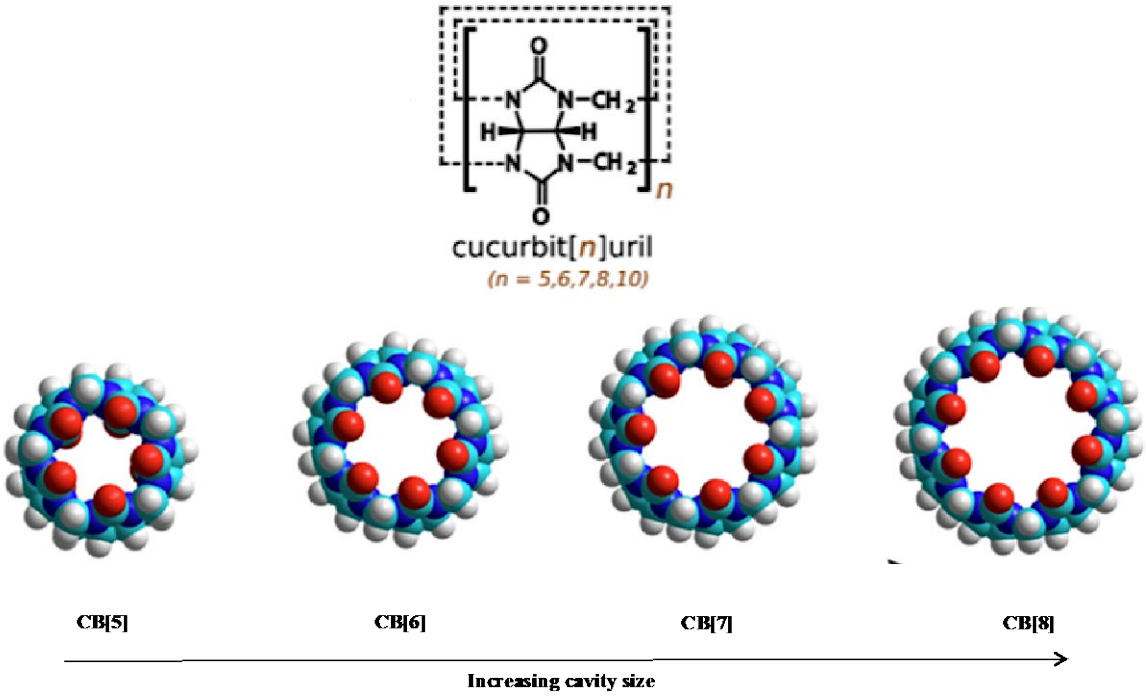

Figure 1.5 Structure of CB[*n*]s and its cavity size

1.3.3. Resorcin[*n*]arenes

Resorcin[*n*]arenes[25] can be synthesized by acid-catalysed condensation of resorcinol with various aliphatic and aromatic aldehydes. Generally, resorcinarenes have a wide upper rim and narrow lower rim. In 1997, MacGillivray and Atwood discovered the self-assembly of C-methylresorcin[4]arene form a chiral hexameric spherical capsules.[26] Later Rebek group[27-29] and Cohen group[30] studied self-assembly of various resoncir[4]arenes and their derivatives to form large supramolecular hexameric capsules. Resorcinarenes can be used to form different types of supramolecular assemblies namely, cavitand, carcerand, hemi-carcerand, and capsules. In 1982, Cram coined the name “cavitands” in which the cavity is wide open so that small molecules can enter and exit. Covalently linked cavitands are called “carcerand” in which if the guest molecules can exit then that is called “hemi-carcerand”.

A capsule is formed when two cavitand forms supramolecular assembly through non-covalent interactions.[31] In 2004, Gibb's group developed a deep-cavity cavitand called Octa acid(OA)[32] which is discussed elaborately in the next section.

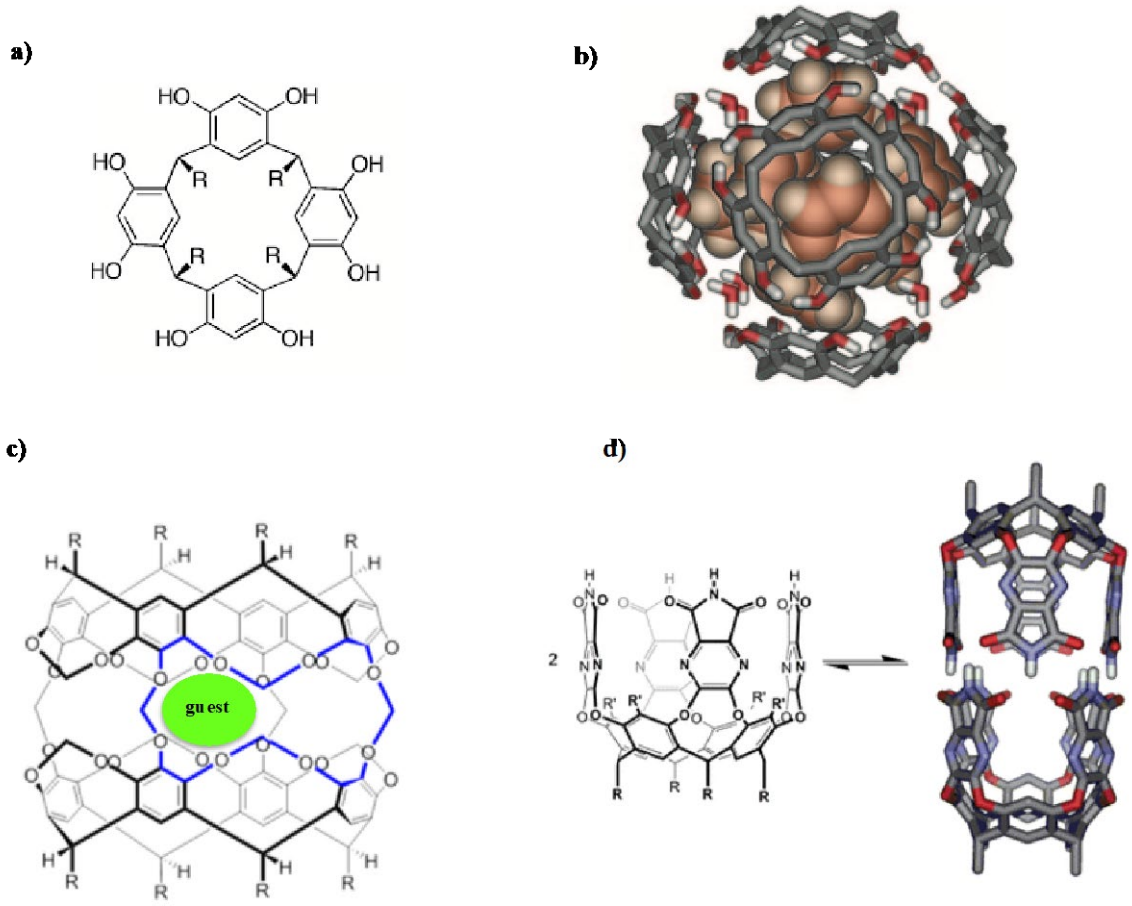

Figure 1.6 a) Structure of resorcin[4]arene; b) Molecular model of hexameric capsules; c) Cram's hermicarcerand; d) structure of Rebek's cavitand and model of capsules.

1.4. Deep-cavitand Octa acid (OA)

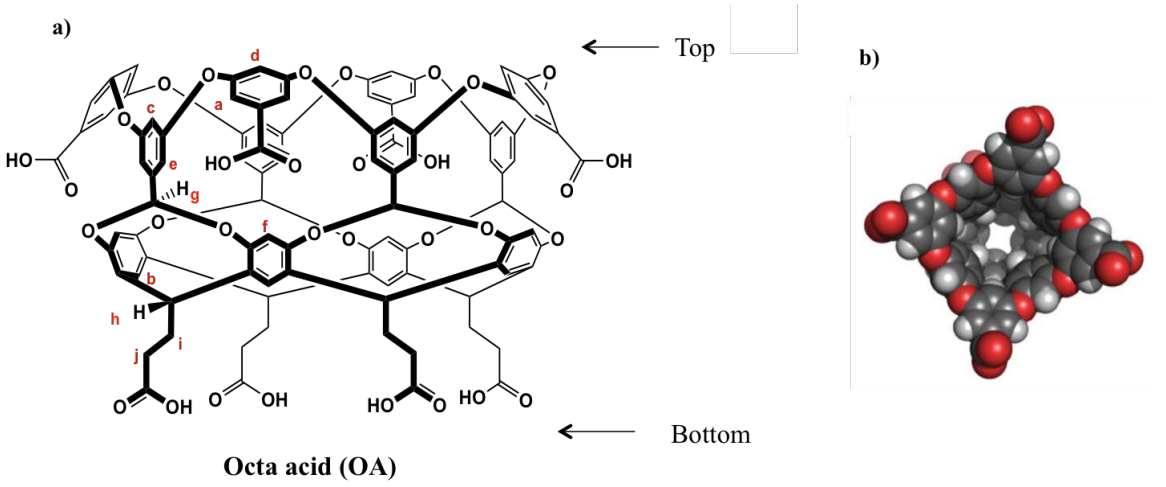

Figure. 1.7 a) Structure of deep water soluble cavitand Octa acid (OA); b) Space-filling model of energy minimized structure of OA.

Gibb and co-workers has synthesized resorcinarene based deep cavity cavitand called Octa acid(OA).[32] OA has eight carboxylic acid(-COOH) groups, four on the top rim and four on the bottom. OA is soluble in water at basic pH (~8.7) and encapsulation of guest molecules is driven by hydrophobic effect. Ramamurthy group has been exploring OA cavitand deeper to study the photochemistry of various organic molecules.[33] The hydrophobic cavity of OA is non-polar "benzene" like which was confirmed by studying various probes such as pyrene, and coumarin-1.[34] OA has the ability to form different types of supramolecular assembly based on the guest molecules. OA forms 1:1 (host-guest) cavitandplex with polar head organic molecules. It can also form 2:1 and 2:2 (host-guest) capsuleplexes(**Figure 1.8**). For example, OA can form 2:2 capsuleplex with small molecules like adamantane. OA can accommodate longer aromatic molecule like tetracene and bulkier aromatic molecule like pyrene.[34] The steroid (+)-dehyroisoandrosterone is the best guest to form strong complex with OA and its length is ideal.[32]

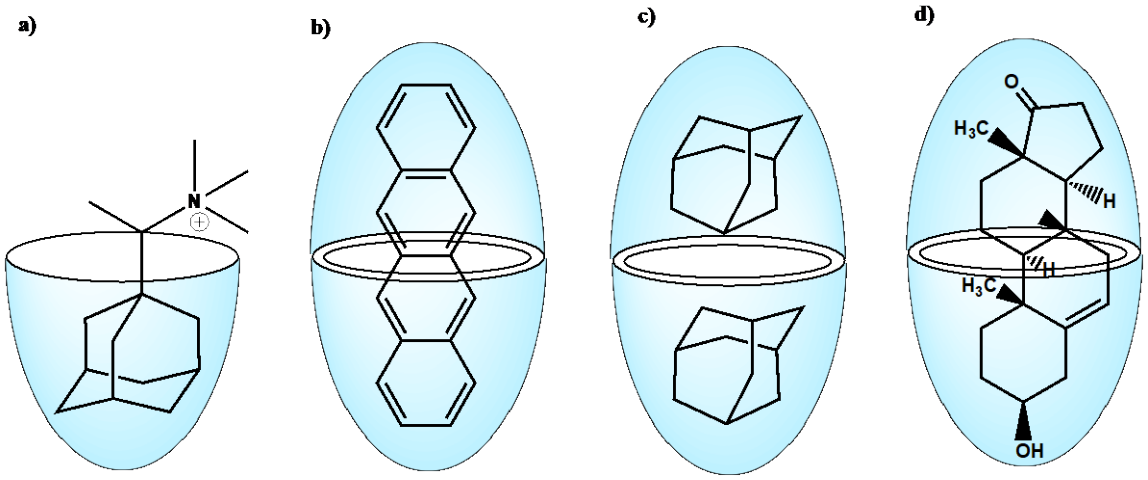

Figure 1.8 a) 1:1 cavitandplex of OA with polar molecule; b) 2:1 complex of longest aromatic molecule (tetracene) with OA; c) 2:2 complex of adamantane with OA; d) Ideal fit of steroid with OA.

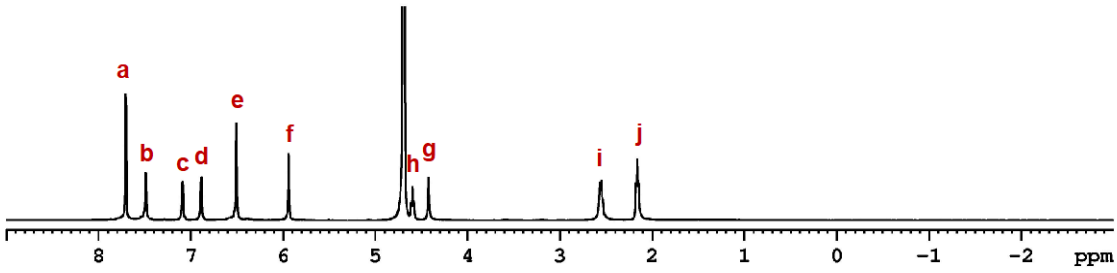

Figure 1.9 ^{1}H NMR spectrum (500 MHz) of OA [1 mM] in 10 mM $Na_2B_4O_7/D_2O$.

OA has distinctive peaks for aromatic region (a-f marked in the **Figure 1.9**) in NMR spectrum. The formation of complexes can be identified by shift in host peaks (a-f) and downfield (δ 0 to -4 ppm) appearance of peaks for aliphatic protons. UV-Vis absorption and fluorescence studies also helped to understand the excited state properties of encapsulated guest molecules. OA has greater impact on photophysical properties of various guest molecules. Lifetime of certain molecules inside OA was extremely longer than in solution. Free rotation of the guest molecules inside OA is restricted due to lack of free space, which also causes change in fluorescence properties of encapsulated guest

molecules.[35] Encapsulated guest molecules mostly donor molecules can communicate to the acceptor molecules which are electrostatically attached to the wall of OA capsule through electron, energy and spin transfer.[36-37] OA has also been used as container for phototriggers, which releases small molecules to the environment upon light radiation.[38-40] Since, OA has carboxylic acid(-COOH) groups, OA-guest complexes found to be stabilized on solid surfaces like, silica, TiO_2 and gold nanoparticles.[37] Surface chemistry of OA still needs to be explored especially in the field of energy conversion, visible light photocatalysis.

1.5 Molecular switches

Photochromic molecules (molecular switches) show change in structure and electronic configuration (affecting their absorption spectra) upon light irradiation. The idea of coupling photoisomerization with supramolecular assembly has attracted much attention as a clean, reliable, easy and in many cases, reversible way of controlling the thermodynamic stability of host-guest complexes. The photoisomerization and photochromic process may control the assembly/disassembly of the capsular complexes. On the other hand, it may also trigger the guest to be released into the environment. Encapsulation of photoactive molecules in supramolecular assembly has created a wide range of applications including, catalysis,[33, 41-43] purification of gases and liquids by trapping method,[44-45] removal of toxic or reactive species from environment,[46-47] drug pharmacokinetics,[48-51] and development of sensors and receptors for small molecules.[52-54] Molecular switches like azobenzenes, stilbenes, spiropyrans, diarylethenes, and fulgicides

have been well-studied (**Figure 1.10**) Encapsulation of these switches with supramolecular assembly has not been explored much.

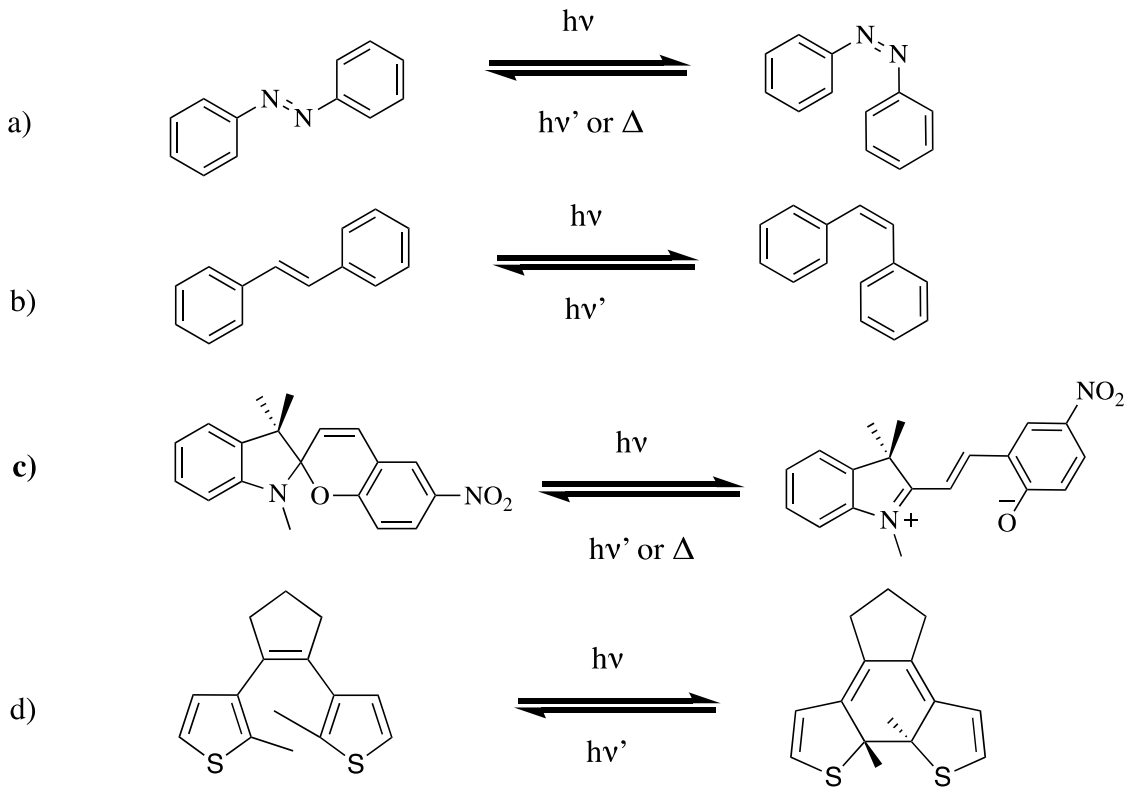

Figure 1.10 Photochemical reactions of commonly used photoswitches.

Rebek group has studied the photophysical properities of classical azobenzenes to understand the assembly/disassembly of the encapsulated complexes (**Figure 1.11**). Azobenzene undergoes reversible *cis-trans* isomerization under UV-Visible light. *Cis* to *trans* isomerization can also be thermally possible. The Rebek group has used their pyrazinamide-extended resoricin[4]arene derivatives to study the photoisomerization of azobenzenes.[55] It forms dimeric capsules through hydrogen-bonding.

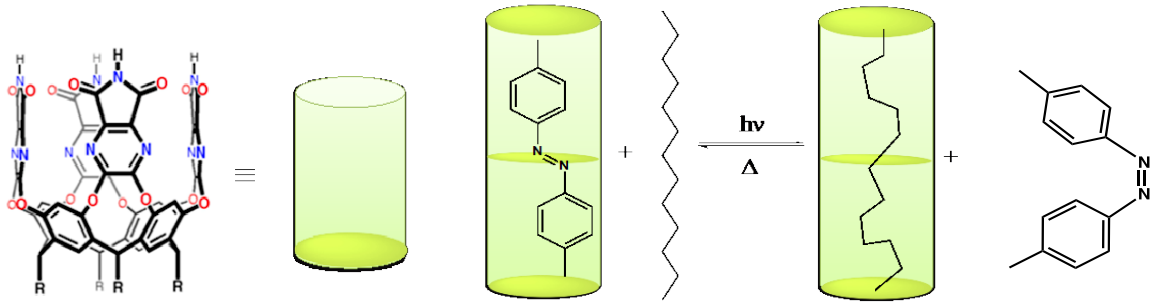

Figure 1.11 Structure of Rebek's cavitand and competive guest binding with azobenzene.

They encapsulated 4,4'-dimethylazobenzene and experimented with competitive guest n-tridecane. While exposing to UV light, trans-isomer isomerize to cis-isomer and expelled out from the capsule and n-tridecane is encapsulated. When the mixture is heated to160 °C for 2 min the trans isomer retains into the capsule by expelling n-tridecane out (**Figure 1.11**). Unexpected fluorescence quenching of 4-methyl-4'-ethylstilbene was observed inside the capsule due to twisted conformation of the molecule inside the capsule.[56] Contrary, enhancement of emission from triplet state of 4,4-dimethylbenzil was seen inside the capsule because of their trans orientation within the capsule.

Chapter 2. Reversible Disassembly-Assembly of Octa Acid-Guest Capsule in Water Triggered by a Photochromic Process

2.1 Overview

Organic molecules behave differently in confined media than in the bulk. Biochemical structures like, pockets of enzymes, interiors of chaperones and inner space of ribosomes are few examples of confined space in nature. Inspired by nature, chemists have developed various synthetic confined spaces like metal-organic frameworks,[57] Zeolites,[58] cyclodextrins,[59] and cucurbiturils[60]. During the last few decades, understanding the properties of photochromic molecules inside the confined spaces has been emerging area of research. Photochromic molecules undergo reversible transformation into two different states under the external stimuli light. Both states have different absorption spectra, conformation and properties. Due to '*on'* and '*off'* nature they found to be useful in many applications including, optical data storage, chemical sensing, ophthalmic lenses, bio-cell imaging, and drug delivery.[61] Few of the photoswitches are listed in **Chapter-1** (**Figure 1.10**). Spiropyran derivatives(SPs) are well known for their photochromism and have been utilized in various applications.[62] For biological applications, molecules need to be soluble and stable in aqueous medium. Unfortunately, spiropyrans are not water-soluble. Numerous efforts have been made to modify the structure of SPs to solubilize in water.[63] Simultaneously to circumvent the poor solubility of SPs in water, attempts were made to encapsulate SPs in water-soluble hosts, such as micelles, vesicles, bile salt aggregates, cyclodextrins, cucurbiturils, and calixarenes.[64-72] This approach also was found to be less successful. Our group has been exploring the water-soluble deep cavity cavitand Octa acid (OA) to understand the

excited state properties of various molecules.[33] Encapsulation of photochromic molecules and their photophysical properties inside the OA cavity is the interesting phenonmenon, which we have not been explored much. This chapter discusses about the encapsulation of spiropyrans and their effect on dynamics of OA capsule.

2.2 Results and discussion

We chose octa acid (OA) as host and spiropyran derivatives 1',3',3'-trimethyl-6-nitrospiro[2H-1-benzopyran-2,2-indoline](6-nitroBIPS),1',3',3'-trimethyl-6-bromospiro[2H-1-benzopyran-2,2-indoline] (6-bromo BIPS), 1',3',3'-trimethyl-spiro[2H-1-benzopyran-2,2-indoline] (BIPS) as guest molecules (**Figure-2.1**).

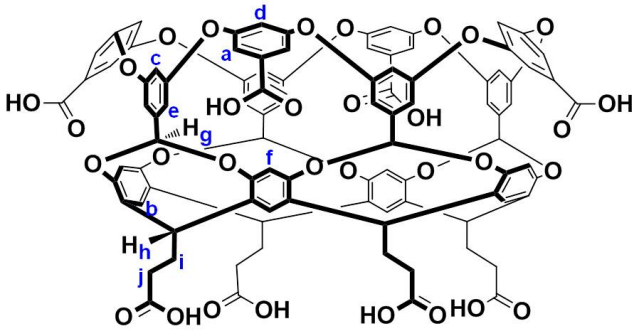

Octa acid (OA)

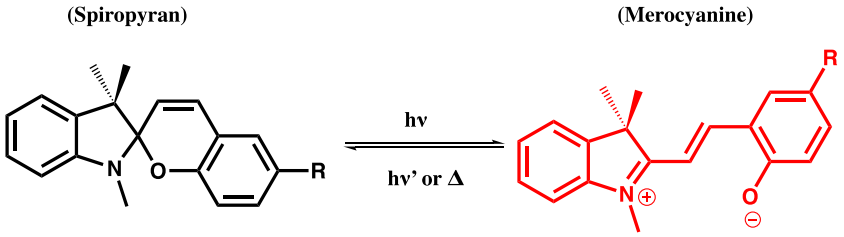

(2.1a) R = NO_2
(2.2a) R = Br
(2.3a) R = H

(2.1b) R = NO_2
(2.2b) R = Br
(2.3b) R = H

Figure 2.1 Chemical structures of host OA and guest molecule

2.2.1 Photochemistry of spiropyrans

Spiropyran (SP) has the structure comprises of two individual indoline and chromene subunits linked together at the central C_{spiro} carbon. Both are orthogonal to each other that break the conjugation. Hence the spiropyran is colorless. It has two absorption maxima, 270-296 nm corresponding to π- π* transition in indoline part and 326-351nm corresponding to the chromene part. Upon UV excitation, the heterolytic cleavage of C_{spiro}-O bond leads to conjugated open merocyanine form. The mechanistic pathway for the ring opening is provided in **Scheme-2.2.** Reversible transformation from merocyanine to spiropyran occurs under the exposure of visible light. Since ground state energy of merocyanine is higher than spiropyran, it will also revert to closed form thermally. Both spiropyran and merocyanine have different properties. Closed spiropyran is colorless, non-planar, neutral, and has low dipole moment (~4 D). On the other hand, merocyanine is colored, planar, zwitterionic and has high dipole moment (~18 D). Since our host OA forms 2:1 or 2:2 capsuleplex with neutral molecules and 1:1 cavitandplex with polar head group, we expected encapsulation of spiropyrans and their photochromic ring opening would be interesting aspects to study.

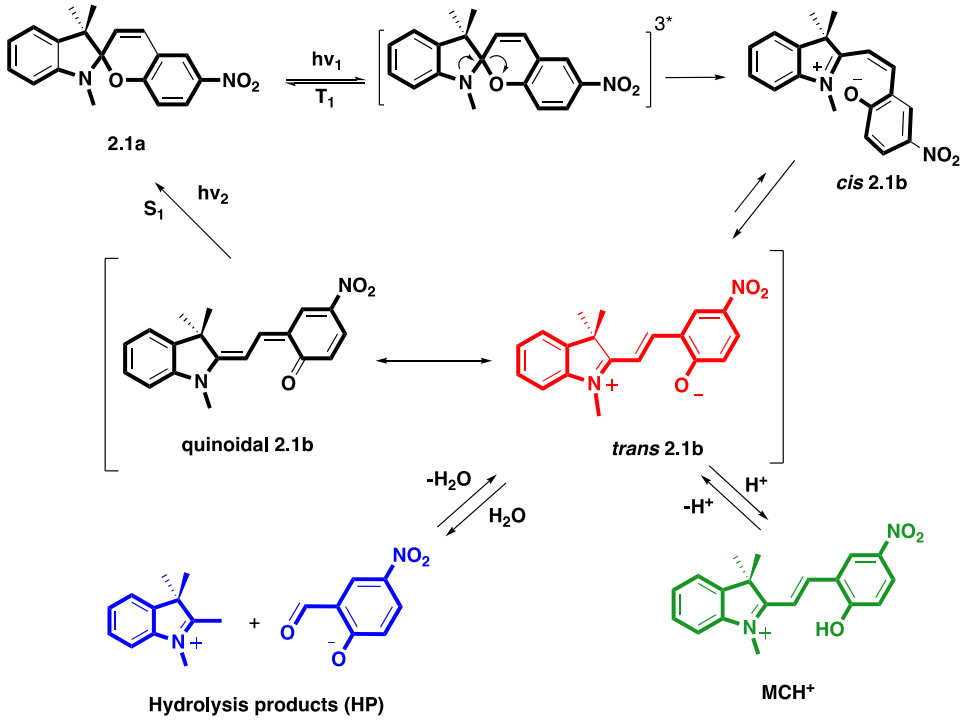

Scheme-2.1 Mechanistic pathway of photointerconversion between **2.1a** and **2.1b** and side reactions of **2.1b.**

2.2.2. ^{1}H NMR studies of spiropyrans with OA

Encapsulation of guest molecules inside the OA cavity normally infer from the ^{1}H NMR titration spectra. Splitting of OA host peaks and upfield appearance (~0-4 ppm) of aliphatic peaks shows those molecules are inside. Diffusion experiment (2D-DOSY) gives information about type of complexes formed with OA. Upon addition of (**2.1 a-2.3a**) to the OA in buffer solution (pH~8.9), the chemical shifts of both are affected, suggesting interaction between OA and the guest molecules. The methyl protons of guest molecules in CD_3CN were upfield shifted (δ -0.2 ppm) in the titration spectra clearly showed the guest inclusion within OA **(Figure 2.2-2.4)**. Titration experiments revealed that addition of more than 0.5 equiv of guest molecules showed no change in the spectra, further suggesting the guest to host ratio to be 2:1. In addition, the integration of the guest methyl and selected host signals as well as the diffusion constant measured by DOSY experiments **(Table-2.1)**

were consistent with the formation of a capsule containing one guest molecule and two molecules of OA. The splitting of OA host peaks (δ 6.5-8 ppm) suggested that inclusion of unsymmetrical guest **2.1a**. Additionally, NOESY spectra of **2.1a@OA$_2$** (guest:host) complex clearly showed the correlation between the three methyl groups of the guest and the host OA protons (H_c, H_d and H_e) suggested that all three methyl groups are located at the middle region of the capsule (**Figure 2.6**).

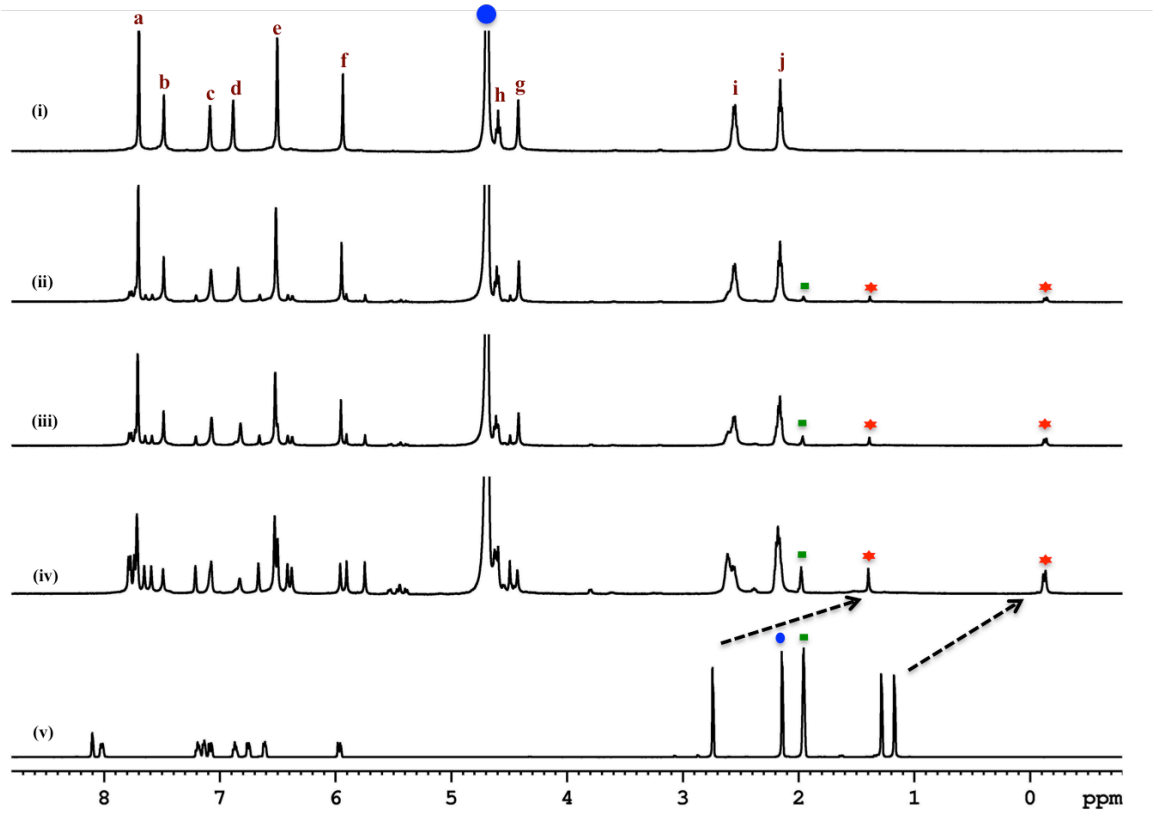

Figure 2.2 ^{1}H NMR (500 MHz) spectra of (i) OA([OA] = 1 mM) in 10 mM $Na_2B_4O_7$ buffer/D_2O; (ii) 2.1a@OA_2 ([OA] = 1 mM), [2.1a] = 0.125 mM) in10 mM $Na_2B_4O_7$ buffer/D_2O; (iii) 2.1a @OA_2 ([OA] = 1 mM), [2.1a] = 0.25 mM) in 10 mM $Na_2B_4O_7$ buffer/D_2O; (iv) 2.1a @OA_2 ([OA] = 1 mM), [2.1a] = 0.50 mM) in10 mM $Na_2B_4O_7$ buffer/D_2O; (v) 2.1a in CD_3CN. "*" indicates the bound guest proton peaks "●"and "■" represent the residual solvent peak of H_2O and CD_3CN, respectively.

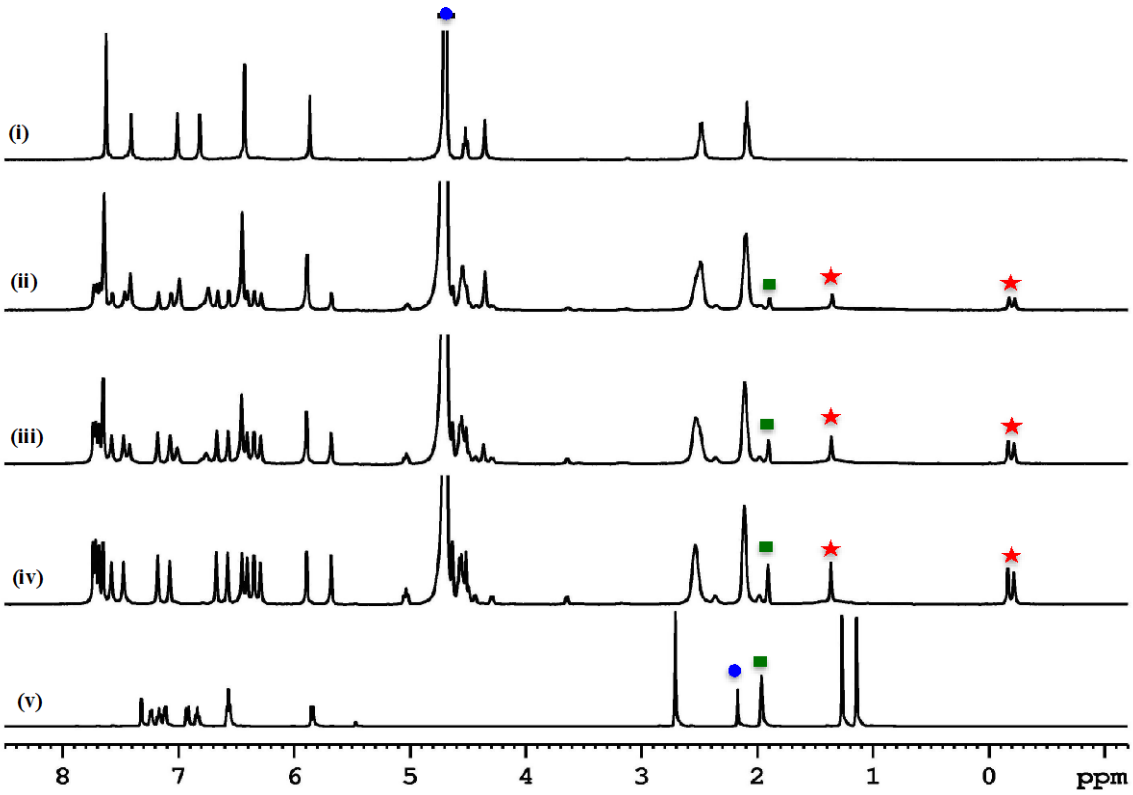

Figure 2.3 ^{1}H NMR (500 MHz) spectra of (i) OA([OA] = 1 mM) in 10 mM $Na_2B_4O_7$ buffer/D_2O; (ii) **2.2a**@OA_2 ([OA] = 1 mM), [**2.2a**] = 0.50 mM) in10 mM $Na_2B_4O_7$ buffer/D_2O; (iii) **2.2a** @OA_2 ([OA] = 1 mM), [**2.2a**] = 1 mM)in10 mM $Na_2B_4O_7$ buffer/D_2O; (iv) **2.2a** @OA_2 ([OA] = 1 mM), [**2.2a**] = 1.5 mM) in10 mM $Na_2B_4O_7$ buffer/D_2O; (v) **2.2a** in CD_3CN. "★" indicates the bound guest proton peaks. "●" and "■" represent the residual D_2O and CD_3CN respectively.

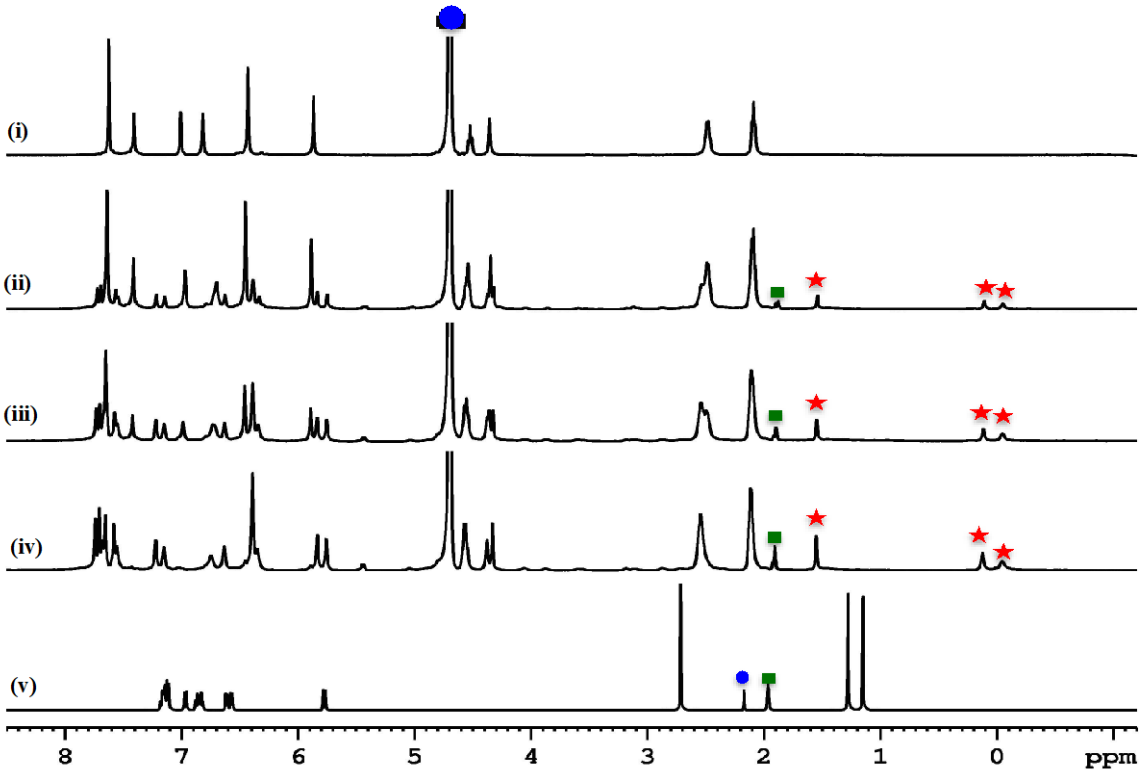

Figure 2.4 ^{1}H NMR (500 MHz) spectra of (i) OA([OA] = 1 mM) in 10 mM $Na_2B_4O_7$ buffer/D_2O; (ii) **2.3a**@OA_2 ([OA] = 1 mM), [**2.3a**] = 0.50 mM) in10 mM $Na_2B_4O_7$ buffer/D_2O; (iii) **2.3a** @OA_2 ([OA] = 1 mM), [**2.3a**] = 1 mM)in10 mM $Na_2B_4O_7$ buffer/D_2O; (iv) **2.3a** @OA_2 ([OA] = 1 mM), [**2.3a**] = 1.5 mM) in10 mM $Na_2B_4O_7$ buffer/D_2O; (v) **2.3a** in CD_3CN. "★" indicates the bound guest proton peaks. "●" and "■" represent the residual D_2O and CD_3CN respectively.

Complex	Diffusion constant(x 10^{-6} cm^2/s)
2.1a@OA_2	1.35
2.2a@OA_2	1.37
2.3a@OA_2	1.44

Table-2.1 Diffusion constant values of the complexes

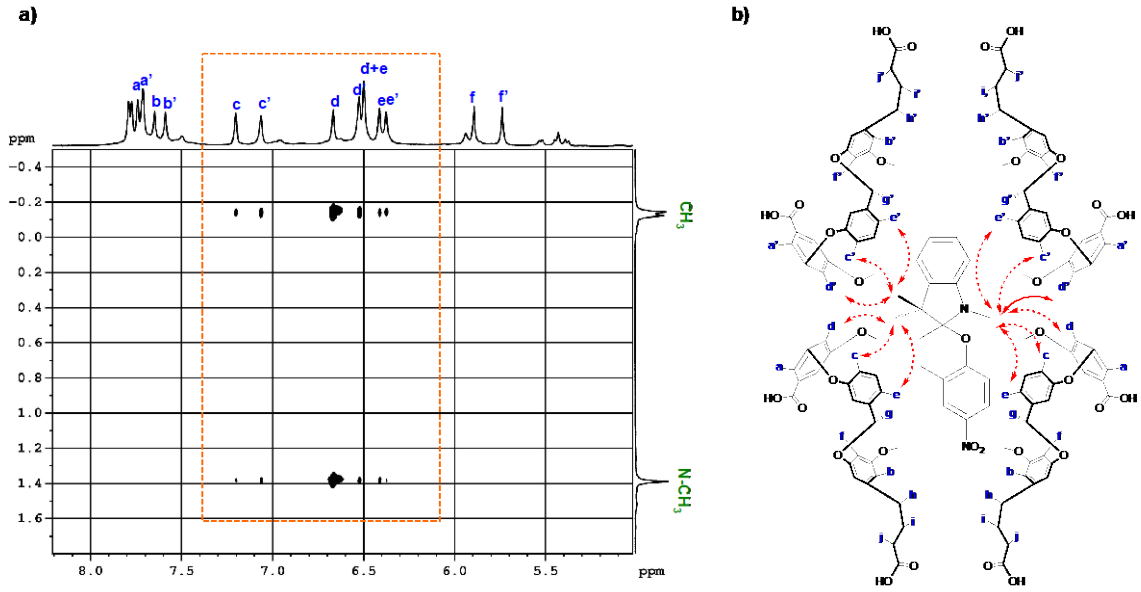

Figure 2.5 a) Partial 2D-NOESY spectra of **2.1a** @OA_2 ([OA] =5mM in 50 mM sodium tetraborate buffer,[1a] = 2.5 mM. Aromatic resonances of host are labeled from (a-f); b) pictorial representation of orientation of **2.1a** inside OA capsule.

2.2.3. Photochromism of 6-nitro BIPS (2.1a)@OA_2 complex

6-nitro BIPS in buffer did not show any absorption due to poor solubility in water. However,the absorption spectra of the complex **2.1a@OA_2** showed the characteristic absorption maxima of closed spiropyran around 340 nm (**Figure 2.6b**). The spectra showed that **2.1a** forms 2:1 complex with OA through hydrophobic effect. Irradiation of the **2.1a@OA_2** complex by UV-light (360 ± 20 nm) for 5 mins showed the colored, open and planar merocyanine form **2.1b@OA_2** in the region around 450-620 nm with λ_{max} at 511nm. As reported in the literature,[62] the absorption spectra of zwitterionic merocyanine form **(2.1b**) depend on the environment. Due to its planar structure and extended conjugation it shows absorption in the visible region with λ_{max} = 550-600 nm in most non-polar solvents. For example, the absorption spectrum of merocyanine in benzene solvent (**2.1b**) shows λ_{max} at 600 nm (**Figure 2.6**). Interestingly, while we irradiate the complex of **2.1a@OA2** under UV light, we observed absorption maxima λ_{max} for merocyanine (**2.1b**) at 511 nm,

which clearly tell us that environment of the **2.1b** in the complex is relatively polar. Our group has established that the OA cavity is non-polar, benzene like nature by using polarity probes like pyrene molecule. If the merocyanine form **(2.1b)** is inside the closed capsule of OA, we should have observed the λ_{max} around 600 nm.

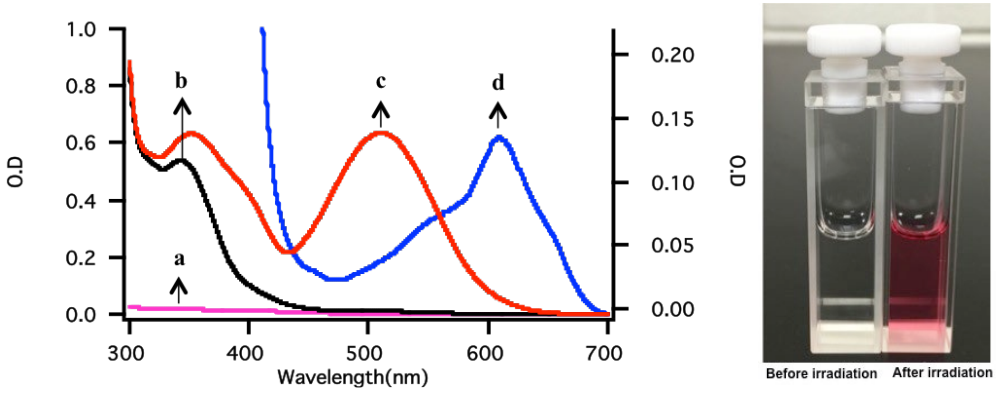

Figure 2.6 Absorption spectra of a) **2.1b** in buffer; b) **2.1a** @OA2 in buffer; c) **2.1b** @ OA in buffer; and d) **2.1b** in benzene. The y-axis scale on the right side (0- 0.25) corresponds to only spectrum (d).

Open-isomer merocyanine of 6-nitro BIPS **(2.1b)** is thermodynamically stable than the other isomers **(2.2b and 2.3b)** due to the presence of electron-withdrawing (-NO_2) group. We were not able to see photochromic behavior of other two guest molecules inside OA (**Figure 2.7)** due to very short lifetime of open merocyanine form. It has been established that presence of nitro group in spiropyran follows triplet pathway and unsubstituted, halo substituted derivatives follow singlet pathway.[73-74]

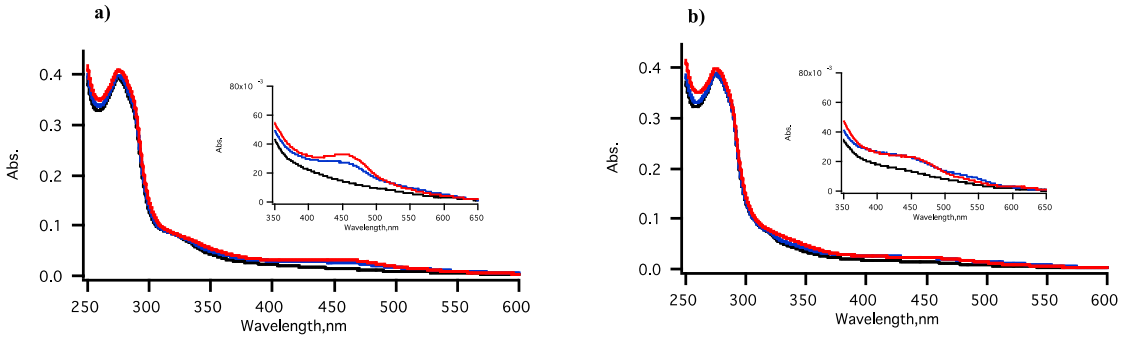

Figure 2.7 Absorption spectra of a) **2.2a @OA2** in buffer; b) **2.3a @OA2** in buffer; before irradiation (black line), after 5 min UV (blue line), after 10 min UV (red line).

2.2.4. Reversible assembly/disassembly of OA triggered by photchromic process

The absorption spectra of 6-nitro-BIPS (**2.1a@OA2**) and its merocyanine form **(2.1b@OA2)** clearly showed that closed spiropyran prefers closed hydrophobic cavity and its open-isomer prefers polar environment. We concluded that photochromic ring opening of spiropyran disassembles the capsule and forms 1:1cavitandplex. The disassembly process of the capsule is due to the formation of open and conjugated zwitterionic nature of merocyanine. The process of forming assembly and disassembly of supramolecular OA capsule is reversible due to the photochromic behavior. We irradiate the complex **2.1a@OA2** in borate buffer (pH- 8.9) under UV and visible light back and forth (5 min irradiation) and recorded the spectra **(Figure-2.8).** We observed the characteristic photochromism of spiropyran inside the OA cavity. Merocyanine formed during the process is quite stable till 20 cycles of irradiation even in polar environment **(Figure-2.8).** There are different ways of disassembly and orientation of the merocyanine inside the cavity OA as shown in **(Scheme-2.2**).

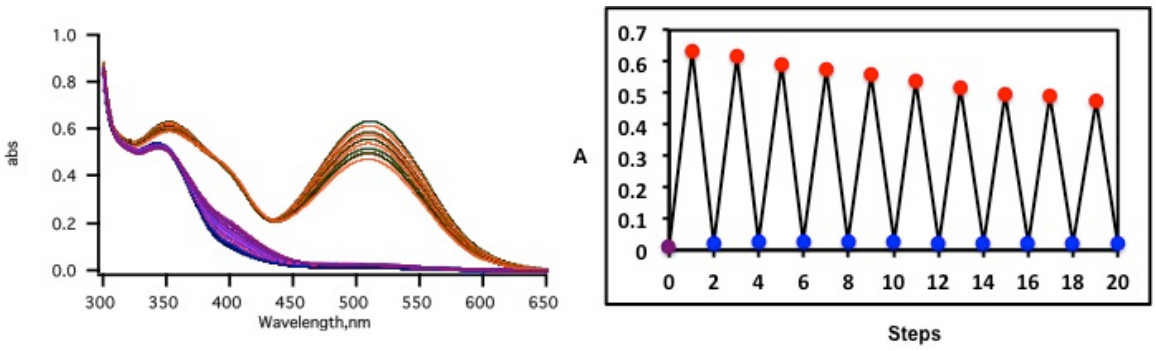

Figure 2.8 Absorption spectrum of photochromism between **2.1a** @OA_2 and **2.1b** @OA and its evolution at 511 nm.

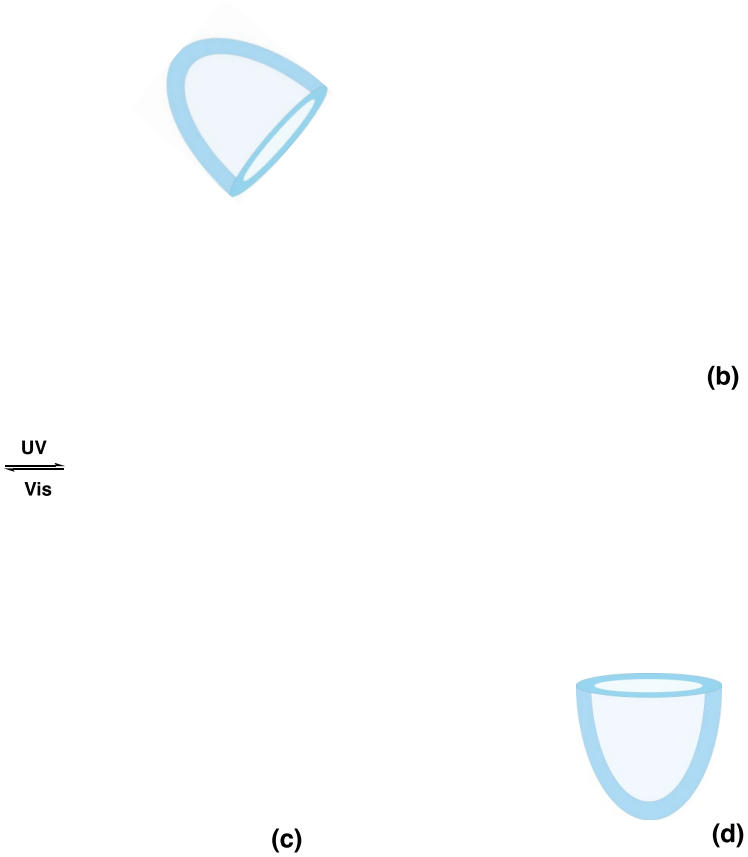

Scheme-2.2 Capsule assembly/disassembly triggered by photochromic process of **2.1a.**

During the photochromic process, we did not observe any turbidity or precipitation. This suggested that one half of the open merocyanine isomer remains intact inside the cavity while the other half exposed to the water. In this stage, we are not certain about the orientation of the merocyanine inside the OA cavity.

2.2.5. Effect of pH

Since the open merocyanine form has higher affinity to the environment, we wanted to study the effect of pH in our system. The absorption studies of the complexes were done in basic pH (8.9). When we irradiate **2.1a@OA$_2$** complex with UV light (360 ± 20 nm) the formed merocyanine disassembles the capsule and exposed in water. We tried to protonate the merocyanine (MC) by reducing the pH of the solution by adding dilute HCl. During

the addition of dil.HCl (pH~6.5), we observed decrease in MC absorbance and appearance of new shoulder around 400 nm which is due to protonated MC (MCH^+)(**Figure-2.9a**). The absorbance of MCH^+ is well-known and various studies have been reported.[62] To confirm the formation of MCH^+, MCH^+ was generated by adding dilute HCl to MC in acetonitrile and the corresponding absorption spectra taken (**Figure-2.10a**). The spectrum of MCH^+ in acetonitrile overlayed well with spectra obtained by reducing pH, suggesting that the MCH^+ formed during this process are identical. This experiment also supported our claim that merocyanine MC is exposed in water and it can be protonated. At the same time, when we increase the pH of the acidified solution by adding borate buffer and irradiated with UV light the recovery of MC from MCH^+ was observed **(Figure-2.9b).** When we lower the pH of **2.1a@OA$_2$** complex without irradiation we did not see any change, which might be due to the capsule formation with OA that does not expose **2.1a** to the environment (**Figure-2.10b**).

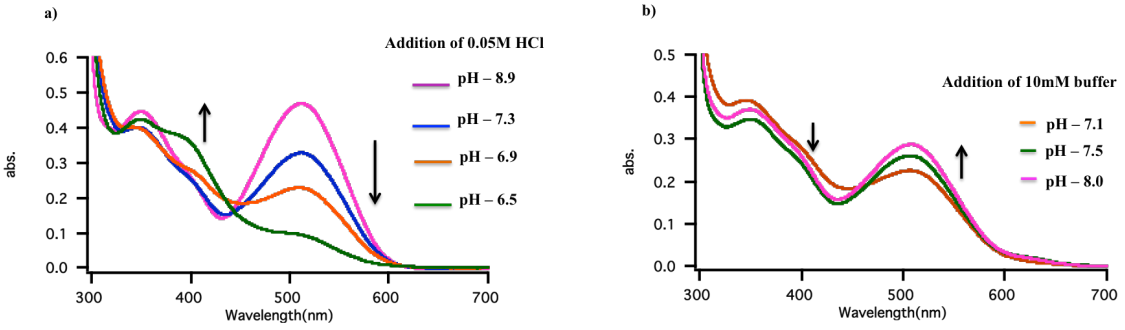

Figure 2.9 a) Absorption spectra of **2.1b**@OA after addition of 0.05 M HCl b) absorption spectra of **2.1b**@OA after addition of 10 mM buffer.

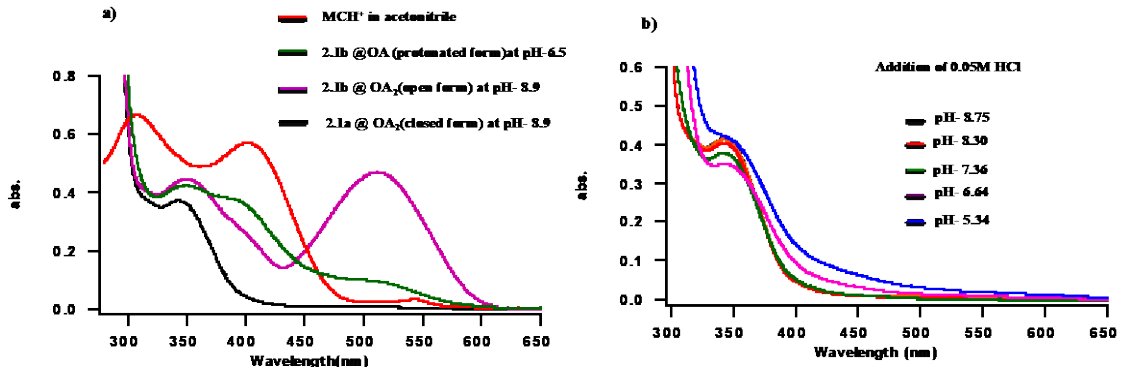

Figure 2.10 a) Absorption spectra of **2.1a**@OA_2 at pH 8.9, **2.1b**@OA at pH 8.9, **2.1b**@OA at pH 6.5 and MCH^+ in acetonitrile; b) Absorption spectra of **2.1a**@OA_2 after addition of 0.05 M HCl .

We checked the stability of merocyanine formed at each cycle of visible irradiation at neutral and basic pH and compared its stability in organic solvent (acetonitrile**)(Figure-2.11)**. Merocyanine **2.1b** is comparatively stable in basic pH than in organic solvent. Merocyanine **2.1b** reverts spontaneously back to **2.1a** normally in organic solvents. But inside the OA cavity it took almost 20 hours for the thermal ring closing to spiropyran. The decay of merocyanine was monitored by its absorption spectra and plotted against time. The reisomerization rate constant of **2.1b** inside OA (1.1×10^{-4} s^{-1}) is one order of magnitude smaller than that (2×10^{-3} s^{-1}) measured in acetonitrile. This suggested that OA cavity greatly enhances the stability of both **2.1a** and **2.1b** in water along with its characteristic photochromic property.

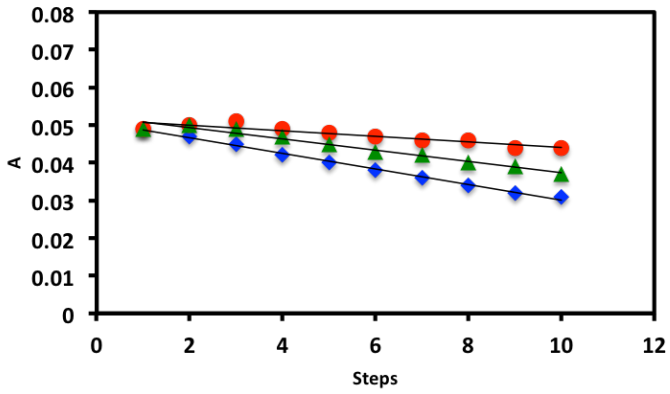

Figure 2.11 Stability of **2a** in acetonitrile (▲); **2a**@OA at pH- 7(●); **2a**@OA at pH-9 (♦)

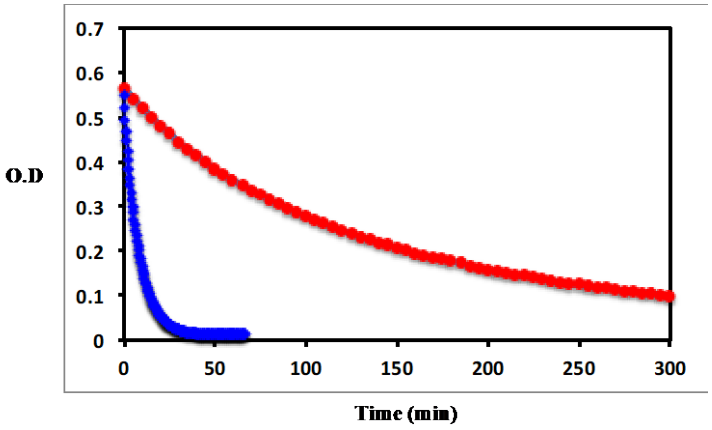

Figure 2.12 Thermal decay of merocyanine **2.1b** to spiropyran **2.1a** within OA (red line) and in acetonitrile (blue line)

2.2.6. Emission and lifetime of Merocyanine inside OA

Excited state properties of Merocyanine have been studied by different research groups.[75-76] Closed spiropyran is weakly emissive but open merocyanine has strong emissive properties. The excited pathway of ring opening of spiropyran is found to be both singlet and triplet excited state.[74, 77-78] The lifetime of merocyanine has been reported to be in sub-picosecond time scale in isotropic solution.[76, 78-79] 2.1b@OA complex shows fluorescence around 625 nm **(Figure 2.13).** The lifetime of 2.1b inside OA was monitored by exciting the complex at 405 ± 5 nm and monitored at 625 nm. The lifetime found to be

bi-exponential decay with τ_1 = 3.3 ns and τ_2 = 0.8 ns which is much longer than in organic solvent **(Figure-2.14)**. This remarkable behavior can be better understood by ultrafast studies. Exciting and emission spectra of the **2.1b@OA** complex (**Figure-2.15-2.16**) did not vary with different wavelength suggested the orientation of **2.1b** inside OA remains intact.

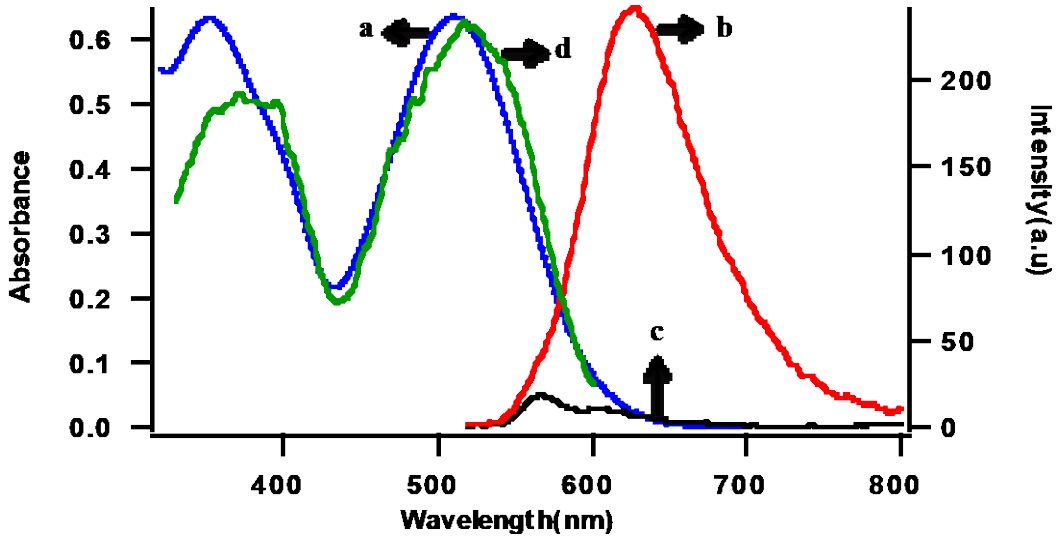

Figure 2.13 a) Absorption spectrum of **2.1a@OA$_2$** b) Emission spectrum of **2.1b@OA** c) Emission spectrum of **2.1a@OA$_2$** d) Excitation spectrum of **2.1b@OA**

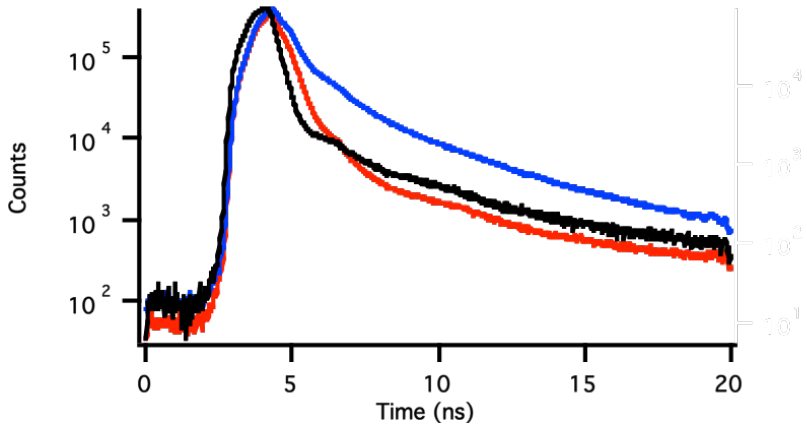

Figure 2.14 Time resolved fluorescence decay of merocyanine **2.1b** within OA (blue line) , in ethanol (blue line) [black line –IRF]

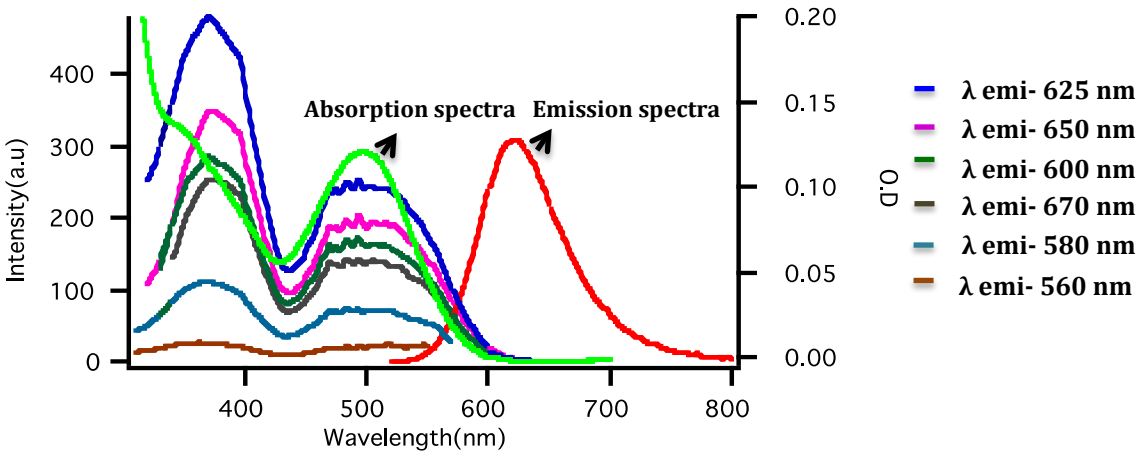

Figure 2.15 Excitation spectra of **2.1b@OA** monitored at different emission wavelength

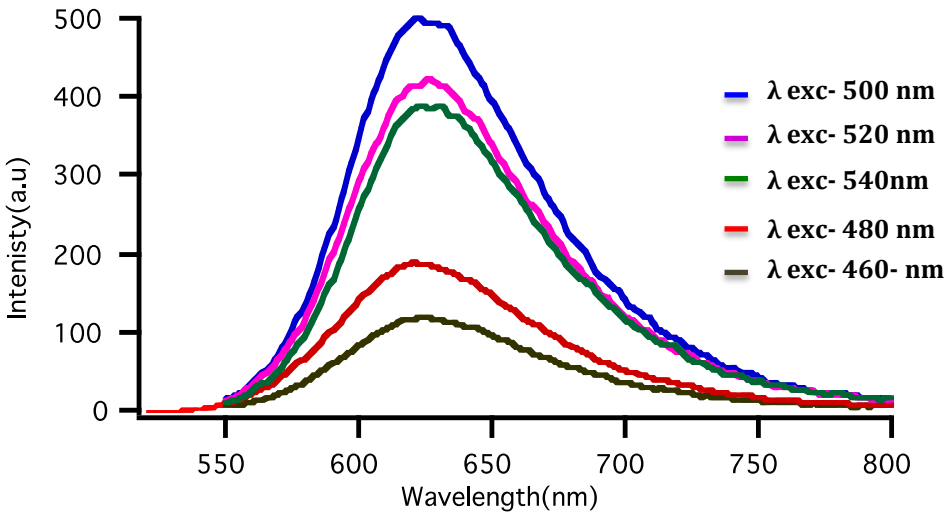

Figure 2.16. Emission spectra of **2.1b@OA** monitored at different excitation wavelength

2.3 Conclusion

We have demonstrated the possibility of reversible disassembly and assembly of the OA capsule by a photochromic process. The influence of OA on the excited state behavior and ground-state stability of a well-known spiropyran system is far superior of those of other organized supramolecular assemblies. The process described here could be useful in transporting and releasing small hydrophobic molecules in a spatially and temporally controlled manner in an aqueous environment. We propose to pursue such studies as well as monitor molecular dynamics of photochromic systems within OA through time-resolved ultrafast studies.

2.4 Experimental section

Materials and methods

Host octa acid (OA) was synthesized and characterized according to the reported procedure.[32] The guest molecule 6-nitro-BIPS (**1a**) was purchased from Sigma-Aldrich and used as received. The 6-bromo-BIPS (**1b**) and parent BIPS (**1c**) were synthesized according to the literature.[80] Absorption spectra were measured with a Shimadzu UV -3150 spectrophotometer. Steady-state luminescence spectra were recorded using a FS920CDT fluorometer (Edinburgh Analytical Instruments). Fluorescence lifetimes were measured by time-correlated single photon counting using a nF920 fluorometer (Edinburgh Analytical Instruments).

General Procedure for guest binding studies probed by NMR

A D_2O stock solution (600 μL) of host OA (1 mM) and sodium borate buffer (10 mM) taken in a NMR tube was titrated with the guest by sequential addition of 0.125 eq of guest (2.5 μL of a 30 mM solution in CD_3CN). The complexation was achieved by shaking the NMR tube for about five minutes. ^1H NMR spectra were recorded at room temperature under aerated conditions on a Bruker 500 MHz NMR. 1:2 complex was achieved by 10 μL of guest solution to 600 μL of 1 mM OA host in 10 mM buffer.

Sample preparation for the photochemical reactions

600 μL of the complex solution was diluted to 6 mL to give the stock solution. The concentration of host and the guest molecules are [OA = 1 x 10^{-4} M], [guest = 5 x 10^{-5} M] respectively. The stock solution was kept in dark for 12 h before doing all measurements. For emission and lifetime measurements, it was further diluted appropriately with 10 mM buffer solution to have the required concentration of bound guest [OA = 1 x 10^{-5} M], [guest

= 5 x 10^{-6} M] purged with N_2 for 30 mins mainly for lifetime measurement. The samples were irradiated with a Luzchem research reactor , UV(Hitachi-FL-8BL-B, 365 nm) and Visible (Luzchem 420).

Chapter 3. Volume Conserving Geometric Isomerization of Encapsulated Azobenzenes in Ground and Excited States and as Radical Ion

3.1 Overview

Many important biological processes, such as photosynthesis[81] and vision[82] are powered by light. Light seems to be an ideal external control element for many chemical and biological manipulations because of its unique properties, including noninvasive, widely available, environment benign and provides high level of spatiotemporal resolution. Additionally, its wavelength and intensity can be precisely regulated. Molecules can be reversibly switched between two states by exposure to light. This phenomenon is known as photochromism and molecules are called photoswitches or photochromic molecules. As discussed in **chapter-2,** molecular switches have been used in various applications including, optical storage devices, triggers for peptide folding, and neuroscience.[83] Examples of molecular photoswitches and importance of spiropyran are discussed in **chapter-2**. Azobenzenes (ABs) form one of the largest and most studied classes of photochromic molecules. Azobenzenes have been used in both biological applications[83] and in electronic devices.[84] Most preferrable properties of photoswitches in biological environments includes water solubility, less toxicity and stability toward side reactions and photo bleaching. In developing nanoswitches and electronic devices, azobenzenes played a vital role. Coupling of photoswitches like azobenzene with metal nanoparticles has been the emerging area of research in developing electronic devices.[85] Encapsulation of ABs in supramolecular cavities or macrocyclic assemblies has been tried by various research groups.[61] However, photoisomerization of azobenzene (*trans* to *cis* form) within these systems causes the *cis*-isomer to disassemble from the capsule subsequently due to the lack

of cavity space to accommodate the *cis*-form. In this chapter, we have studied the encapsulation of azobenzene derivatives with deep cavitand

Octa acid (OA) and studied their photoisomerization within the cavity. We also utilized the surface binding capacity of OA to understand the interaction between gold nanoparticles and encapsulated ABs.

Azobenzenes undergo photoisomerization from thermodynamically stable *trans* isomer to *cis* isomer under UV-light excitation. The back isomerization from *cis-trans* isomer is achieved by visible light. The reversible *cis-trans* isomerization also occurs readily at room temperature in dark. This is due to lower activation energy (23 kcal mol^{-1}) for thermal *cis-trans* isomerization.[86] The structurally similar stilbenes undergo photoisomerization via volume demanding 180° bond flip (rotation around C=C) but azobenzene proceeds through pyramidalization (inversion) along with rotation. In this chapter, we compared the geometric isomerization of stilbene and azobenzene inside OA capsule.

3.2 Results and discussion

We chose alkyl substituted azobenzenes and its stilbene analogue as guest molecules and Octa acid (OA) as water-soluble host. *trans*-azobenzenes and stilbene analogue **3.1-3.6** (**Scheme 3.1**) were synthesized, purified and characterized by methods reported in the literature.[56, 87]

Encapsulation of *trans*-ABs (**3.1-3.5**) with OA capsule was characterized by ^{1}H NMR spectra (**Figure-3.1**). The upfield shift (δ 0 to -4 ppm) of alkyl protons of azobenzenes clearly indicates the encapsulation of the guest molecules. The splitting of OA peaks and shift within aromatic region also indicates the interaction between OA and ABs. Individual

NMR titration spectra of each guest molecules with OA are also shown in (**Figure-3.2-3.6**). We measured the diffusion constant of the complexes from 2D-DOSY spectra and tabulated the values in **Table-3.1.** The values are in the range of (1.23 x 10^{-6} cm^2/s to 1.40 x 10^{-6} cm^2/s) confirmed the host : guest ratio is 2:1.

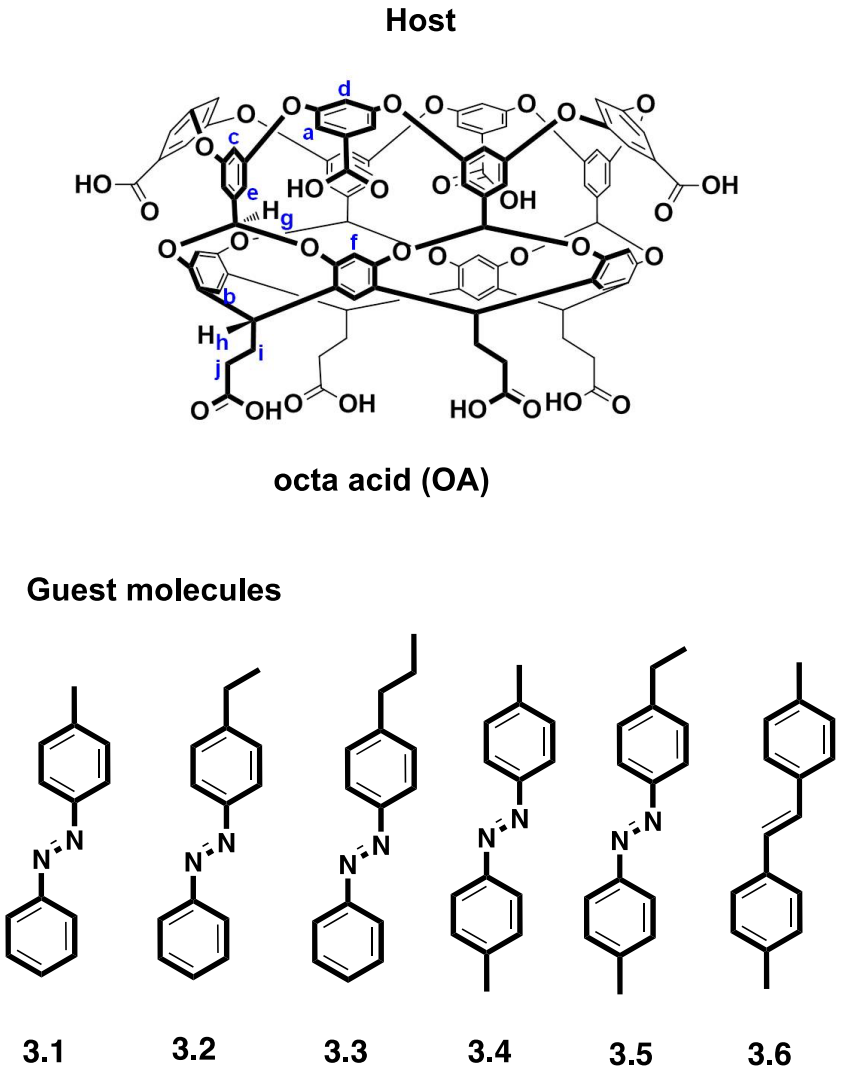

Scheme-3.1 Structures of the host and the guest molecules

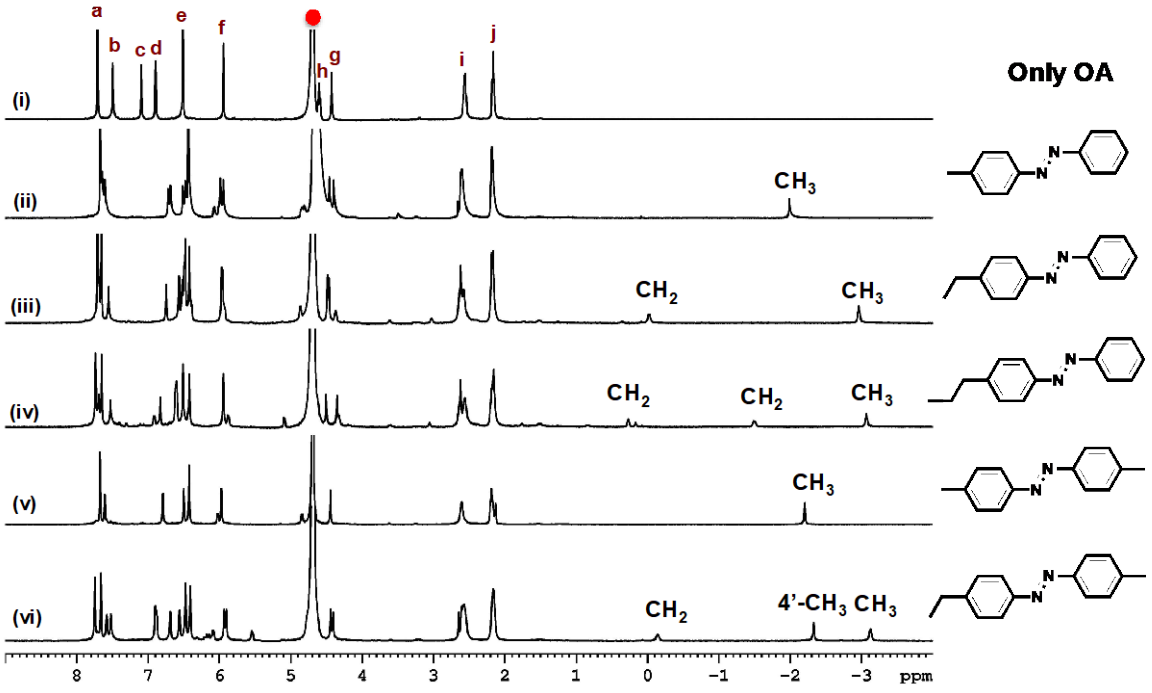

Figure 3.1 ^{1}H NMR (500 MHz) spectra of (i) OA (1 mM) in 10 mM $Na_2B_4O_7$ buffer/D_2O; (ii) **3.1@OA$_2$**; (iii) **3.2@OA$_2$** ; (iv) **3.3@OA$_2$** ; (v) **3.4@OA$_2$** ; (vi) **3.5@OA$_2$** ([OA] = 1 mM [**3.1-3.5**] = 0.5 mM); "●"represent the residual D_2O.

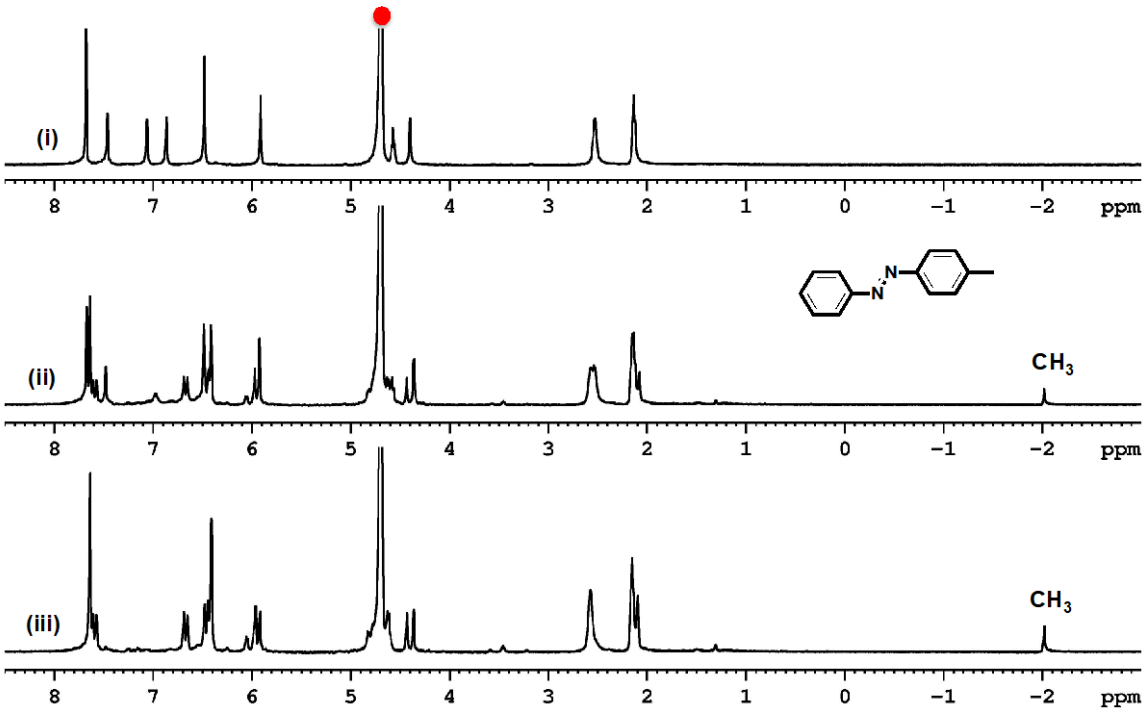

Figure 3.2 ^{1}H NMR (500 MHz) spectra of (i) OA (1 mM) in 10 mM $Na_2B_4O_7$ buffer/D_2O; (ii) **3.1**@OA ([OA] = 1 mM), **[3.1**] = 0.25 mM); (iii) **3.1**@OA ([OA] = 1 mM), [3.**1**] = 0.5 mM); "●"represent the residual D_2O.

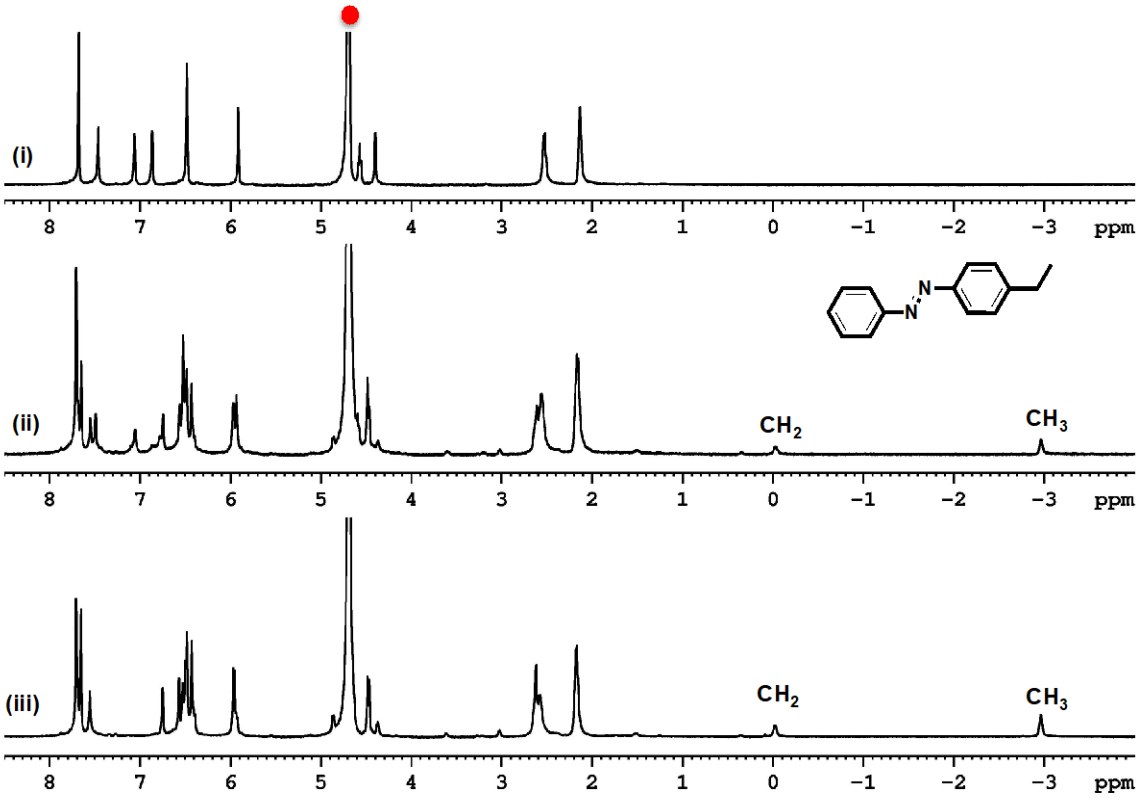

Figure 3.3 ^{1}H NMR (500 MHz) spectra of (i) OA (1 mM) in 10 mM $Na_2B_4O_7$ buffer/D_2O; (ii) **3.2**@OA ([OA] = 1 mM), **[3.2]** = 0.25 mM); (iii) **3.2**@OA ([OA] = 1 mM), [**3.2**] = 0.5 mM); "●"represent the residual D_2O.

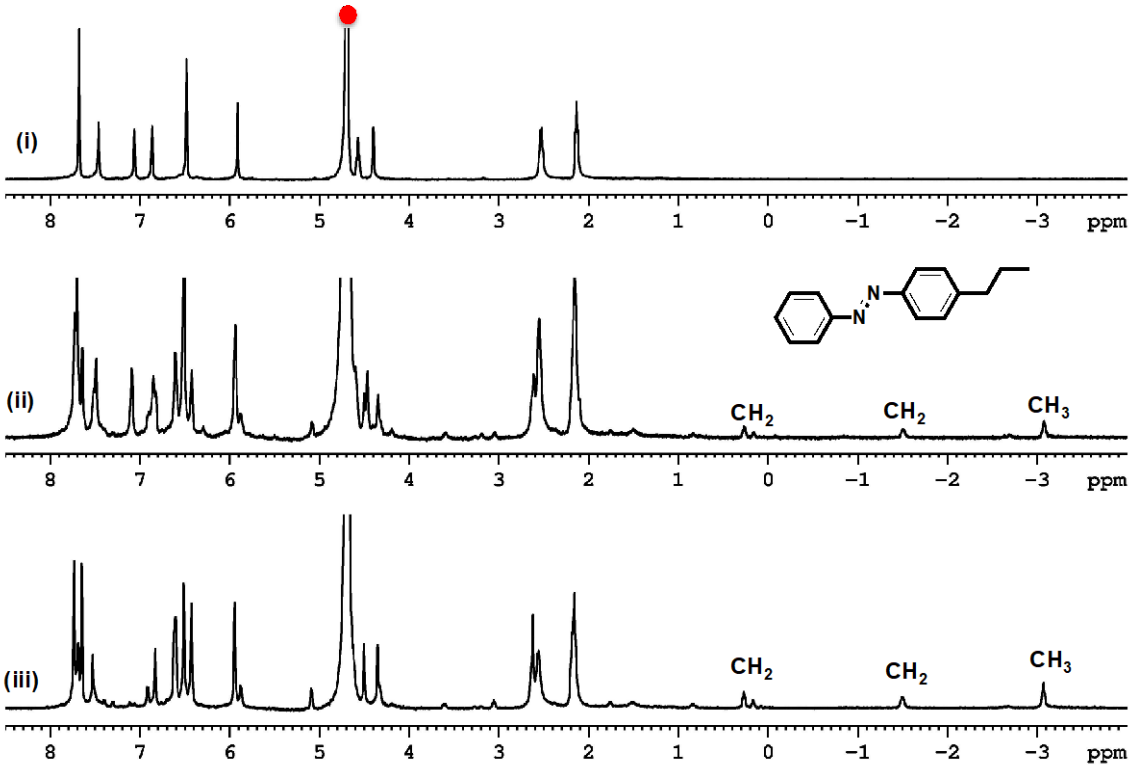

Figure 3.4 ^{1}H NMR (500 MHz) spectra of (i) OA (1 mM) in 10 mM $Na_2B_4O_7$ buffer/D_2O; (ii) **3.3**@OA ([OA] = 1 mM), **[3.3]** = 0.25 mM); (iii) **3.3**@OA ([OA] = 1 mM), [**3.3**] = 0.5 mM); "●"represent the residual D_2O.

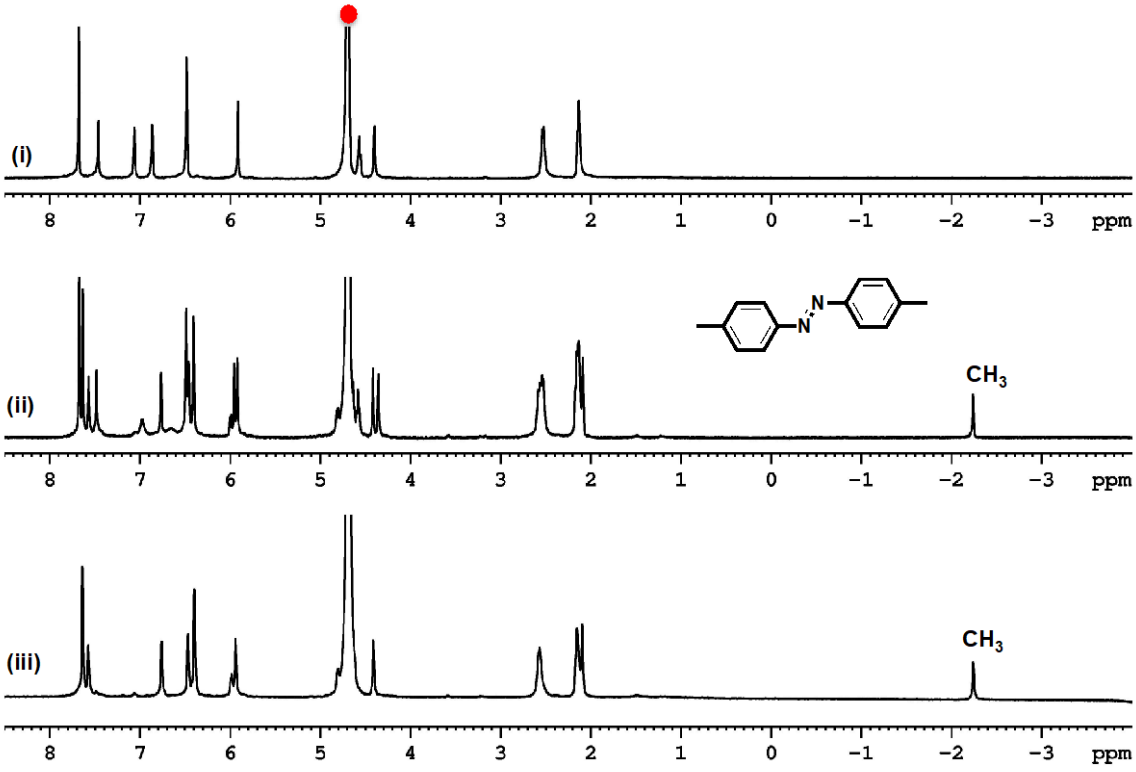

Figure 3.5 ^{1}H NMR (500 MHz) spectra of (i) OA (1 mM) in 10 mM $Na_2B_4O_7$ buffer/D_2O; (ii) **3.4**@OA ([OA] = 1 mM), **[3.4]** = 0.25 mM); (iii) **3.4**@OA ([OA] = 1 mM), [**3.4**] = 0.5 mM); "●"represent the residual D_2O.

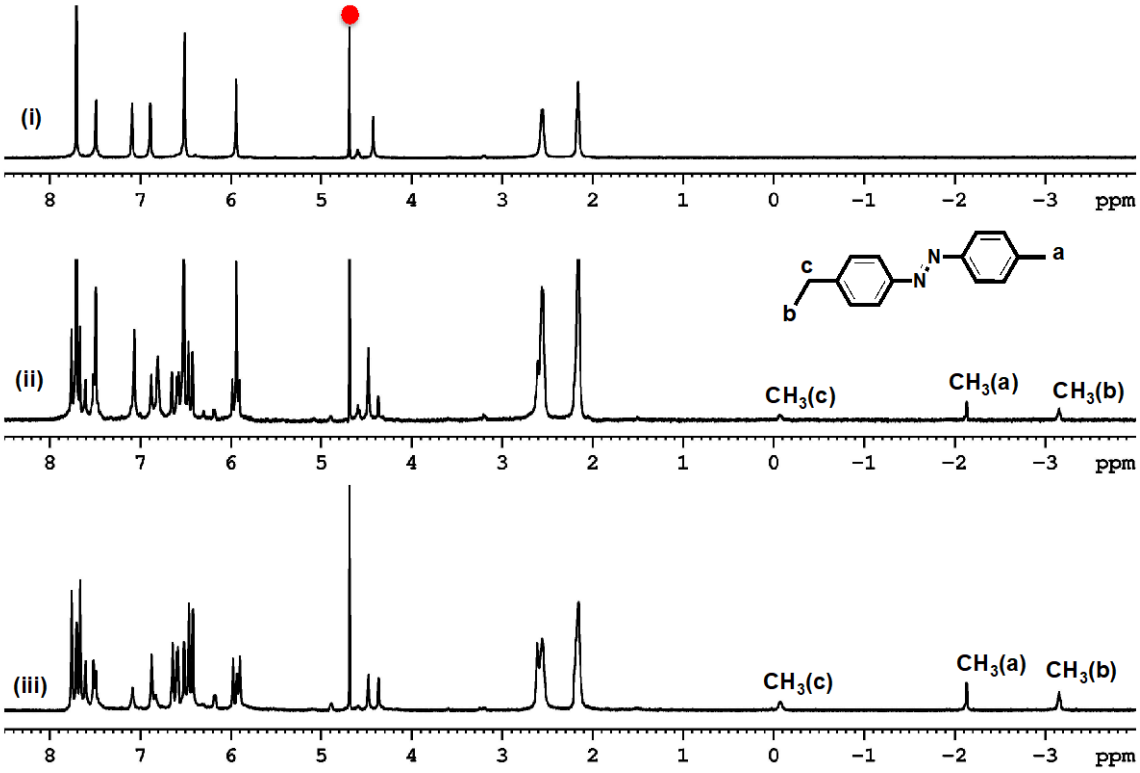

Figure 3.6 ^{1}H NMR (500 MHz) spectra of (i) OA (1 mM) in 10 mM $Na_2B_4O_7$ buffer/D_2O; (ii) **3.5**@OA ([OA] = 1 mM), **[3.5]** = 0.25 mM); (iii) **3.5**@OA ([OA] = 1 mM), [**3.5**] = 0.5 mM); "●"represent the residual D_2O.

Compound	Diffusion constant (cm^2/s)
Only OA	1.91×10^{-6}
3.1@OA_2	1.40×10^{-6}
3.2@OA_2	1.34×10^{-6}
3.3@OA_2	1.28×10^{-6}
3.4@OA_2	1.38×10^{-6}
3.5@OA_2	1.23×10^{-6}

Table 3.1 Diffusion constant values of azobenzene derivatives complexes with OA by 2D-DOSY NMR.

3.2.1 Absorption spectra of azobenzenes within OA

Absorption spectra of all *trans*-ABs@OA_2 showed characteristic absorption maxima, 350 ± 10 nm due to π-π* transition and 440 ± 10 nm due to n- π* transition (**Figure 3.7**). The absorption of OA host molecules is around 290 nm is not shown in the spectra. The *trans*-AB@OA_2 complexes were irradiated with UV light (350 ± 20 nm) using Luzchem reactor for 30 mins to reach photostationary state (PSS). The PSS in the absorption spectra showed enhancement of visible region (n- π* transition) around 450 nm and decrease in the absorbance in UV region, which is due to the formation of *cis*-isomer during photoisomerization (**Figure 3.7)**. This process of photoswitching between *trans* and *cis*-isomer is reversible and can be easily monitored by absorption spectra (**Figure 3.8**).

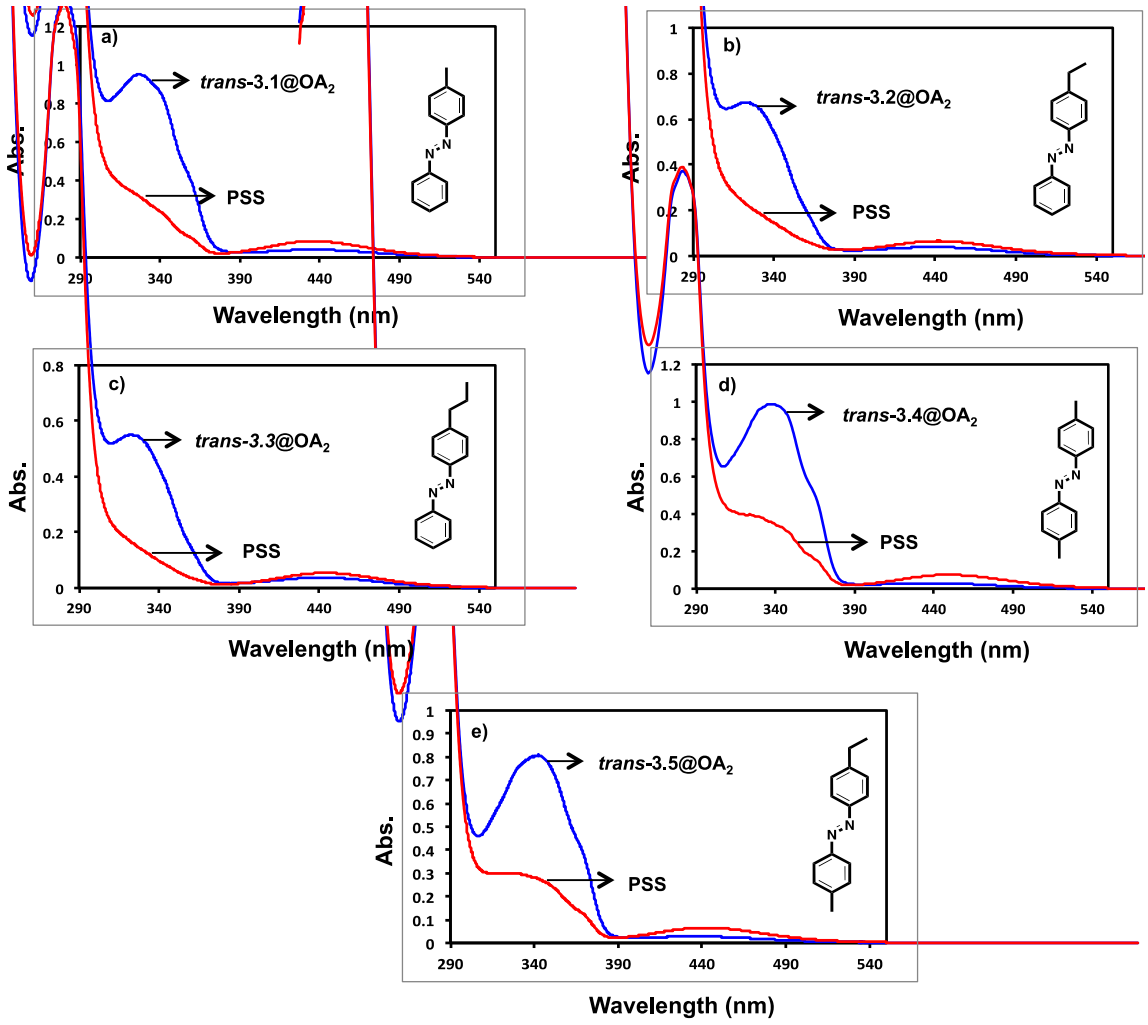

Figure 3.7 Absorption spectra of trans and cis-azobenzene complexes a) **3.1**@OA_2; b) **3.2**@OA_2; c) **3.3**@OA_2; d) **3.4**@OA_2; e) **3.5**@OA_2 ; ([OA]= 1 x 10^{-4} M, [guest] = 5 x 10^{-5} M) Luzchem reactor, 350 ± 20 nm and 420 ± 20 nm lamps for UV and visible, respectively, were used

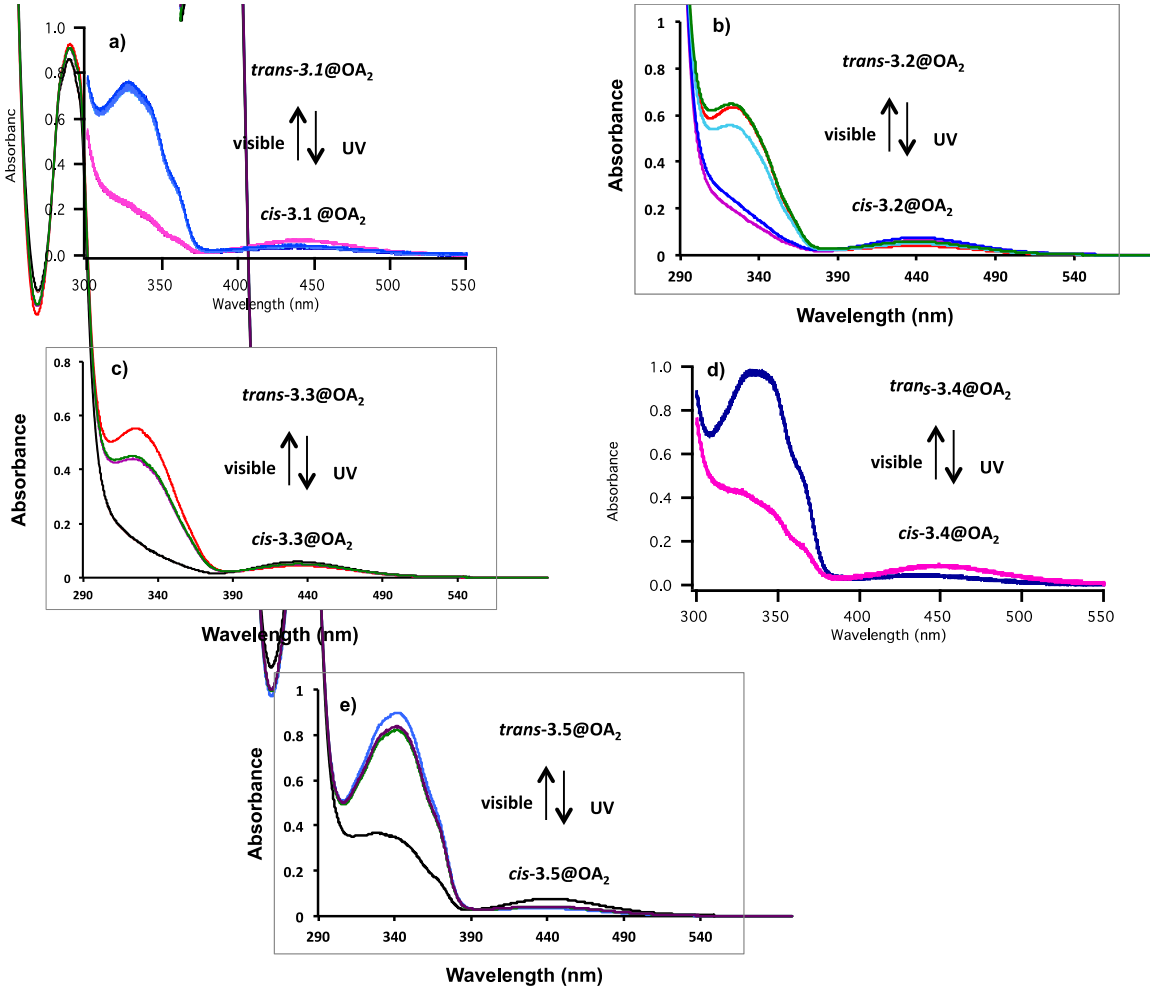

Figure 3.8 Absorption spectra of *trans*-azobenzene@OA_2 complexes recorded after every 5 min UV and visible irradiation in sequence: a) **3.1**@OA_2; b) **3.2**@OA_2; c) **3.3**@OA_2; d) **3.4**@OA_2; e) **3.4**@OA_2 ; ([OA]= 1 x 10^{-4} M, [guest] = 5 x 10^{-5} M). Luzchem reactor, 350 ± 20 nm and 420 ± 20 nm lamps for UV and visible, respectively, were used.

3.2.2 Photoinduced *trans* to *cis* isomerization of Azobenzenes within OA

All *trans*-AB@OA_2 complexes were irradiated with UV light (350 ± 20 nm) and corresponding NMR spectra were taken. Reversible *cis* to *trans* isomerization was monitored by irradiating the sample with visible light (420 ± 20 nm). This process repeated for few cycles with each irradiation about 30 minutes. When the *trans*-AB complex with OA was irradiated with UV light, appearance of new peaks along with existing *trans* peaks in the upfield region was observed. New peaks are due to the formation of encapsulated *cis*-isomer inside the OA cavity. Similarly, irradiation with visible light causes the disappearance of *cis*-isomer peaks and enhancement in peak of *trans* isomer peaks. **Figure 3.9** shows the photoisomerization of encapsulated *trans*-4-methyl azobenzene (**3.1**) derivative. The methyl (-CH_3) proton for encapsulated *trans*-4-methylazobenzene appears at δ -2.0 ppm. After UV irradiation, new peak around δ -0.6 ppm was observed along with decrease in peak of corresponding *trans* isomer. This new peak around δ -0.6 ppm corresponds to the cis-isomer. After visible light irradiation of the *cis*-isomer, the peak around δ -0.6 ppm almost disappears due to the back isomerization of *cis to trans.* Similar trend was observed for the rest of the complexes (**Figure 3.10-3.13**). The ratio between *trans* and isomers were mentioned in the corresponding figures.

One of the interesting examples of all *trans* complexes is 4-propylazobenzene (**3.3)**. When we irradiated **3.3@OA_2** using UV light, we observed about 96% enrichment of *cis*-isomer in the PSS composition. But when we reversibly irradiated with visible light, we found only about 50% conversion to *trans* isomer and remaining 50% stays as *cis* isomer inside OA. This might be due to preferable orientation between *cis* and *trans* propyl azobenzene is *cis* isomer within OA cavity. Once cis-4-propylazobenzene forms during

photoisomerization and it found hard to go back to *trans*. This peculiar behavior is rationalized by the orientation of the guest molecule (***cis*-3.3**) inside OA cavity.

Partial ^{1}H NMR spectra for all the complexes revealed that the photoswitchable property of azobenzene inside OA cavity. Unlike expulsion of *cis* isomer from the cavity that is observed in the literature, [56] we were able to see the photoisomerization from *trans* to *cis* and vice-versa inside the cavity. The PSS for all the complexes after UV light irradiation was quantified by NMR integration and listed in **Table-3.2**. We also measured the PSS of all guest molecules in toluene (**Table-3.2**) for comparison.

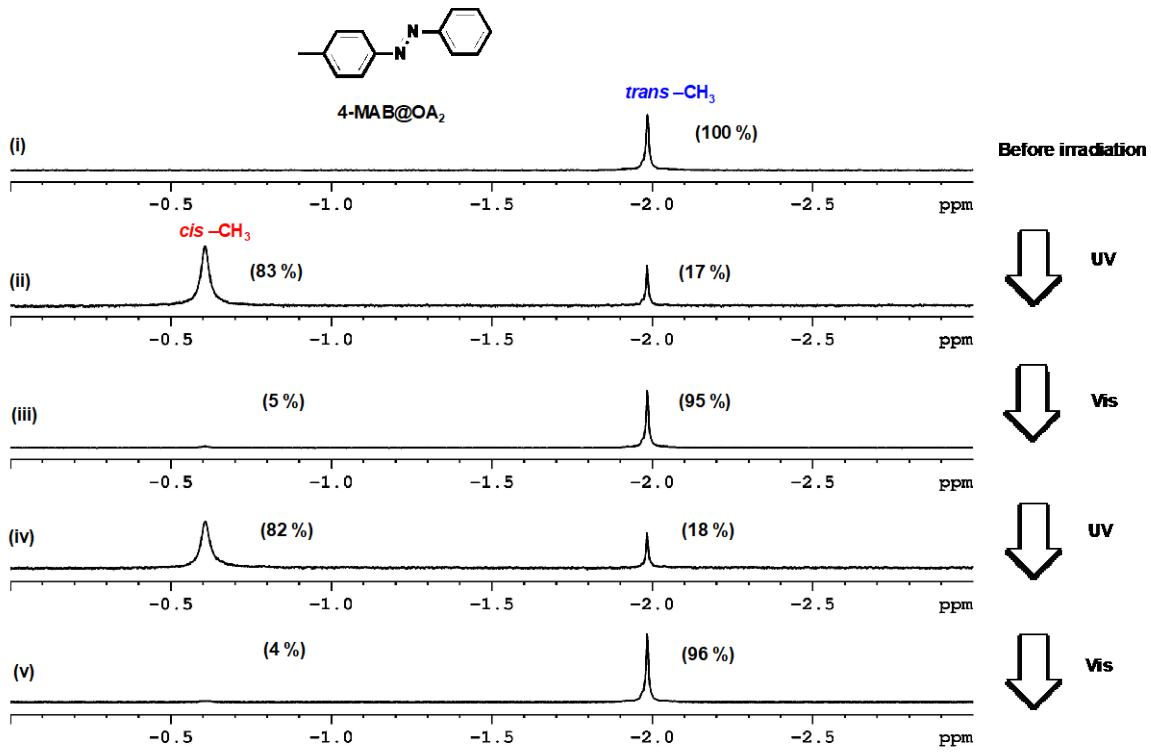

Figure 3.9 Partial ^{1}H NMR spectra of **3.1**@OA_2 (i) before irradiation; (ii) after 30 min UV irradiation; (iii) after 30 min visible irradiation; (iv) after 30 min UV irradiation; (v) after 30 min visible irradiation. ([OA]= 1 mM, [**3.1**] = 0.5 mM). Luzchem reactor, 350 ± 20 nm and 420 ± 20 nm lamps for UV and visible, respectively, were used.

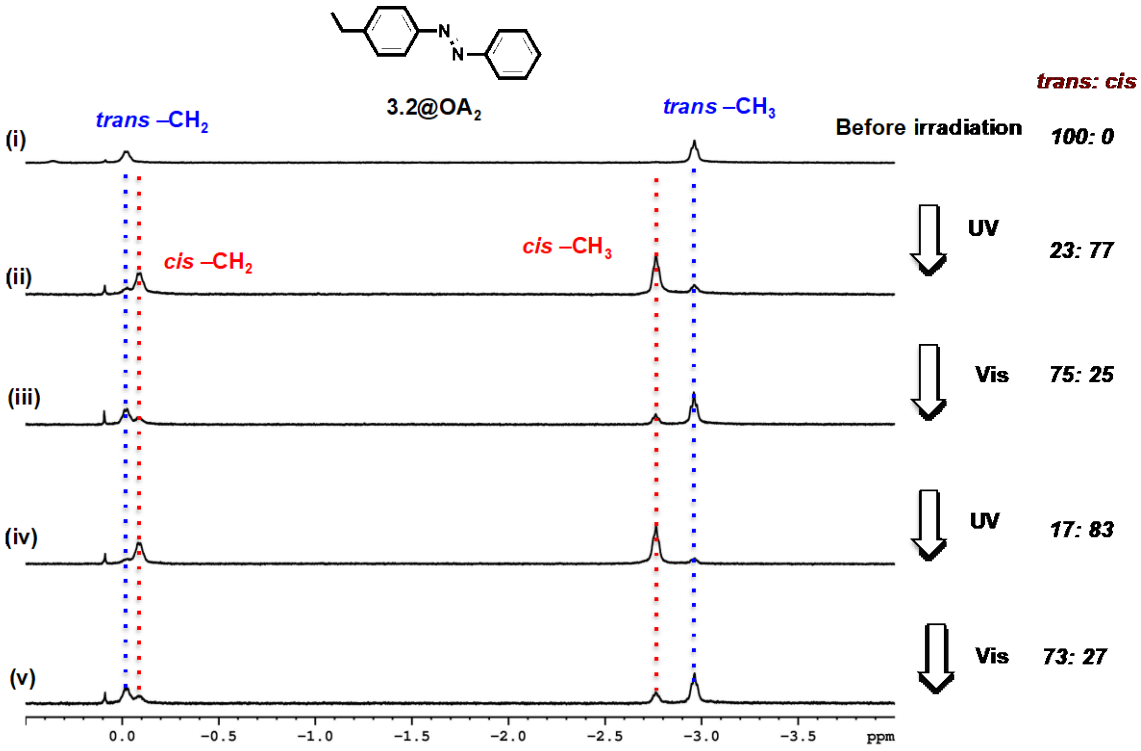

Figure 3.10 Partial ^{1}H NMR spectra of **3.2**@OA_2 (i) before irradiation; (ii) after 30 min UV irradiation; (iii) after 30 min visible irradiation; (iv) after 30 min UV irradiation; (v) after 30 min visible irradiation. ([OA]= 1 mM, [**3.2**] = 0.5 mM).

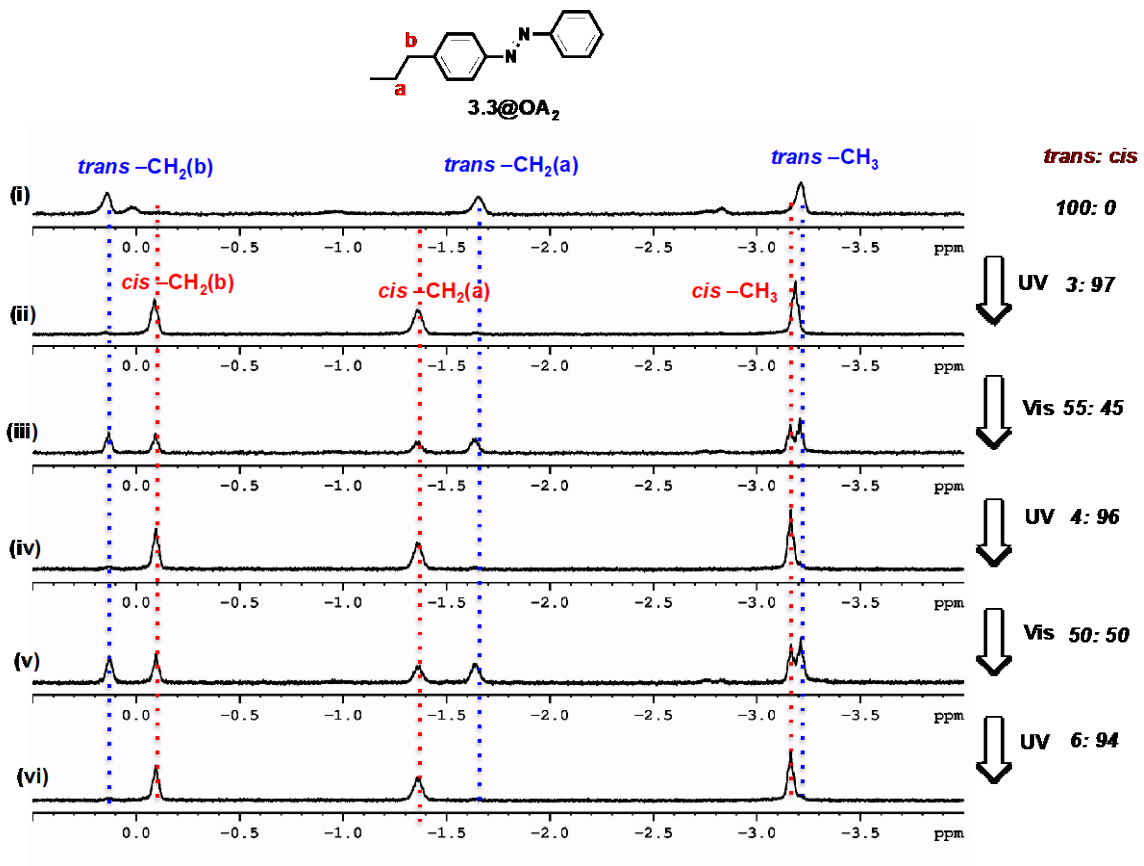

Figure 3.11 Partial ^{1}H NMR spectra of **3.3**@OA_2 (i) before irradiation; (ii) after 30 min UV irradiation; (iii) after 30 min visible irradiation; (iv) after 30 min UV irradiation; (v) after 30 min visible irradiation. ([OA]= 1 mM, [**3.3**] = 0.5 mM).

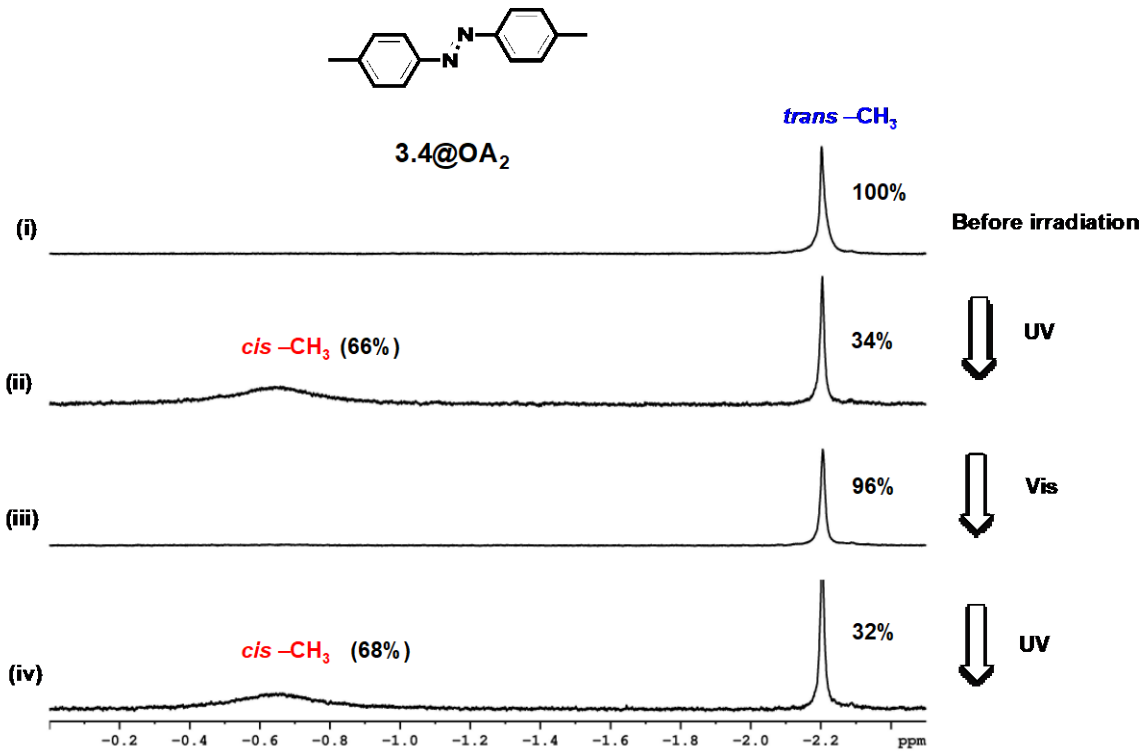

Figure 3.12 Partial ^{1}H NMR spectra of **3.4**@OA_2 (i) before irradiation; (ii) after 30 min UV irradiation; (iii) after 30 min visible irradiation; (iv) after 30 min UV irradiation; (v) after 30 min visible irradiation. ([OA]= 1 mM, [**3.4**] = 0.5 mM).

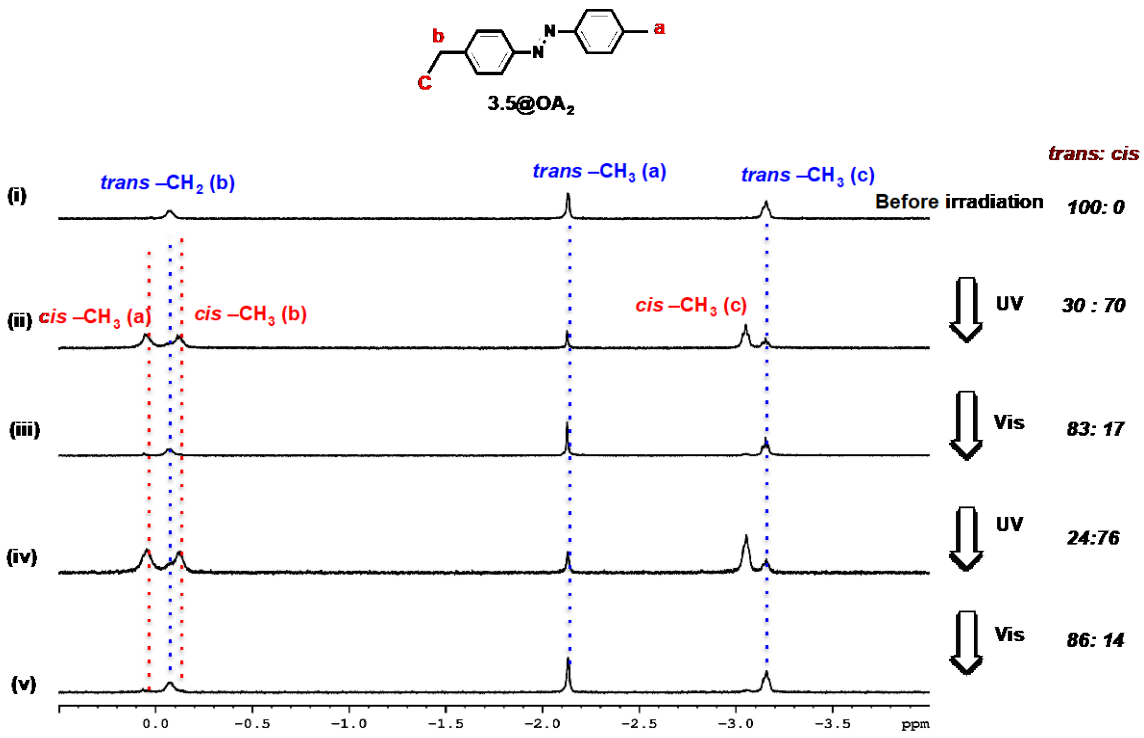

Figure 3.13 Partial ^{1}H NMR spectra of **3.5**@OA_2 (i) before irradiation; (ii) after 30 min UV irradiation; (iii) after 30 min visible irradiation; (iv) after 30 min UV irradiation; (v) after 30 min visible irradiation. ([OA]= 1 mM, [**3.5**] = 0.5 mM).

Compound	Photostationary state in toluene (*cis: trans*)	Photostationary state inside OA (*cis: trans*)
3.1	86:14	83:17
3.2	90:10	77:23
3.3	88:12	97:3
3.4	95:5	68:32
3.5	91:9	70:30

Table 3.2 Photostationary state composition of the *cis* and *trans* isomers of azobenzenes (**3.1-3.5**) in toluene and as complexes with OA in water. Irradiations were conducted with (Luzchem reactor, 350 ± 20 nm)

3.2.3 Comparison of stilbene and azobenzene photoisomerization influenced by OA

Geometrical isomerization from *trans* to *cis* isomer of stilbenes involves rotation around C=C bond. On the other hand, azobenzene isomerization follows two types of mechanisms (i) rotation and (ii) inversion or pyramidalization. In our group, we have already studied the photoisomerization of various stilbene derivatives inside OA capsule and we established that geometric isomerization could be controlled within a well-defined space.[88] Of various stilbene derivatives, 4,4'-dimethylstilbene(**3.6**) showed unusual behavior. Photoisomerization of *trans*-4,4'-dimethylstilbene reaches photostationary state enriched with *trans* isomer (*trans: cis* 80: 20) due to restricted rotation inside the cavity. We wanted to compare the photoisomerization of 4,4'-dimethylstilbene(**3.6**) and its analogue 4,4'-dimethylazobenzene(**3.4**). We believe nearly the same ^{1}H NMR shift of the methyl groups of **3.6**@OA_2 and **3.4**@OA_2 (**Figure 3.14**) suggesting their placement in a similar environment within OA. Weak CH-π interaction between the dimethyl group and the capsular wall and lack of free space around the aryl ring likely restricted the isomerization of *trans* 4,4'-dimethylstilbene to the *cis* within OA via C=C bond rotation. Despite the two guest molecules has similar environment within OA, photoisomerization of **3.4**@OA_2 reaches the photostationary state with 68% *cis* isomer (**Figure 3.14b).** We trace the above variance to the mechanistic difference of the isomerization in the excited state of two chromophores. While C=C can isomerize only by 180° rotate, the N=N can do so by either a 180° rotation or by volume conserving pyramidalization process. This implicates that both compounds follow different pathway to reach the PSS. We concluded

that the photoisomerization of ABs follow different pathway than corresponding stilbene derivative. We are collaborating with Professor Chris Elles in University of Kansas to study the ultrafast dynamics of both stilbenes and azobenzenes to elucidate our initial observation.

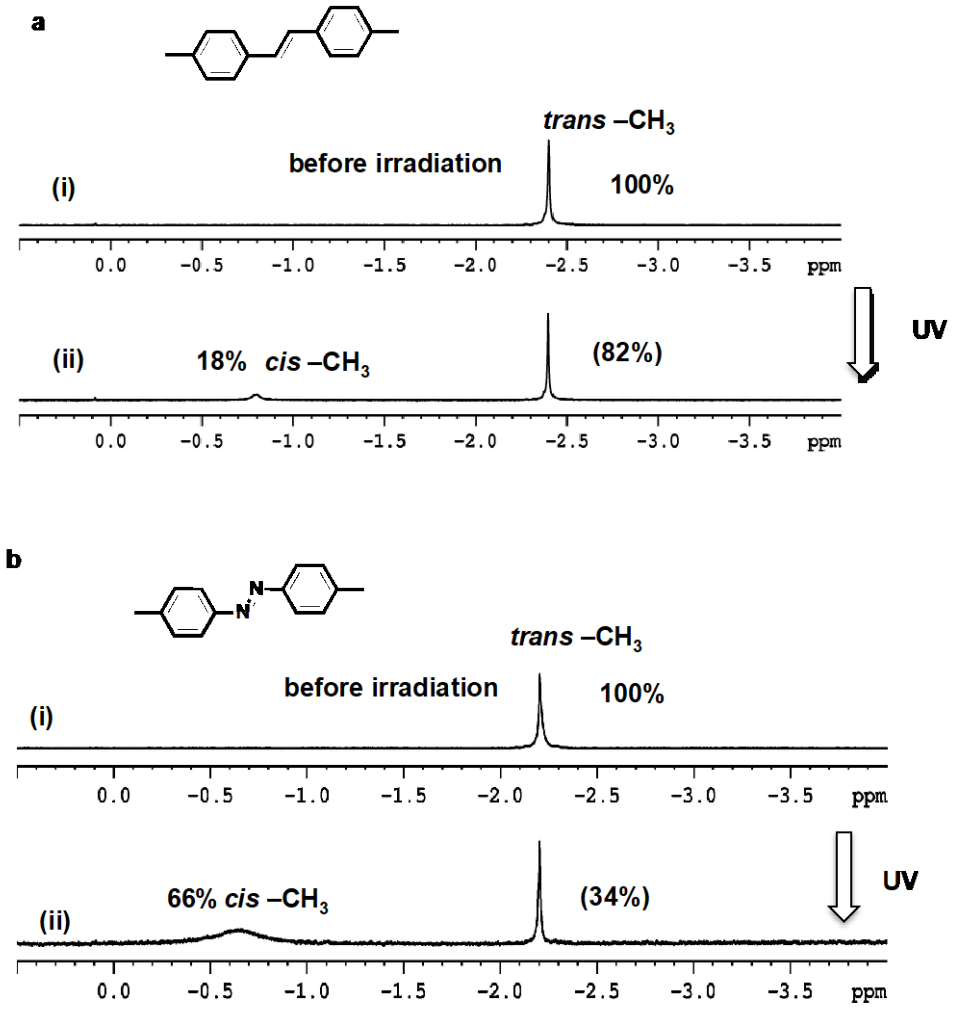

Figure 3.14 Partial NMR (500 MHz) spectra a) (i) **3.6**@OA_2 before irradiation; (ii) **3.6**@OA_2 after 30 min UV; b) (i) **3.4**@OA_2 before irradiation; (ii) **3.4**@OA_2 after 30 min UV; ([OA]= 1 mM [**3.4** & **3.6**] = 0.5 mM

3.2.4 Thermal back isomerization of *cis*-azobenzenes in presence of OA

Trans azobenzenes are thermodynamically stable compared to *cis* azobenzenes. *Cis* azobenzenes are known to isomerize to *trans* isomers at ambient temperature in the dark due to relatively low activation energy barrier. We carried out thermal back isomerization by irradiating the *trans* isomer under UV light for 30 mins kept at dark and followed the *cis*-*trans* isomerization by recording absorption spectra with time. We monitored the thermal back isomerization of *cis* azobenzenes within OA capsule as well as in toluene solution (**Figure-3.15 & 3.16**). The thermal back isomerization from *cis* to *trans* isomer took 5- 8 days in toluene solution for all the guest molecules. However, in the case of inside OA, the thermal back isomerization inside OA capsule varies from day to months. For the guest molecules, 4-methyl **(3.1**), 4,4'-dimethyl (**3.4)** and 4-methyl-4'-ethyl derivatives (**3.5**) it took almost a week. In the case of 4-ethyl (**3.2)** and 4-propyl **(3.3)** it took more than months. Especially, 4-propylazobenzene took 78 days to complete the back isomerization process thermally. This can be explained by the fact that *cis*-isomer of 4-propyl azobenzene is oriented energetically favorable position inside the OA capsule. We also noticed this unique behavior by NMR studies.

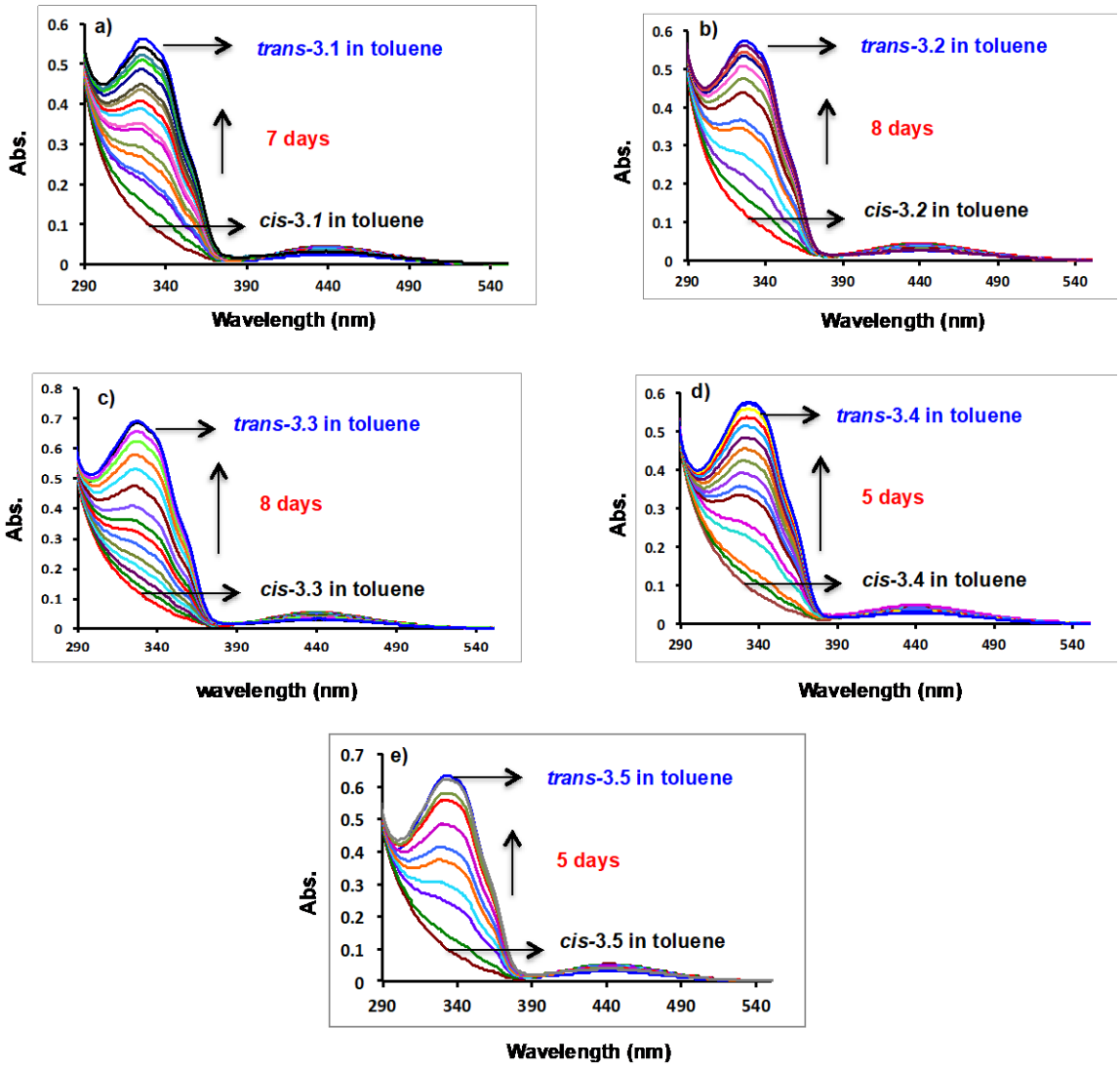

Figure 3.15 Absorption spectra of thermal isomerization of *cis*-azobenzene derivatives (after 30 min UV) in toluene: a) **3.1**; b) **3.2**; c) **3.3**; d) **3.4**; e) **3.5**. ([**3.1-3.5**] = 25 uM).

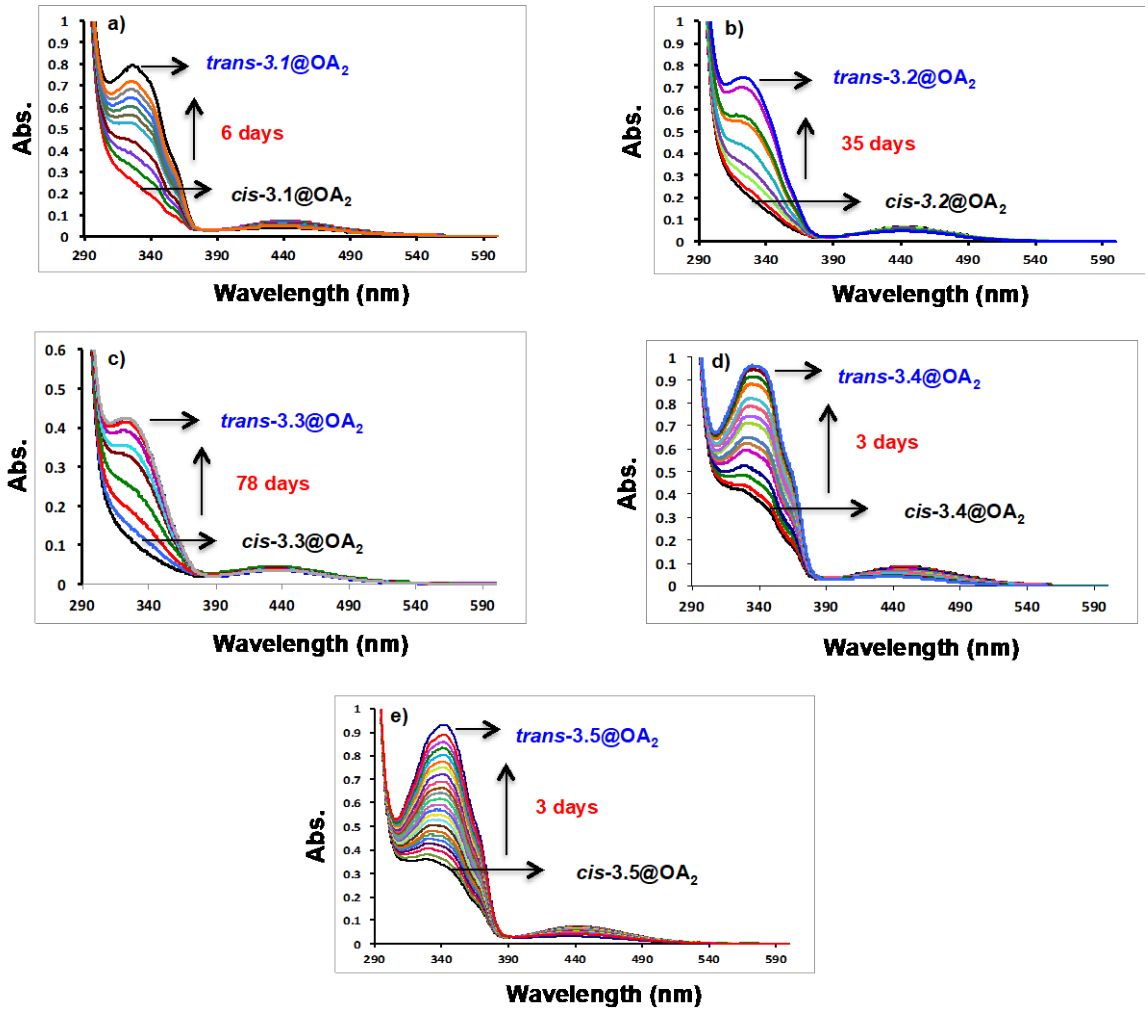

Figure 3.16 Absorption spectra of thermal isomerization of *cis*-azobenzene derivatives (after 30 min UV) within OA capsule a) **3.1**@OA_2; b) **3.2**@OA_2; c) **3.3**@OA_2; d) **3.4**@OA_2; e) **3.5**@OA_2 ([OA]= 1 x 10^{-4} M, [guest] = 5 x 10^{-5} M)

3.2.5 Rapid thermal back isomerization induced by gold nanoparticles

Thermal back isomerization from *cis* to *trans* isomer of azobenzenes generally takes several hours to days. Recently it was found that presence of gold nanoparticles (AuNP) induces the back isomerization within several minutes.[89-92] Catalytic property of gold nanoparticles and unique behavior of photoswitches attracted scientists to study their mechanism and its applications. Most of the reported literature involved direct coupling of azobenzene with metal surface by modification of the azobenzene structure.[89, 93] This kind of approach had drawback of aggregation of metal nanoparticles. Sciano *et al* reported that addition of *pseudo naked* AuNPs to the aqueous solution of unbounded azobenzene derivatives enhanced the thermal back isomerization drastically. They proposed a mechanism that involves electron transfer from azobenzene to the gold surface via generation of radical cation of azobenzene as an intermediate.[91] But spectrophotometrical and electrochemical studies of azobenzene revealed that azobenzene radical anion isomerizes rapidly from *cis* to *trans*.[94-95] The actual mechanism for the enhancement of the rate of thermal back isomerization of azobenzene due to gold nanoparticles is still not clearly understood. We are interested in investigating the mechanism of thermal back isomerization of *cis* azobenzenes inside our capsule. Our group had already established that OA can stabilize the gold nanoparticles and photochemistry of encapsulated guest molecules was observed.[96] We also demonstrated that electron transfer from encapsulated donor to acceptor outside the capsule across the wall is possible.[36] In this work, addition of gold nanoparticles to the encapsulated azobenzene solution facilitates the rate of thermal back isomerization even without direct contact between azobenzene and AuNPs.

Metastable gold nanoparticle (mAuNP) was prepared by reported procedure[97] and characterized by UV and DLS experiments (**Figure 3.17 & 3.18)**. UV light irradiation of *trans*-ABs@OA_2 complexes causes enrichment of *cis* isomer inside the capsule, which was recorded by absorption spectra. Addition of 200 uL of metastable gold nanoparticle (mAuNP) solution to the complex induces the electron transfer and enhances the thermal back isomerization within in minutes for all the complexes. **Figure 3.21** shows the rapid thermal back isomerization of cis-azobenzene@OA_2 complexes. The kinetic plot of this process is shown as inset in **Figure 3.21**. Thermal back isomerization of all the complexes except *cis*-4-propyl derivatives completed within 15 minutes. *cis*-4-propylazobenzene@OA2 took 60 minutes to complete the process. We have tried the same experiments with citrate-capped gold nanoparticle (cAuNP), which is bulkier and stable than metastable gold nanoparticles (mAuNP). We observed rapid thermal isomerization with the addition of cAuNp**(Figure 3.22).** The proposed mechanism is shown in the **scheme-3.1.** We believe that the rapid thermal isomerization from *cis* to *trans* isomer of azobenzene induced by AuNP is due to the electron transfer from Au surface to the encapsulated azobenzene. The generation of azobenzene radical anion during the electron transfer process enhances the rate of isomerization. The electron transfer from outside the wall to the guest molecule inside OA capsule across the wall is interesting observation. This kind of approach can be useful in the future to develop a photocatalyst which would bind to the capsule and induce selective photochemical reaction inside the capsule.

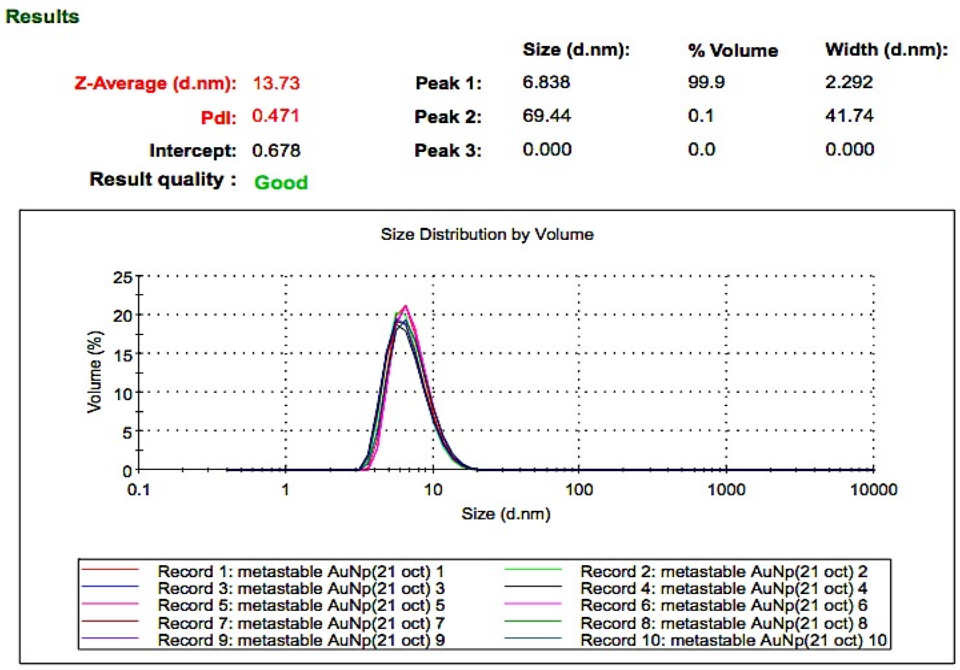

Figure-3.17 Size of metastable gold nanoparticles (mAuNP) by DLS.

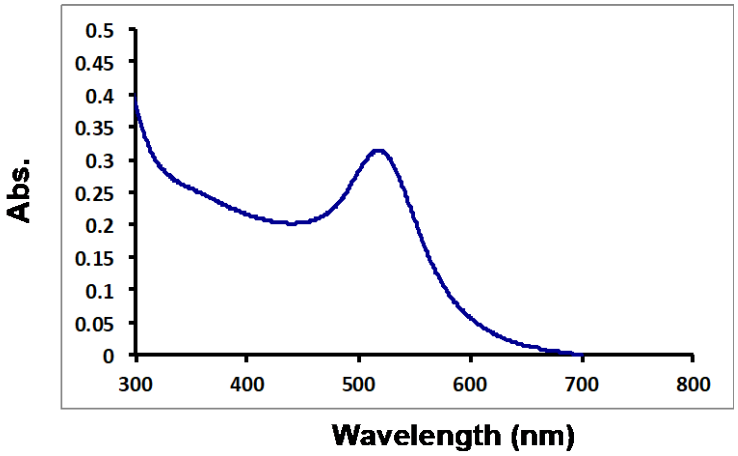

Figure-3.18 Absorption spectrum of metastable gold nanoparticle (mAuNP).

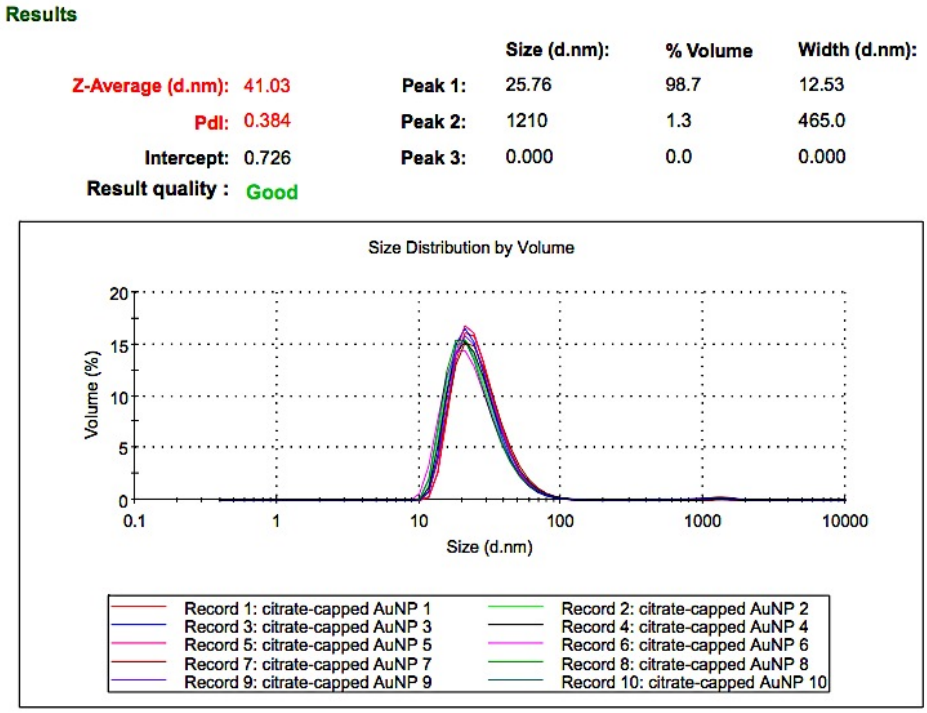

Figure-3.19 Size of the citrate capped AuNP by DLS.

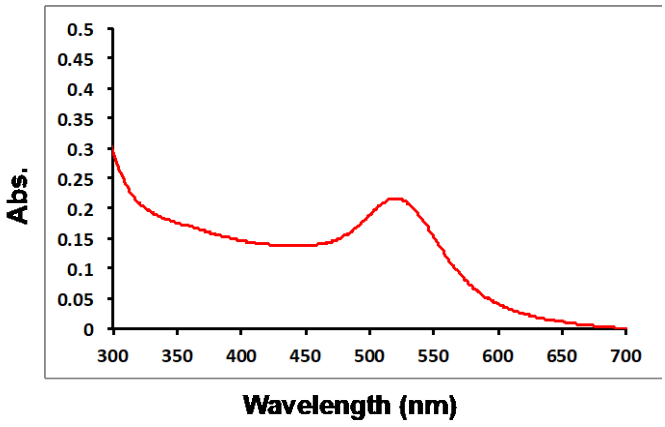

Figure-3.20 Absorption spectrum of citrate capped gold nanoparticle (cAuNP)

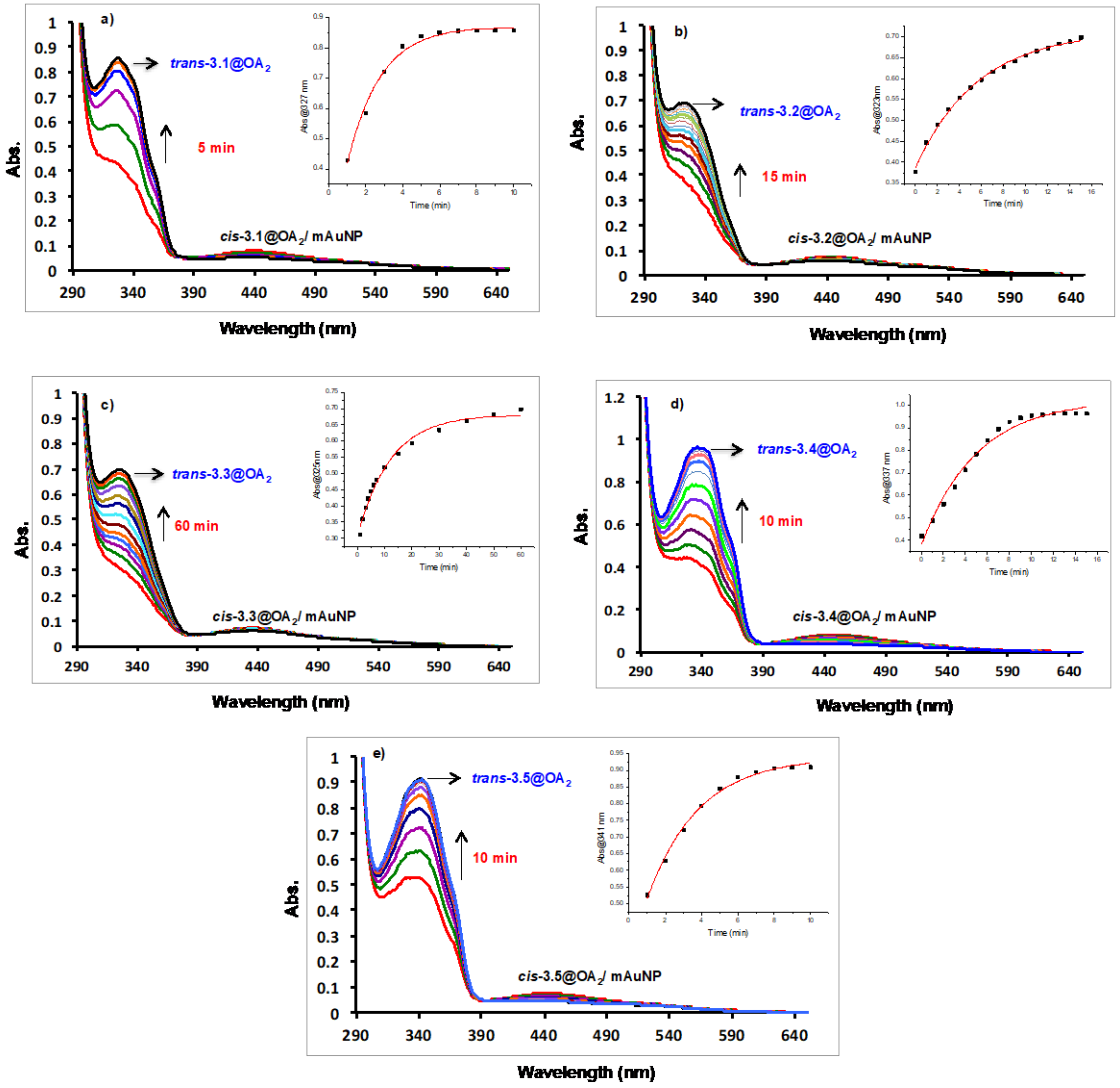

Figure 3.21 Absorption spectra of thermal isomerization of *cis*-azobenzene derivatives inside OA capsule in presence of metastable AuNP. a) **3.1**@OA_2; b) **3.2**@OA_2; c) **3.3**@OA_2; d) **3.4**@OA_2; e) **3.5**@OA_2. ([OA]= 1 x 10^{-4} M, [guest] = 5 x 10^{-5} M); Inset figures depict the growth of the trans isomers as function of time monitored at λ_{max} of trans isomers.

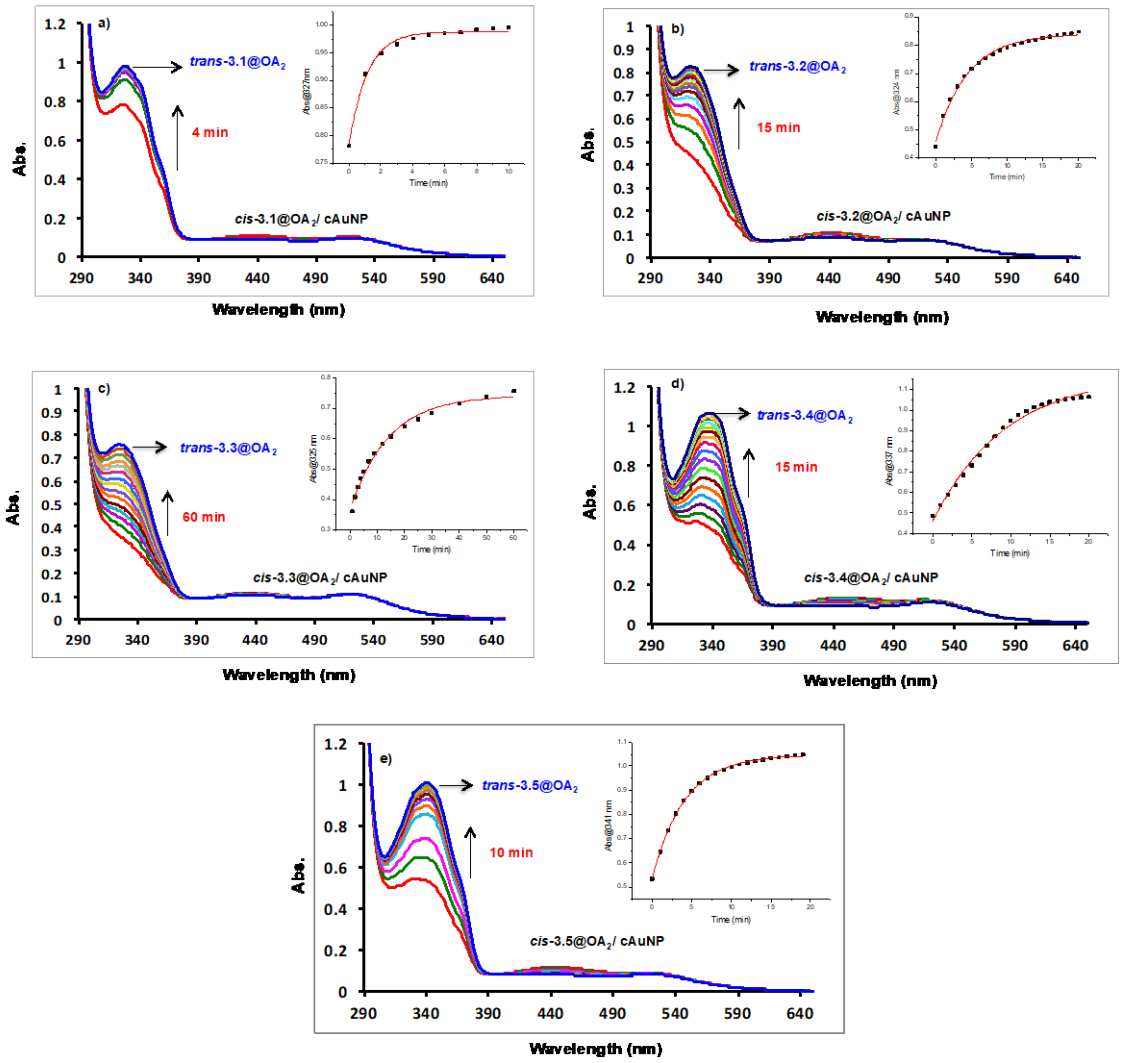

Figure 3.22 Absorption spectra of thermal isomerization of *cis*-azobenzene derivatives inside OA capsule in presence of citrate capped AuNP. a) **3.1**@OA_2; b) **3.2**@OA_2; c) **3.3**@OA_2; d) **3.4**@OA_2; e) **3.5**@OA_2. ([OA]= 1 x 10^{-4} M, [guest] = 5 x 10^{-5} M); Inset figures depict the growth of the trans isomers as function of time monitored at λ_{max} of the trans isomers.

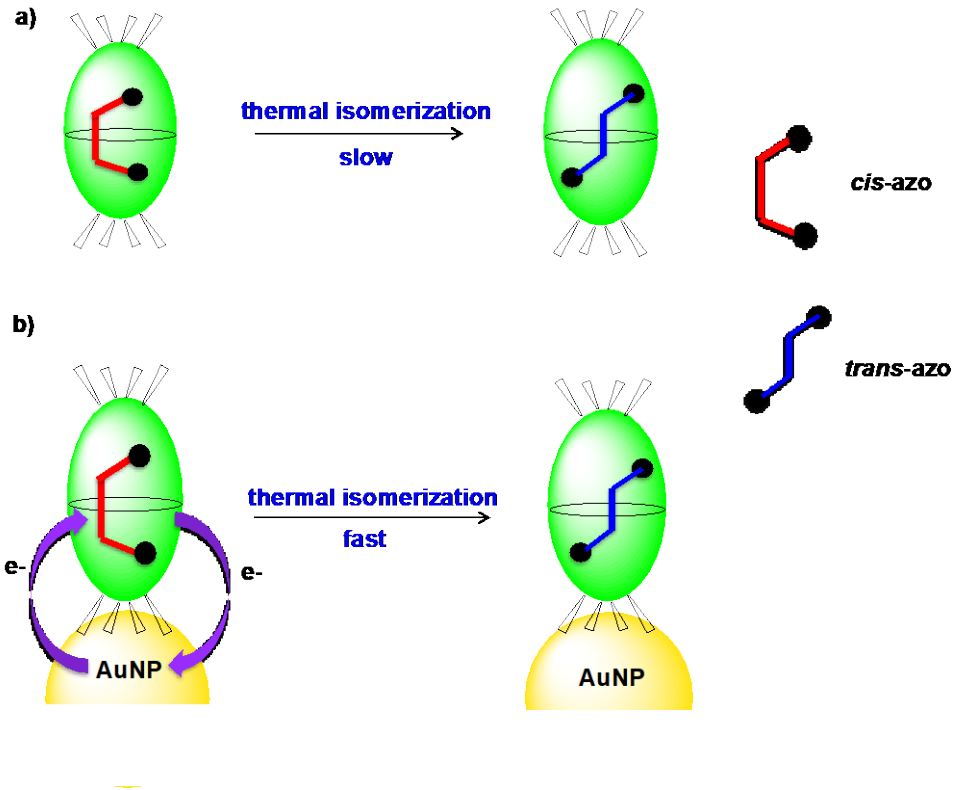

Scheme-3.2 Cartoon representation of thermal isomerization of *cis*-ABs a) with OA and b) with OA in the presence of AuNPs

To probe whether the formation of azobenzene radical cation would enhance the rate of thermal back isomerization, we used N-methylacridinium iodide (NMI) as an electron acceptor. We selectively excited NMI with band pass filter (Corning 7-60, cut off region 320-400 nm) in the presence of *cis*-**3.3**@OA_2 (**Figure 3.22**). We observed isomerization from *cis* to *trans*, suggesting the formation of azobenzene radical cation also induces isomerization. Based on our results, we were not able to unequivocally state

whether ABs act as the electron donor or acceptor with respect to AuNP during thermal catalytic isomerization.

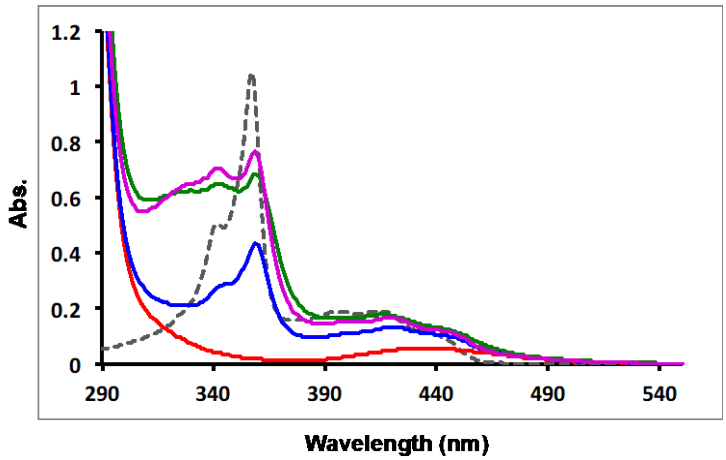

Figure 3.23 UV-Vis spectra establishing N-methylacridinium iodide (NMI) can sensitize the isomerization of *cis*-azobenzene. Absorption spectra of N-methylacridinium iodide (NMI)(grey dashed), *cis*-**3.3**@OA_2 with NMI (blue), *trans*-**3.3**@OA_2 with NMI (purple), *cis*-**3.3**@OA_2 without NMI after UV irradiation (red), *cis*-**3.3**@Owith NMI after UV irradiation (green). ([OA]= 10^{-4} M, [**3.3**] = 5 x 10^{-5} M), [NMI]= 30 uM).

3.3 Conclusion

In this Chapter, we have demonstrated that photoswitchable property of azobenzenes could be observed within OA cavity. This shows that role of confined space in controlling both ground and excited state reactions. We also discussed that small variations in the length of alkyl chain of guest molecules could change the photophysical properties of the encapsulated azobenzenes. We were also able to differentiate the geometrical isomerization of both azobenzene and stilbene inside OA. We could explain the electron transfer process from or to azobenzene is possible without direct contact with metal surface. This opens up new possibility for us to explore electron transfer reactions.

3.4. Experimental section

Materials and Methods

The host Octa acid was synthesized following published procedure.[32] Azobenzene derivatives used in this work were synthesized using the following literature procedure.[87] 4,4'-dimethylstilbene was synthesized following the literature procedure.[36] Metastable (bare) AuNP , citrate-stabilized AuNP also synthesized according to the standard reported procedure[97] as follows.

Synthesis of metastable gold nanoparticles (mAuNp)

135 uL of 30 mM of Gold salt ($HAuCl_4$) was added to 40 mL distilled water and stirred for 5 minutes. Then 100 uL of freshly prepared 0.1M $NaBH_4$ solution was added to the mixture and stirred for 1 h to get purple color solution. Size of the nanoparticle was measured by DLS. UV-Vis spectrum also recorded. About 200 uL of this fresh solution was added to the *cis*-ABs @OA_2 (2 mL).

Synthesis of citrate-capped gold nanoparticles (cAuNp)

Add 20 mL of 1 mM of gold salt into a 50 mL Erlenmeyer flask on a stirring hot plate. Add a magnetic stir bar and bring the solution to rolling boil. To the rapidly stirred boiling solution, quickly add 2 mL of 1% citrate solution. Remove from heat when the solution has turned deep. Size of the nanoparticle was measured by DLS. UV-Vis spectrum also recorded. About 100 uL of this fresh solution was added to the cis-ABs @OA_2(2 mL).

General Procedure for guest binding studies probed by NMR

A D_2O stock solution (600 μL) of host OA (1 mM) and sodium borate buffer (10 mM) taken in a NMR tube was titrated with the guest by sequential addition of 0.25 eq of guest (2.5 μL of a 60 mM solution in $DMSOd_6$). The complexation was achieved by shaking the NMR tube for about five minutes. ^1H NMR spectra were recorded at room temperature under aerated conditions on a Bruker 500 MHz NMR. 1:2 complex was achieved by 5 μL of guest solution to 600 μL of 1 mM OA host in 10 mM buffer. This complexes were irradiated for 30 min with a Luzchem research reactor, UV (Hitachi-FL-8BL-B, 365 nm) and Visible (Luzchem 420).

Sample preparation for the photochemical reactions

600 μL of the complex solution was diluted to 6 mL to give the stock solution. The concentration of host and the guest molecules are [OA = 1 x 10^{-4} M], [guest = 5 x 10^{-5} M] respectively. For UV-Vis studies, the samples were irradiated for 30 min with a Luzchem research reactor, UV(Hitachi-FL-8BL-B, 365 nm) and Visible (Luzchem 420). The irradiated samples were kept in dark for monitoring the thermal isomerization. About 200 uL and 100 uL of freshly prepared metastable AuNP and citrate-capped AuNP were added to the irradiated sample respectively and followed the UV-Vis of thermal isomerization from *cis* to *trans* configuration for all five ABs.

Chapter 4. Role of Confined Space in Controlling the Photoinduced Geometrical isomerization

4.1 Overview

Photochemical *cis-trans* isomerization of olefins is one of the important reactions among organic and bioorganic chemists.[98] Photoinduced geometrical isomerization plays vital role in various biological events, like vision (rhodopsin), photoreceptors (phytochromes) ,triggering ion transport in membranes and negative phototaxis.[98] *Cis-trans* isomerization of stilbenes, polycylic olefins, 1,2-diphenyl cyclopropanes has been studied extensively in last few decades.[99-100] Photoinduced cis-trans isomerization of olefins and its selectivity in solution is entirely different from the confined medium. For instance, cis-retinal isomerizes selectively 100% to all-trans isomer inside confined environment of protein pocket (Opsin), which is responsible for the vision. This kind of selectivity for cis-retinal was not observed in organic solvents.[101-103] In this context, photoinduced isomerization of stilbenes, 1,2-diphenylcyclopranes and polycyclic olefins has been studied in molecular containers such as organic and inorganic hosts, cavitands, zeolites, crystals, and antibodies that mimic the confined biological environment.[104-107] Our group had used molecular container 'Octa acid' to study the geometrical isomerization of stilbenes and 1,4-diaryl-1,3-butadienes.[35, 88, 108] We also used Zeolites to study the photoisomerization of 1,2-diphenylcyclopropanes.[107] In case of stilbenes, position of alkyl groups in stilbenes and their interaction with OA controls their photostationary states. Confinement of 4,4'-dimethylstilbene entirely alters their photostationary states upon irradiation.[88] We explained that trans-isomer is orientated in such a way the CH-π interactions is stronger inside OA capsule. MD simulations studies in the case of 1,4-diaryl-1,3-butadienes showed that cis-isomer is the preferred conformer inside

the OA capsules.[108] Based upon cation-π binding, cis-1,2-diphenylcyclopropane is preferred isomer inside the Zeolites.[107]

In this chapter, we wanted to understand the role of OA cavity deeply in the photoisomerization of stilbenes and diphenylcyclopropanes. The guest molecules were selectively chosen from our experience shown in **Figure 4.1**.

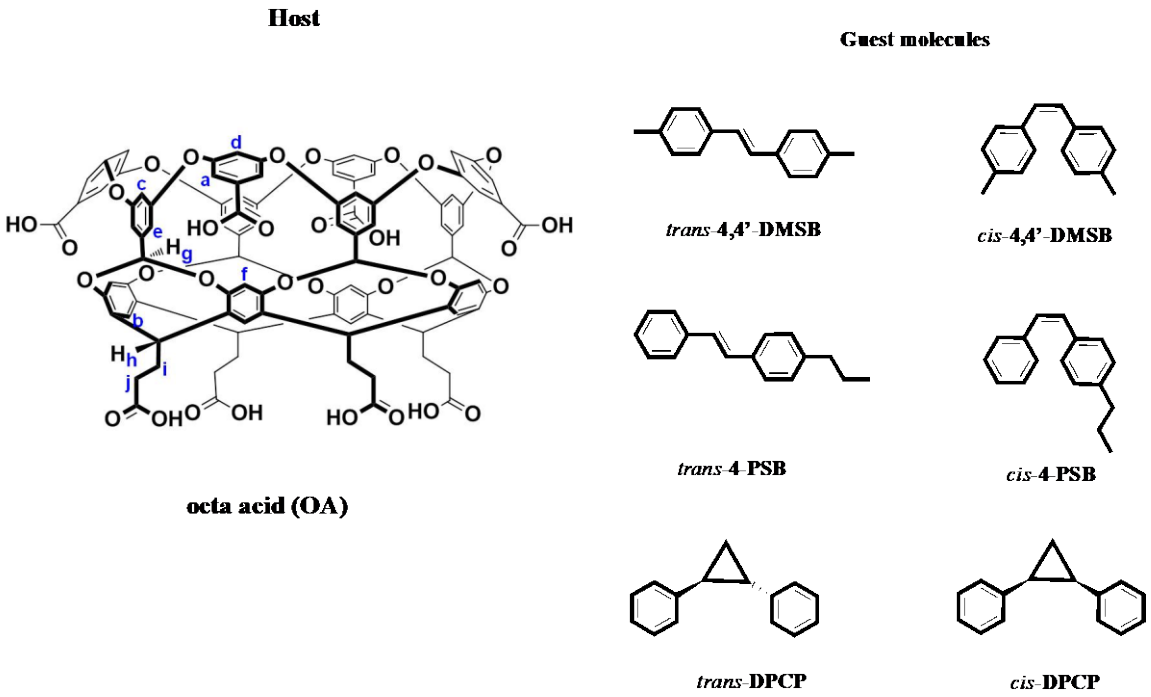

Figure-4.1 Structures of the host and guest molecules used in this study.

4.2 Results and discussion

The guest molecules used in this chapter were synthesized according to the reported literatures.[35, 109] We used ^{1}H NMR technique for the complexation of guest molecules and 2D-DOSY experiments for the type of complexes. We used MD simulation studies to find the stable isomer inside the capsule and its binding energy.

4.2.1 ^{1}H NMR studies for the complexes

Complexes of stilbenes (*cis* and *trans* **4.1-4.2**) with OA were characterized by ^{1}H NMR and 2D-DOSY experiments. Addition of *trans*-4,4'-dimethylstilbene (*trans*-**4.1**) to the OA in borate buffer showed upfield shift of methyl protons around (δ -2.4 ppm), confirmed the complexation of *trans*-**4.1**with OA . It also indicates the position of methyl group is deeper inside the capsule **(Figure 4.2**). Absence of splitting in host OA protons indicates that the *trans*-4,4'-dimethyl stilbene occupies a symmetrical position within the capsular complex making the top and bottom halves identical. When the *cis*-4,4'-dimethylstilbene(*cis*-**4.1)** was added to OA, the methyl proton corresponds to *cis*-**4.1** appears upfield (δ -0.8 ppm) **(Figure 4.3**). This difference in position of methyl protons between *cis* and *trans* isomer, indicates that orientation of trans-isomer is much deeper than cis-isomer. Our group had already established the orientation of stilbene derivatives inside OA using NOESY spectra.[88] 2D-DOSY spectra for above complexes recorded and the diffusion constant values for the complexes are listed in **Table-4.1**.

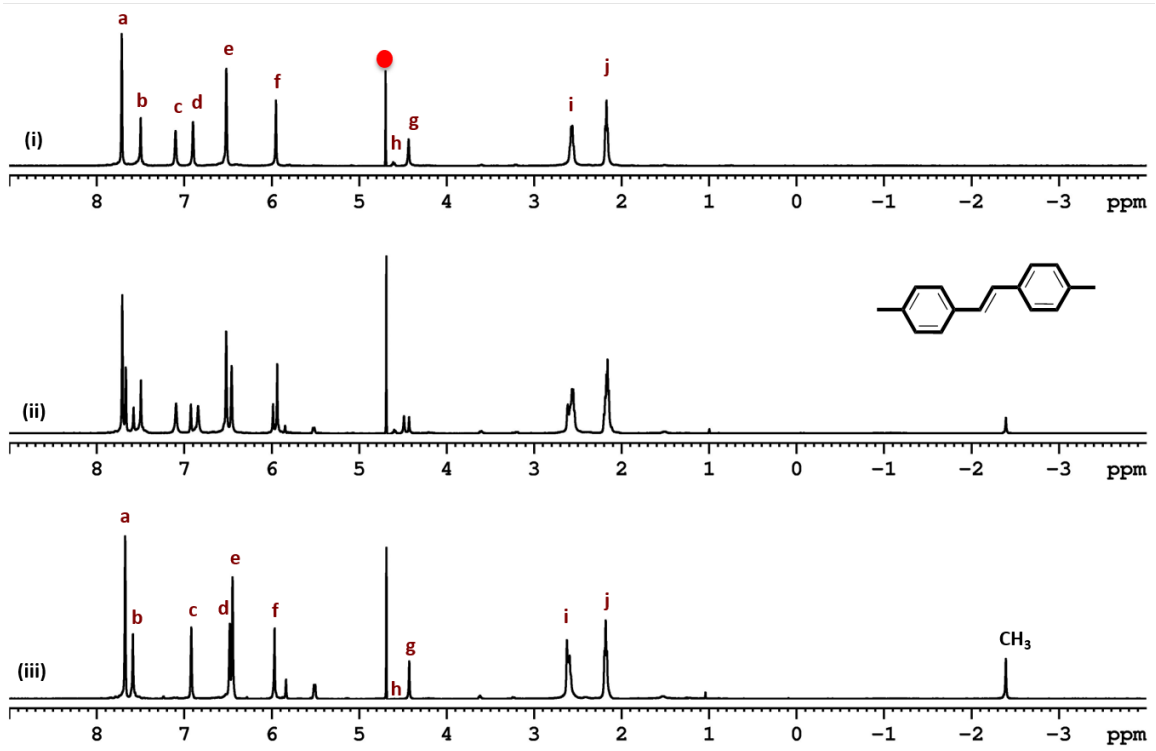

Figure 4.2 ^{1}H NMR (500 MHz) spectra of (i) OA (1 mM) in 10 mM $Na_2B_4O_7$ buffer/D_2O; (ii) ***trans*-4.1**@OA ([OA] = 1 mM), **[***trans*-**4.1**] = 0.25 mM); (iii) ***trans*-4.1** @OA ([OA] = 1 mM), [*trans*-**4.1**] = 0.5 mM); "●"represent the residual D_2O.

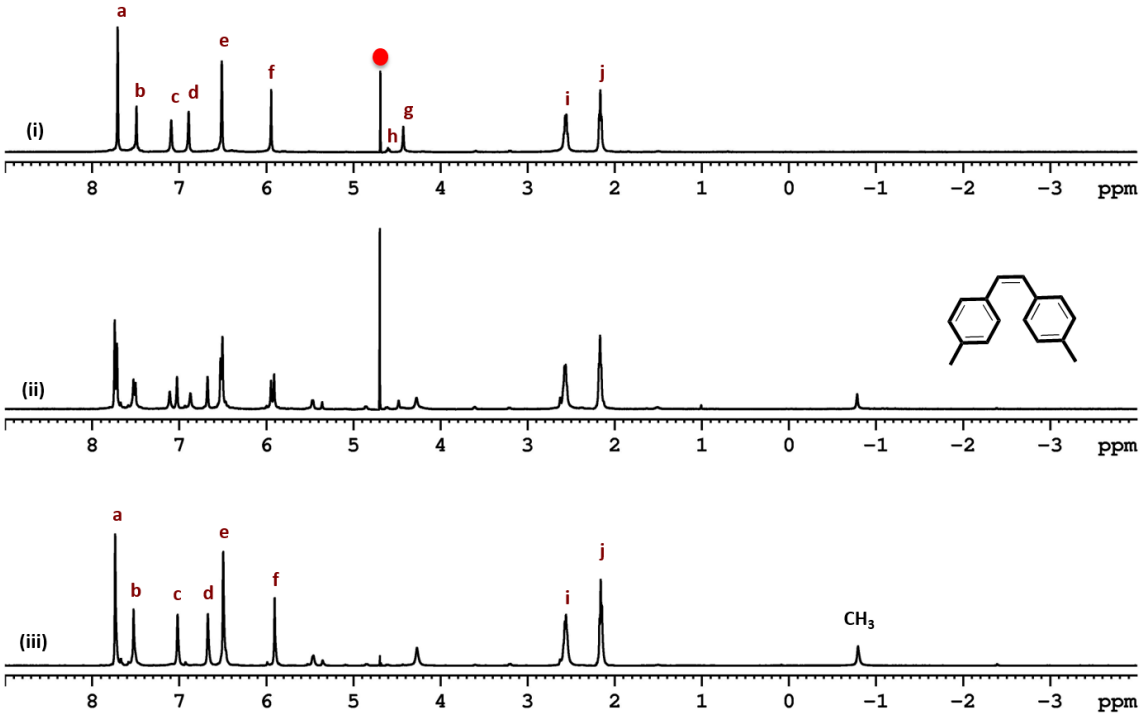

Figure 4.3 ^{1}H NMR (500 MHz) spectra of (i) OA(1 mM) in 10 mM $Na_2B_4O_7$ buffer/D_2O; (ii) ***cis*-4.1**@OA ([OA] = 1 mM), **[***cis*-**4.1**] = 0.25 mM); (iii) ***cis*-4.1**@OA ([OA] = 1 mM), [*cis*-**4.1**] = 0.5 mM); "●"represent the residual D_2O.

^{1}H NMR titration spectra for both *trans* and *cis* isomer of 4-propystilbenes with OA are shown in **Figure 4.4 and 4.5**. **Figure 4.4 and 4.5** showed the upfield shift of alkyl protons, confirmed the encapsulation of *trans*-**4.2** and *cis*-**4.2**. The upfield shift (δ -3.1ppm) for methyl protons indicates that alkyl group reaches the deeper end of the cavity of OA. There is slight difference between *trans* and *cis* propyl protons inside OA capsule.

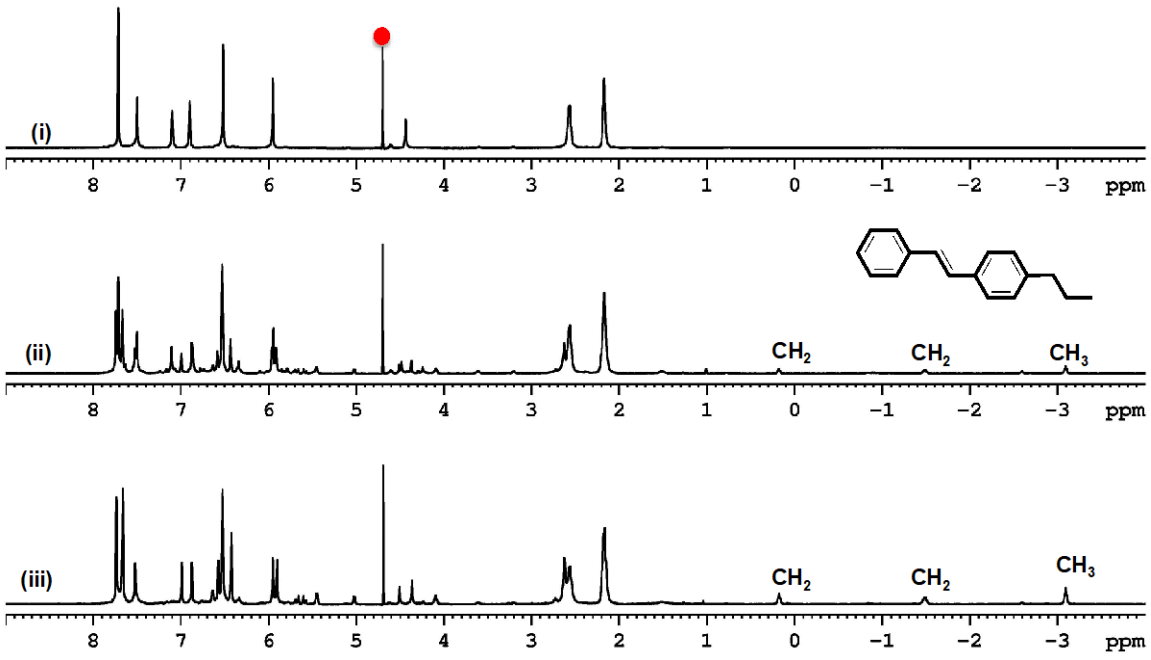

Figure 4.4 ^{1}H NMR (500 MHz) spectra of (i) OA(1 mM) in 10 mM $Na_2B_4O_7$ buffer/D_2O; (ii) ***trans*-4.2**@OA ([OA] = 1 mM), [*trans*-**4.2**] = 0.25 mM); (iii) ***trans*-4.2** @OA ([OA] = 1 mM), [*trans*-**4.2**] = 0.5 mM); "●"represent the residual D_2O.

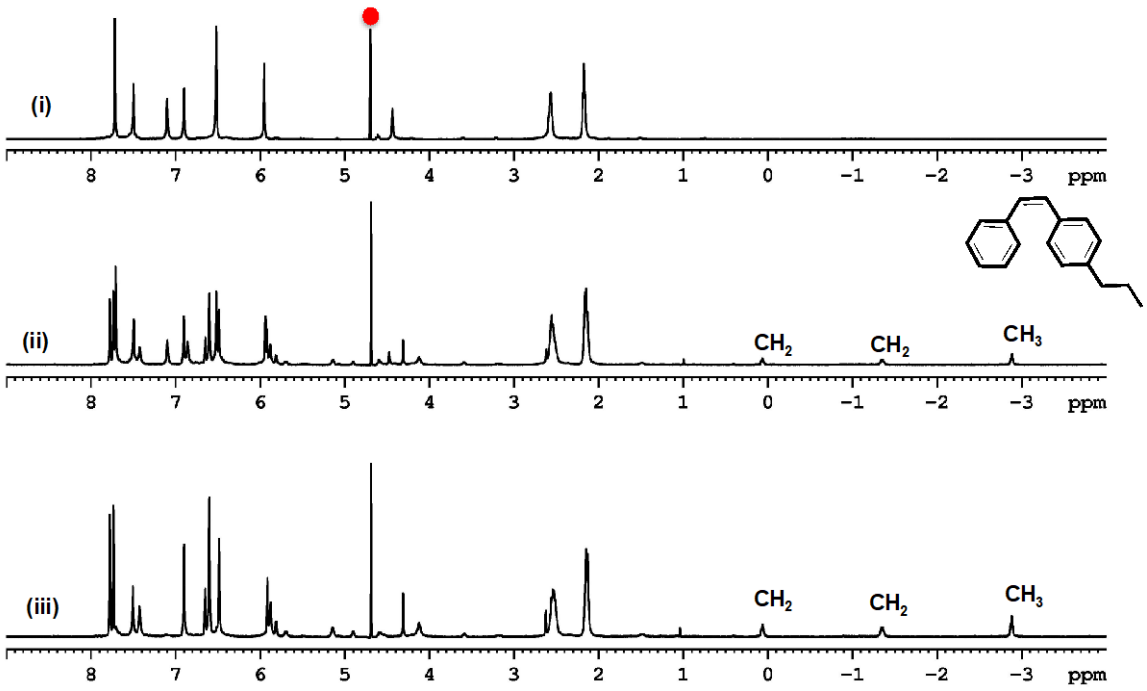

Figure 4.5 ^{1}H NMR (500 MHz) spectra of (i) OA(1 mM) in 10 mM $Na_2B_4O_7$ buffer/D_2O; (ii) ***cis*-2**@OA ([OA] = 1 mM), **[***cis*-**4.2**] = 0.25 mM); (iii) ***cis*-2** @OA ([OA] = 1 mM), [*cis*-**4.2**] = 0.5 mM); "●"represent the residual D_2O.

Complexation of *trans* and *cis* 1,2-diphenylcyclopropanes (DPCP) with OA are shown in **Figure 4.6 and 4.7.** The –CH_2 protons of the cyclopropyl ring appears between (δ 1.0 and 0.0 ppm), which is not shifted upfield like stilbene molecules. This shows that cyclopropyl ring located in the middle region of the two cavitand of OA. The broadening of the peaks is due to the weak complexation of the *cis*-**4.3** with OA. However, spectra corresponding to *trans* **4.3** with OA showed sharp triplet peaks in the region around δ 1.0 and 0.0 ppm with slight shift. The host OA protons are also sharp and shifted indicates the stronger complexation of *trans*-**4.3** with OA. There are some peaks corresponding to encapsulated *cis* isomer also seen, because of the less purity of the *trans* isomer. Partial NMR spectra for all the guest shown in **Figure 4.8**, where we could see the distinctive peaks corresponding to both *cis* and *trans* isomer of all the complexes. The diffusion constant

values for all the complexes are listed in **Table-4.1.** The values showed that all the guest molecules forms 1:2 (guest:host) complex with OA.

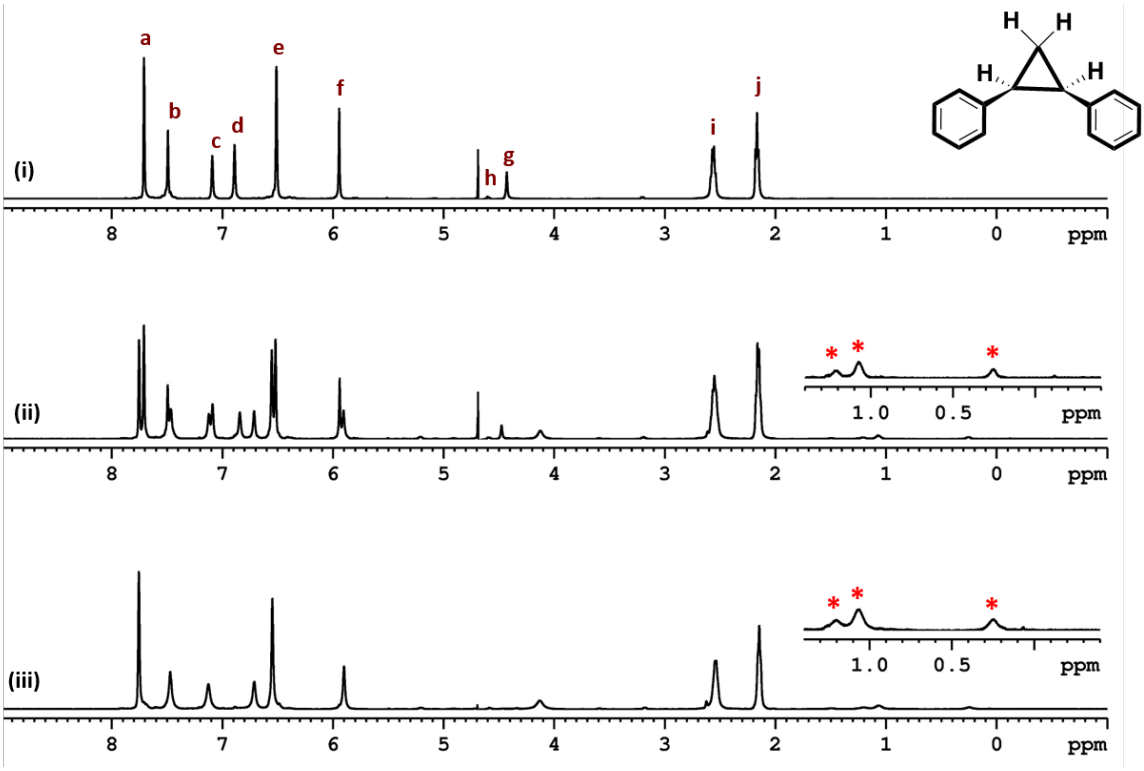

Figure 4.6 ^{1}H NMR (500 MHz) spectra of (i) OA(1 mM) in 10 mM $Na_2B_4O_7$ buffer/D_2O; (ii) ***cis-4.3***@OA ([OA] = 1 mM), [*cis*-**4.3**] = 0.25 mM); (iii) ***cis-4.3*** @OA ([OA] = 1 mM), [*cis*-**4.3**] = 0.5 mM); "*" represent the bound protons of the ***cis-4.3***.

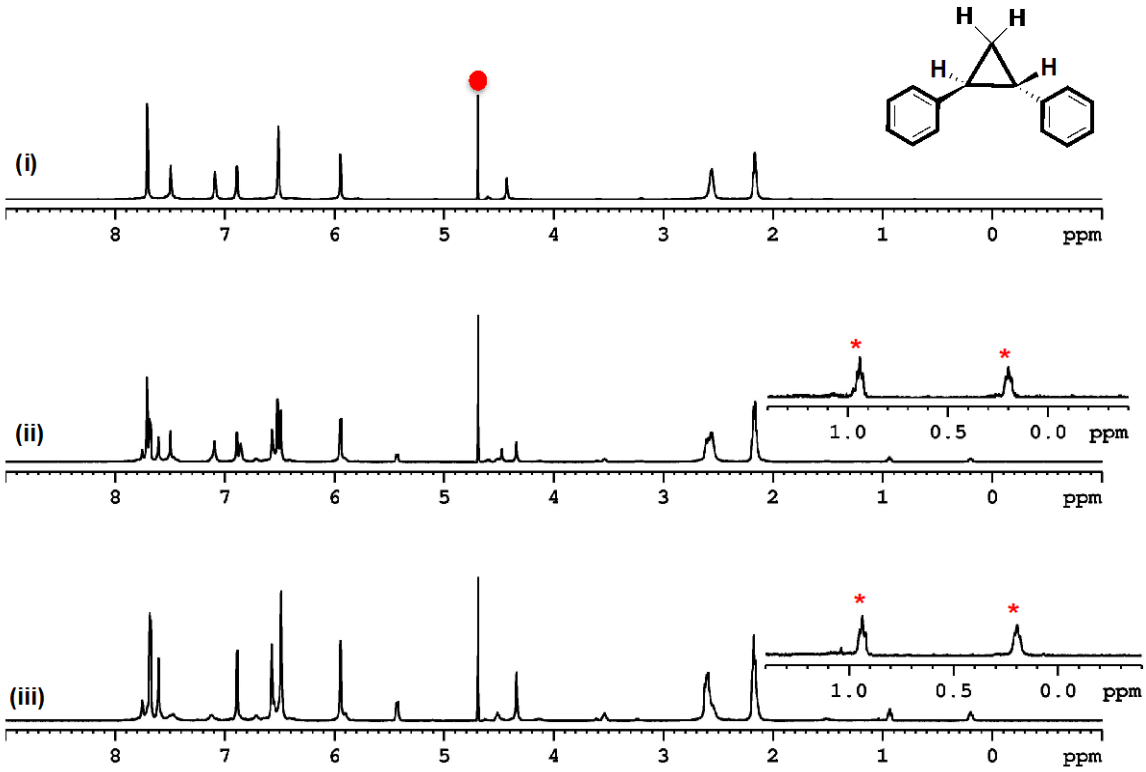

Figure 4.7 ^{1}H NMR (500 MHz) spectra of (i) OA(1 mM) in 10 mM $Na_2B_4O_7$ buffer/D_2O; (ii) ***trans-4.3***@OA ([OA] = 1 mM), **[***trans*-**4.3**] = 0.25 mM); (iii) ***trans-4.3***@OA ([OA] = 1 mM), [*trans*-**4.3**] = 0.5 mM); "*" represent the bound protons of the ***trans*-4.3** and"●"represent the residual D_2O.

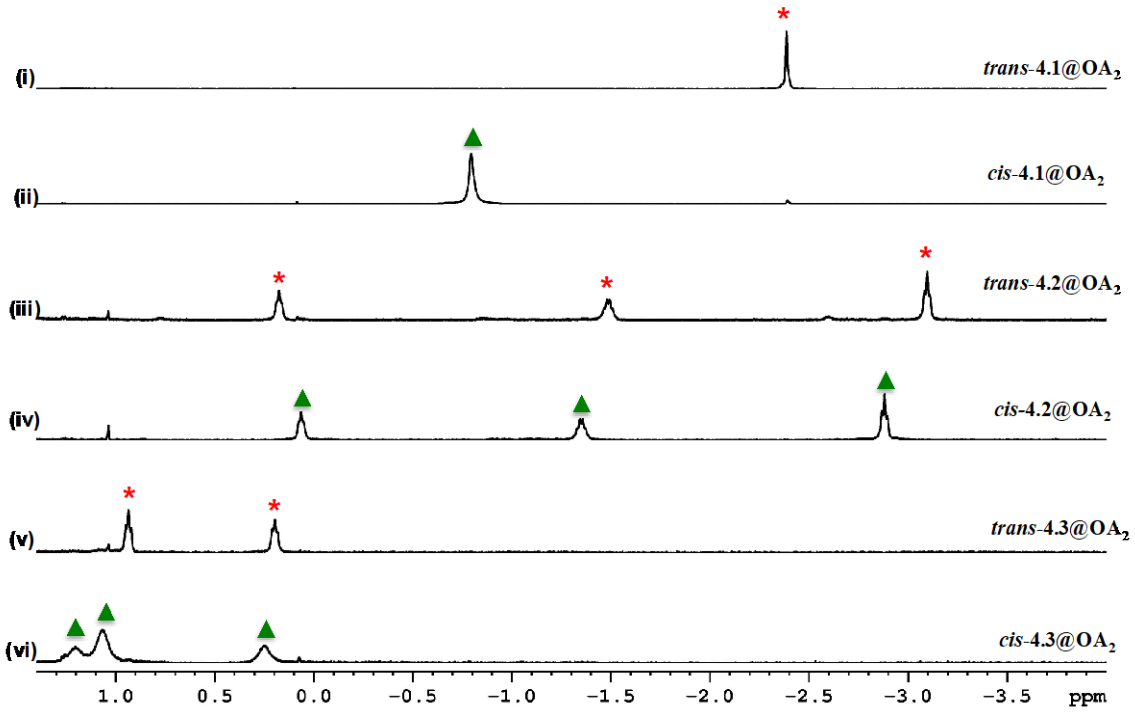

Figure 4.8 Partial ^{1}H NMR (500 MHz) spectra of (i) 1: 2 complex of ***trans*-4.1**@OA_2 ;(ii) 1: 2 complex of ***cis*-4.1**@OA_2; (iii) 1: 2 complex of ***trans*-4.2**@OA_2 ;(iv) 1: 2 complex of ***cis*-4.2**@OA_2 ; (v) 1: 2 complex of ***trans*-4.3**@OA_2 ;(vi) 1: 2 complex of ***cis*-4.3**@OA_2. "*" represent the bound protons of trans isomers and " " ▲ represent the bound protons of cis isomers.

Compound	Diffusion constant (cm^2/s)
Only OA	1.88×10^{-6}
***trans*-4.1**@OA_2	1.27×10^{-6}
***cis*-4.1**@OA_2	1.39×10^{-6}
***trans*-4.2**@OA_2	1.37×10^{-6}
***cis*-4.2**@OA_2	1.30×10^{-6}
***trans*-4.3**@OA_2	1.36×10^{-6}
***cis*-4.4**@OA_2	1.45×10^{-6}

Table 4.1. Diffusion constant of complexes of guest molecules with OA by 2D-DOSY NMR.

4.2.2 Competitive NMR studies of the guest molecules

We wanted to check whether the *cis* or *trans* isomer of the guest molecules form stronger complex with OA using NMR techniques. We recorded the NMR of the spectra of the *trans*-isomer@OA_2 of the complex and we added the *cis*-isomer from the stock solution to the *trans*-isomer@OA_2 complex. The above mixture was sonicated and the NMR was recorded again. We also did the same procedure for *cis*-complexes by taking *cis*-isomer@OA_2 and adding the *trans*-isomer to the complex. We observed very interesting results for our complexes. More stable isomer forms stronger complex with OA by displacing the less stable isomer without depending on the mode of addition of *cis* and *trans* isomer to OA. In case of 4,4-dimethylstilbene, gradual addition of *trans*-**4.1** to the *cis*-**4.1**@OA_2 complex slowly displaces the *cis*-**4.1** from the OA capsule and form stronger complex with OA (**Figure 4.9**). **Figure 4.9** shows the disappearance of cis-peaks and appearance of sharp trans-peaks with gradual addition of *trans*-**4.1.** But addition of *cis*-**4.1** to the *trans*-**4.1**@OA_2 complex did not displace the *trans*-**4.1 (Figure 4.10).** This observation clearly confirmed *trans*-4,4'-dimethyl stilbene is the preferable isomer inside OA capsule.

In case of 4-propylstilbene, gradual addition of *trans*-**4.2** to the *cis*-**4.2**@OA_2 did not displace the c*is*-**4.2** (**Figure 4.11**). On the contrary, gradual addition of c*is*-**4.2** to the *trans*-**4.2**@OA_2 complex displaces the *trans*-**4.2** (**Figure 4.12**). This shows that cis-4-propylstilbene is the preferred isomer inside OA than trans isomer. In case of 1,2-diphenylcyclopropane, *trans*-**4.3** displaces c*is*-**4.3** from the complex *cis*-**4.3**@OA_2, but c*is*-**4.3** could not displace *trans*-**4.3**@OA_2 (**Figure 4.13 & 4.14**). This indicates that *trans*-**4.3** is the preferable inside OA capsule than corresponding *cis* isomer.

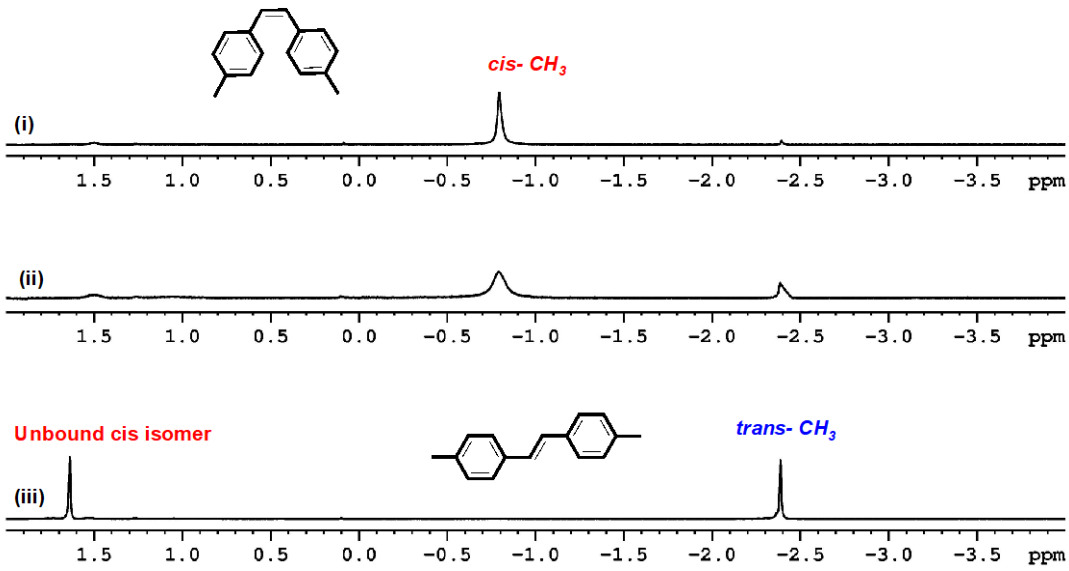

Figure 4.9 Competition experiments between *cis* and *trans* isomers of **4.1** towards OA capsule. Partial ^{1}H NMR (500 MHz) spectra of (i) 1: 2 complex of ***cis*-4.1**@OA_2; (ii) upon addition of 0.25 equiv. of ***trans*-4.1** to (i); (iii) upon addition of 0.5 equiv. of ***trans*-4.1** to (i).

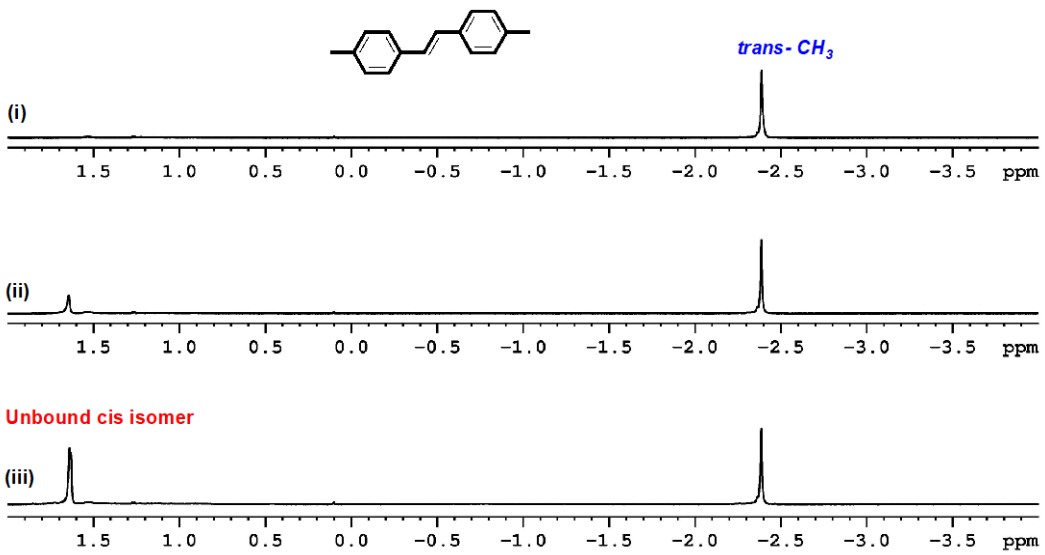

Figure 4.10 Competition experiments between *cis* and *trans* isomers of **4.1** towards OA capsule. Partial ^{1}H NMR (500 MHz) spectra of (i) 1: 2 complex of ***trans*-4.1**@OA_2; (ii) upon addition of 0.25 equiv. of ***cis*-4.1** to (i); (iii) upon addition of 0.5 equiv. of ***cis*-4.1** to (i).

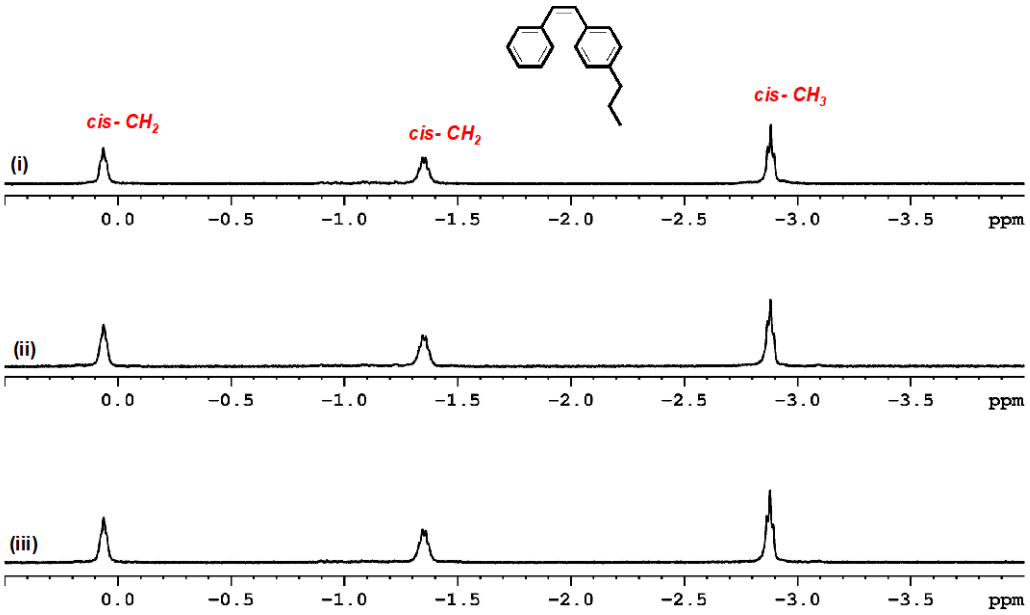

Figure 4.11. Competition experiments between *cis* and *trans* isomers of **4.2** towards OA capsule. Partial ^{1}H NMR (500 MHz) spectra of (i) 1: 2 complex of ***cis*-4.2** @OA_2; (ii) upon addition of 0.25 equiv. of ***trans*-4.2** to (i); (iii) upon addition of 0.5 equiv. of ***trans*-4.2** to (i).

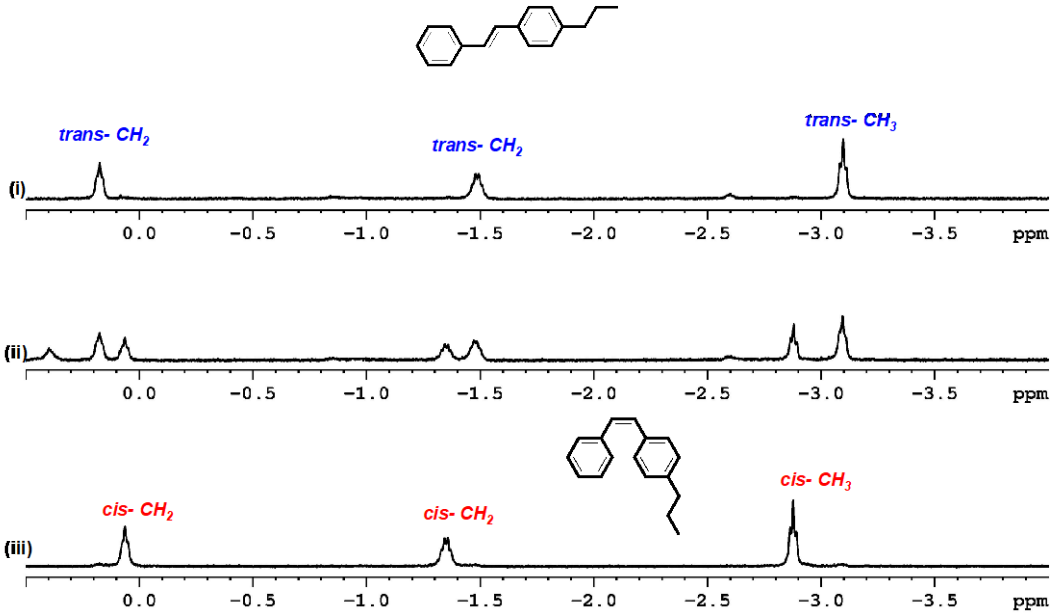

Figure 4.12 Competition experiments between *cis* and *trans* isomers of **4.2** towards OA capsule. Partial ^{1}H NMR (500 MHz) spectra of (i) 1: 2 complex of ***trans*-4.2** @OA_2; (ii) upon addition of 0.25 equiv. of ***cis*-4.2** to (i); (iii) upon addition of 0.5 equiv. of ***cis*-4.2** to (i).

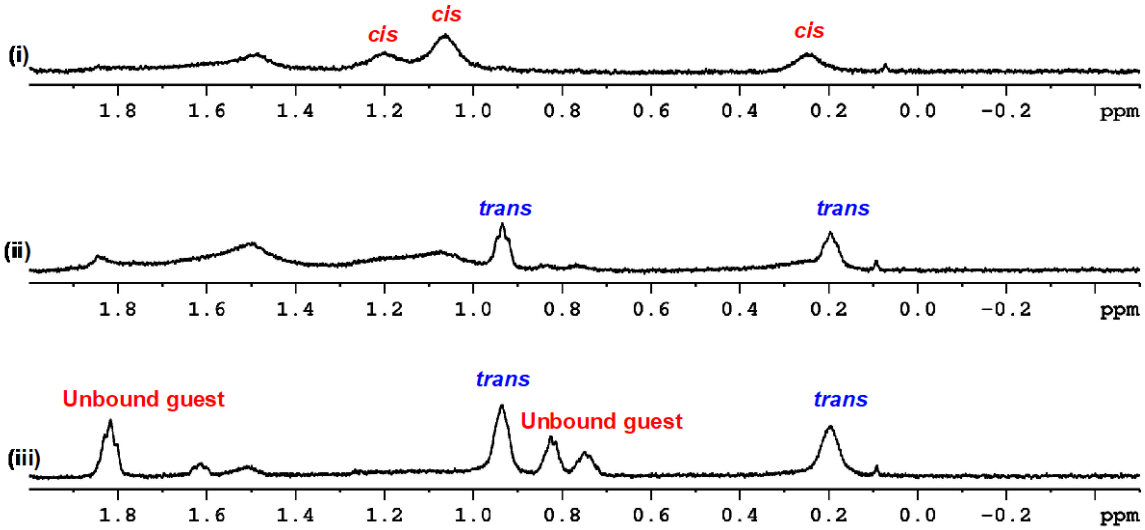

Figure 4.13 Competition experiments between *cis* and *trans* isomers of **4.3** towards OA capsule. Partial ^{1}H NMR (500 MHz) spectra of (i) 1: 2 complex of ***cis*-4.3**@OA_2; (ii) upon addition of 0.25 equiv. of ***trans*-4.3** to (i); (iii) upon addition of 0.5 equiv. of ***trans*-4.3** to (i).

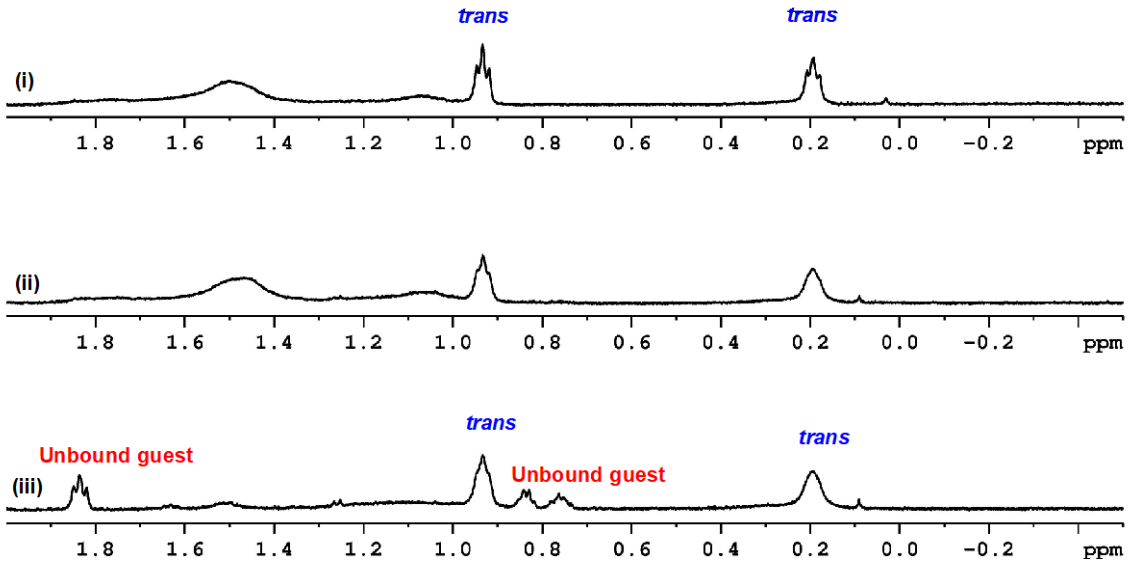

Figure 4.14 Competition experiments between *cis* and *trans* isomers of **4.3** towards OA capsule. Partial ^{1}H NMR (500 MHz) spectra of (i) 1: 2 complex of ***trans*-4.3** @OA_2; (ii) upon addition of 0.25 equiv. of ***cis*-4.3** to (i); (iii) upon addition of 0.5 equiv. of ***cis*-4.3** to (i).

To confirm our observation from NMR studies, we also did molecular modeling with the collaboration with Prof. Rajeev Prabhakar. Molecular models for the most preferable isomer within OA for all the guest molecules were shown in **Figure 4.15**. The binding energy for the host:guest complexes were calculated and listed in the **Table-4.2.**

S.No	**Compound**	**Binding Free Energy (KJ/mol)**	
		***cis*@OA$_2$**	***trans*@OA$_2$**
1	4,4'-dimethylstilbene	-196.3	-215.4
2	4-propylstilbene	-212.0	-148.3
3	1,2-diphenylcyclopropane	-85.3	-98.8

Table-4.2 Binding energy of the complexes of *cis* and *trans* isomer with OA.

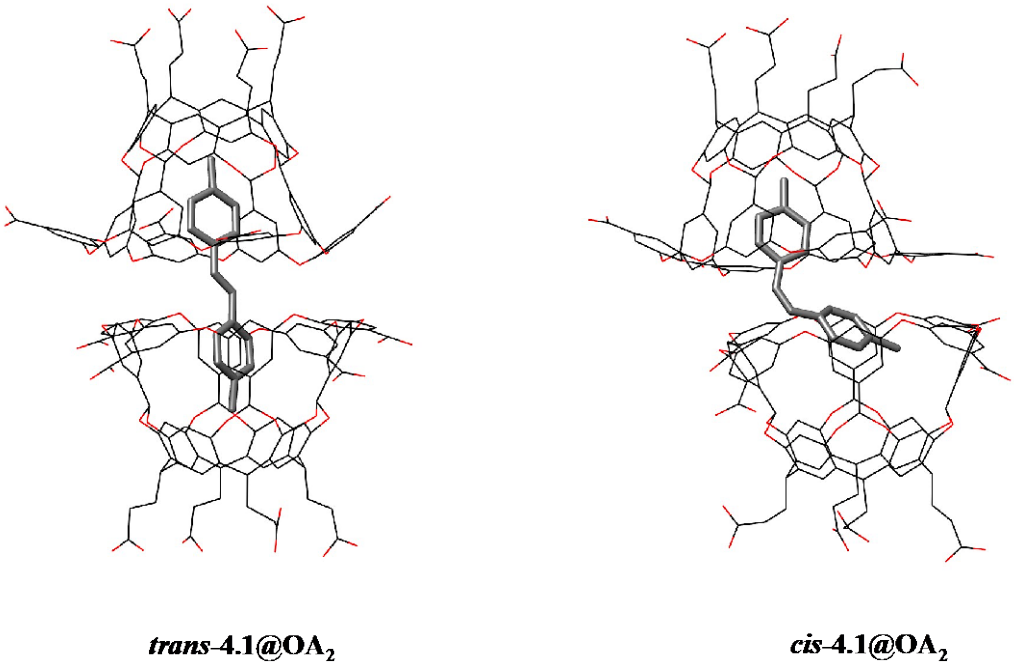

Figure 4.15 Most representative structures of *trans*-**4.1**@OA_2 and *cis*-**4.1**@OA_2 obtained from MD simulations.

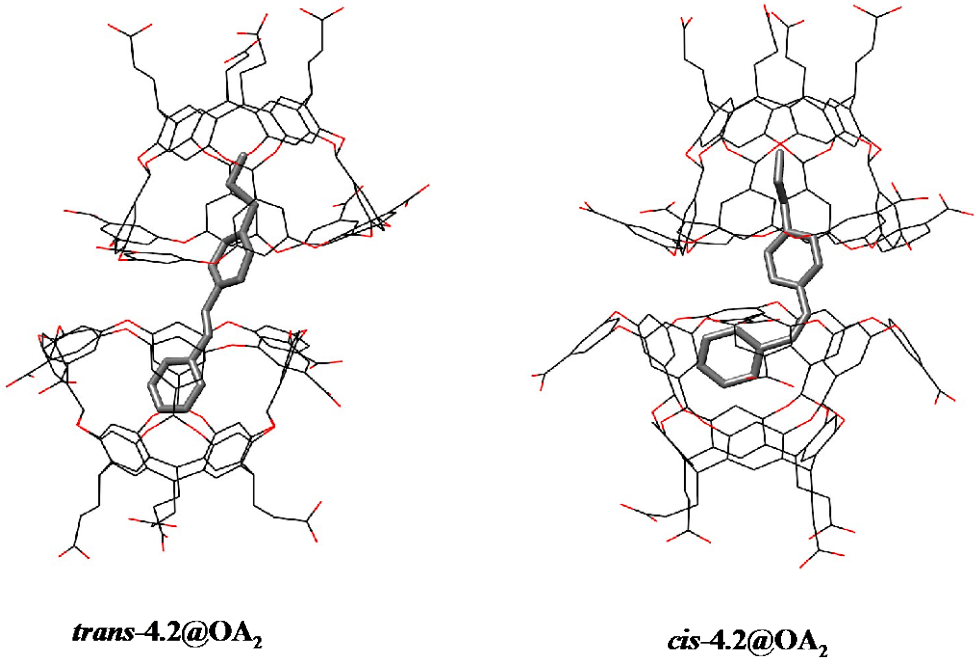

Figure 4.16 Most representative structures of *trans*-**4.2**@OA_2 and *cis*-**4.2**@OA_2 obtained from MD simulations.

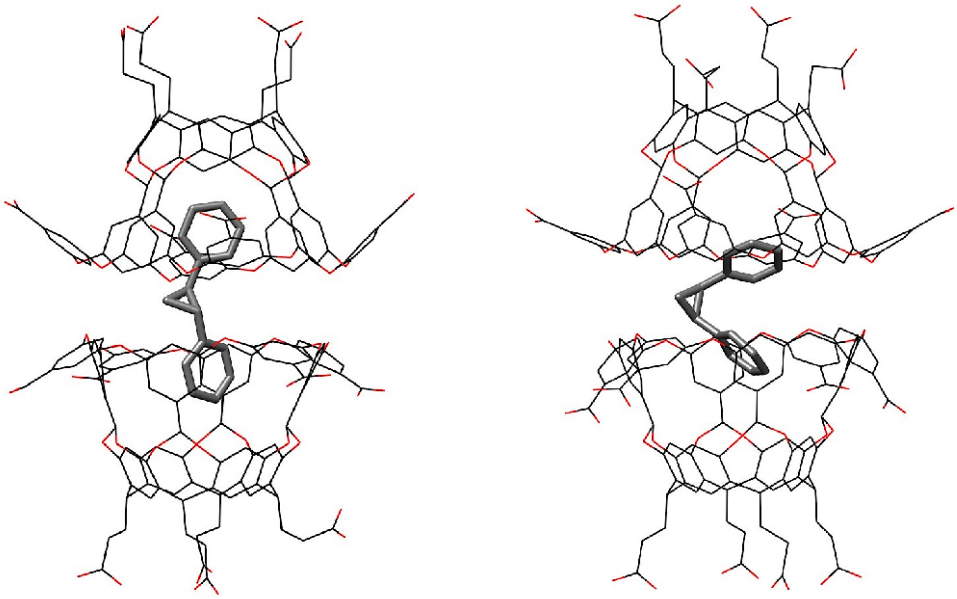

Figure 4.17. Most representative structures of *trans*-**4.3**@OA_2 and *cis*-**4.3**@OA_2 obtained from MD simulations.

From the MD stimulation results and from the **Table 4.2,** we concluded that *trans* **4.1** isomer is the preferred isomer than *cis* **4.1**, *cis* **4.2** is the preferred structure than *trans* **4.2** and *trans* **4.3** is the preferred isomer than *cis* **4.3** inside the OA capsule.

4.2.3 Photophysical results

The photoisomerization of stilbene has been studied for more than 50 years. Trans-stilbene is thermodynamically more stable than *cis*-isomer. The photoisomerization of stilbene can occur either by direct irradiation (via excited singlet state) or by triplet sensitization (via excited triplet state).[99] The potential energy diagram for stilbene photoisomerization is shown in **Figure 4.19**. Similarly, the photoisomerization of 1,2-diphenylcyclopropane (DPCP) also can also occur either by direct irradiation or by triplet sensitization.[100] The PE diagram for DPCP photoisomerization is shown in **Figure 4.20.**

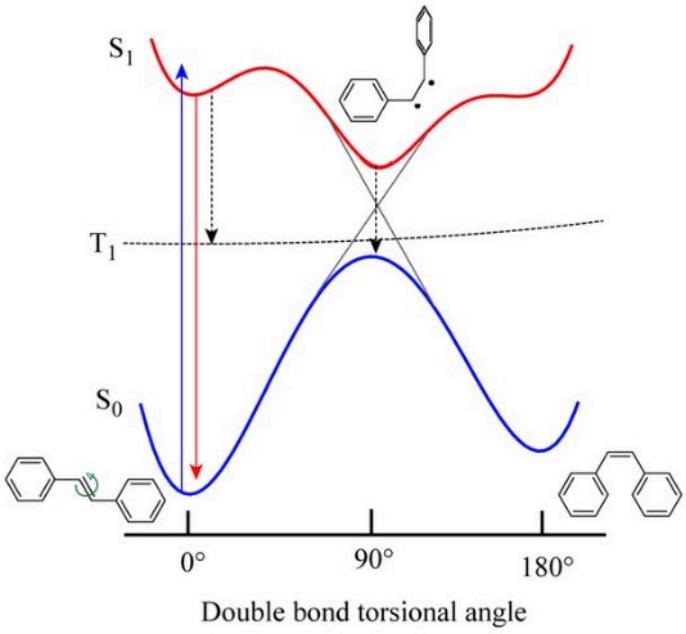

Figure 4.19 Potential energy diagram of photoisomerization of stilbene.

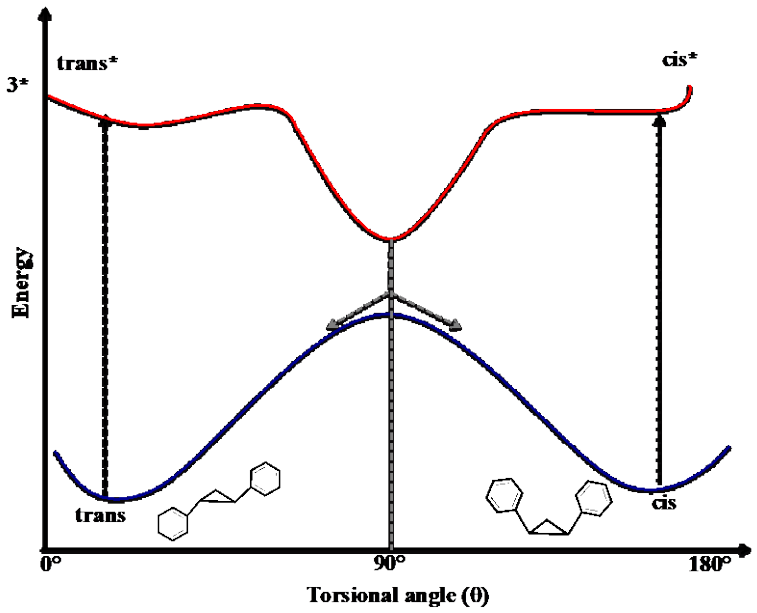

Figure 4.20 Potential energy diagram of photoisomerization of 1,2diphenylcyclopropane.

Photoisomerization of stilbenes was monitored by NMR spectra by irradiating the complex using UV light (>310 nm using cut-off filter). The cut-off filter (0-52) is used to avoid direct excitation of OA (**Figure-4.21**).[88] Photostationary states (PSS) were calculated based on NMR data and listed in **Table 4.3**. PSS in solution also recorded for comparison. *cis*-**4.1**@OA_2 upon irradiation reaches PSS consisting of 80% *trans* and 20% *cis* isomer very quickly. On the other hand, when we irradiate *trans*-**4.1**@OA_2, PSS contains 80% *trans* and 20% *cis* isomer. In case of 4,4'-dimethylstilbene, trans-isomer did not reach the PSS due to restricted rotation inside the capsule, but *cis* isomer reaches expected PSS without any problem. This suggested that confined space of OA plays a vital role in controlling the excited state behavior of the guest molecule. When we irradiated the propyl derivative, the situation is entirely different. *trans*-**4.2**@OA_2 upon UV irradiation isomerized to 97% *cis* isomer quickly inside OA capsule. However, when we irradiate *cis*-**4.2**@OA_2, *cis* isomer did not isomerize to *trans* isomer. PSS reaches 97% *cis*: 3% *trans* and did not change even

after prolonged irradiation. We think that the orientation of *cis*-4-propylstilbene inside OA which hinders the photoisomerization.

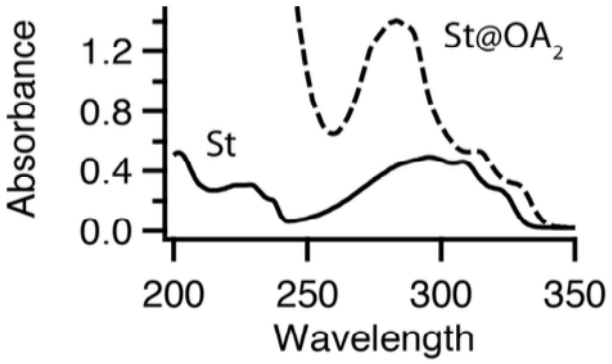

Figure 4.21 Absorption spectra of stilbene@OA_2 (dashed) in borate buffer and stilbene in cyclohexane (thick).

We induced photoisomerization of 1,2-diphenylcylcopropane using triplet sensitization. Since DPCP@OA_2 absorption overlaps with OA absorption (**Figure 4.22**), we irradiate OA by using UV light (> 290 nm) using pyrex NMR tube. In our group, we have already established OA capsule can be used as triplet sensitizer because of its lower triplet energy (73 kcal/mol) and we observed triplet-sensitized reaction of benznorboradiene inside the capsule itself.[110] Since triplet energy of DPCP is about 60 kcal/mol, OA seems to be perfect triplet sensitizer for photoisomerization reaction. When we irradiate *cis*-**4.3**@OA_2 complex under UV light (> 290 nm), we observed photoisomerization of *cis* to *trans* isomer (**Figure 4.23**). But when we irradiate the *trans*-**4.3**@OA_2 we did not observe the isomerization of *trans* to *cis* **(Figure 4.24)**. The photostationary state (90% *cis* and 10% *trans*) was obtained. But when we did the photoirradiation in the solvent using p-methoxyacetophenone as triplet sensitizer, we got 45% *cis* and 55% *trans* (**Table-4.3**). This indicates, that confined space of OA controls the photochemistry of the guest molecules in the excited states.

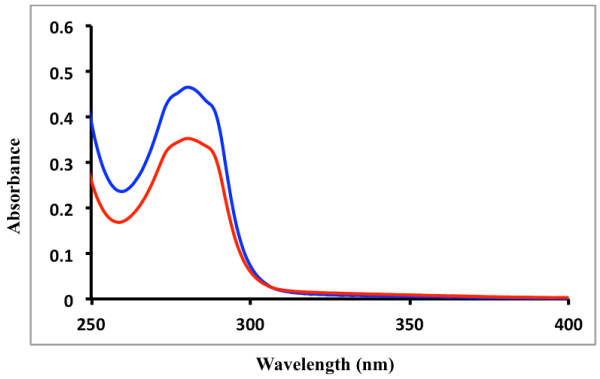

Figure 4.22 Absorption spectra of cis-4.3@OA_2 (blue) and OA cavitand (red) in borate buffer.

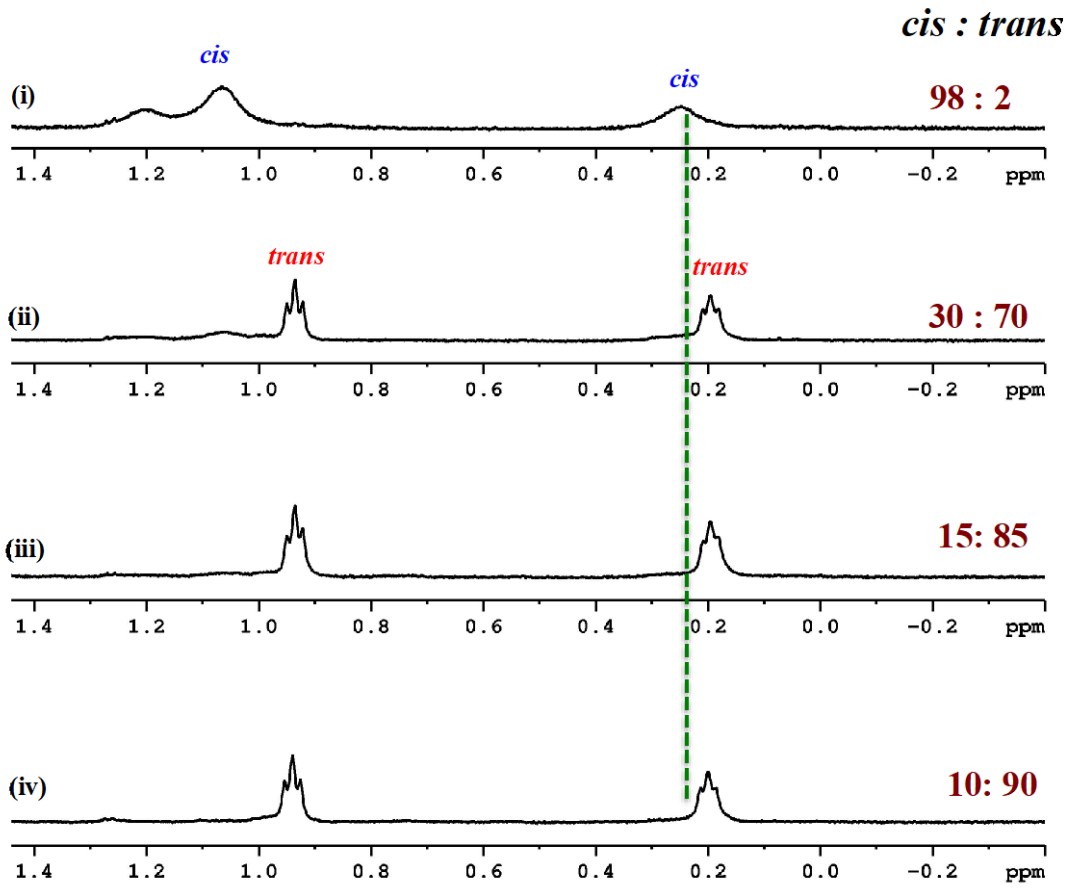

Figure 4.23 Partial ^{1}H NMR (500 MHz) spectra of (i) 1: 2 complex of ***cis*-4.3** @OA_2 before irradiation; (ii) after 2 hour irradiation; (iii) after 5 hour irradiation ; (iv) after 8 hour irradiation (irradiation wavelength > 290 nm).

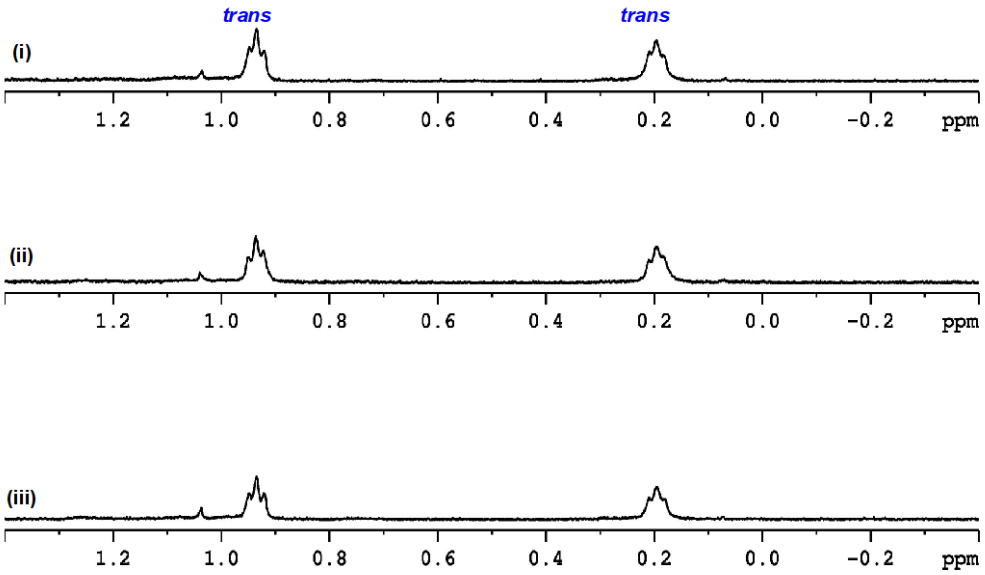

Figure 4.24 Partial ^{1}H NMR (500 MHz) spectra of (i) 1: 2 complex of ***trans*-4.3** @OA_2 before irradiation; (ii) after 2 hour irradiation; (iii) after 5 hour irradiation(irradiation wavelength > 290 nm).

S.No	Compound	Solution	OA
		trans : cis	***trans : cis***
1	4,4'-dimethylstilbene	20 : 80	80 : 20
2	4-propylstilbene	15 : 85	3 : 97
3.	1,2-diphenylcyclopropane	55 : 45	90 : 10

Table-4.3 Photostationary state of guest molecules in solution and inside OA capsule (values quantified by NMR)

4.3. Conclusion

In summary, the role of confined space of OA on photoisomerization of stilbenes and 1,2-diphenylcyclopropane was discussed in this chapter. NMR techniques were used as tool to understand the complexation and the dynamics of guest within the complex. We have established that PSS depends on the interactions of the guest with walls of the cavitand and available free volume for the encapsulated guest. The change of alkyl group at para position entirely changed the photochemistry of the encapsulated stilbenes. We are doing ultrafast studies with collaboration with Prof. Chris Elles (University of Kansas) to understand the excited state dynamics of stilbene derivatives with OA in detail.

4.4. Experimental section

Materials and Methods

The host Octa acid was synthesized following published procedure.[32] *Cis* and *trans* isomers of 4,4'-dimethylstilbene (**4.1**), 4-propylstilbene (**4.2**) and 1,2-diphenylcyclopropane (**4.3**) were synthesized and characterized by reported procedure.[88, 109]

General Procedure for guest binding studies probed by NMR

A D_2O stock solution (600 μL) of host OA (1 mM) and sodium borate buffer (10 mM) taken in a NMR tube was titrated with the guest by sequential addition of 0.25 eq of guest (2.5 μL of a 60 mM solution in $DMSOd_6$). The complexation was achieved by shaking the NMR tube for about five minutes. ^1H NMR spectra were recorded at room temperature under aerated conditions on a Bruker 500 MHz NMR. 1:2 complex was achieved by 5 μL of guest solution to 600 μL of 1 mM OA host in 10 mM buffer. Competition studies were done by taking *cis* isomer complex in NMR tube and added slowly the *trans* isomer and recorded NMR spectra and vice versa.

Photoirradiation of the complex

1mM concentration of the host-guest complexes (2:1) prepared as above mentioned procedure. The NMR tube was kept in UV-reactor and irradiated using 450 W medium pressum Hg lamp kept in a Pyrex jacket. Cut off filter (0-54) used to irradiate the stilbene complexes.

Molecular Simulations procedure

MD simulations were performed using the following multistep strategy. In the first step, a three-dimensional structure of OA was taken from out previous work[111] and optimized using the Gaussian09 program.[112] The guests were modeled using the Gaussview program package and were optimized without any geometrical constraint by using Gaussian09 program. Antechamber, an inbuilt tool in Amber, was used in the calculation of RESP charges and making topology files.[113] Autodock Vina 1.5.6 software was used to perform molecular docking to investigate the binding of Guest to OA.[114] The size of the grid was chosen to cover the OA, and the spacing was kept to 1.00 Å which is a standard value for Autodock Vina. The molecular dynamics (MD) simulations of OA with Guest were performed using the GROMACS[115] program utilizing the AMBER03[116] force field. The starting structures were placed in a cubic box with dimensions of 60 × 60 × 60 Å. The box was filled with TIP3P water molecules.[117] In the next step, some of the water molecules were replaced by Na and Cl ions to neutralize the system and to maintain the physiological ion concentration (154 mM) of the system. Before running the structures for MD, they were energy minimized for 3000 steps. The results of these minimization produced the starting structures for the MD simulations. All the MD simulations were performed for 100 ns. The MD simulations were carried out with a constant number of particles (N), pressure

(P), and temperature (T) (NPT ensemble). The bond lengths and angles of the water molecules, were constrained by SETTLE[118] algorithm and LINCS[119] algorithm was used to constrain the bond lengths of the OA. Particle-Mesh Ewald (PME) method was used to calculate the long-range electrostatic interactions. The MD trajectories were computed for each model with a time step of 2 fs. Cluster analysis was performed to derive the most representative structures of the OA. Yasara[120] and Chimera[121] programs were used for visualization and for the preparation of the structural diagrams presented in this study.

Chapter 5. Ultrafast Electron Transfer from Upper Excited State of Encapsulated Azulenes to Acceptors across an Organic Molecular Wall

5.1 Overview

Nature inspires lot of scientists for their innovation. Plants produce energy using sunlight (photosynthesis) in which electron and energy transfer process constitute main reactions. Photoinduced electron transfer (PET) from a donor to acceptor is widely studied to mimic the natural photosynthetic center for solar energy conversion. PET process has been studied extensively by various groups in the area of visible light photocatalysis, dye-sensitized solar cell.[122-124] One of the main drawbacks in PET process is the back-electron transfer (BET) from acceptor to donor molecule in the system. In the natural photosynthetic system, the electron transfer occurs via cascades of donor and acceptor units to avoid BET. Many efforts have been made to circumvent the BET process. Our group has studied the PET process by encapsulating the donor molecule inside a capsule and the acceptor in the proximity of the capsule to slow down the BET process.[36, 125] We have already established that the PET process could be occurred from the donor inside the capsule to acceptor outside across the wall.[36] Azulene known to exhibit fluorescence from higher electronic state S_2 violating Kasha's rule.[126] Azulene derivatives have been studied in energy and electron transfer reactions.[127-128] This unique behavior of azulene led us to investigate their electron donating capability within confined space. In this chapter, we will discuss the photoinduced electron transfer from upper excited state of azulene derivatives to various acceptors through a molecular wall.

5.2 Results and discussion

In this work, we chose Azulene(Az) and Guaiazulene(GAz) as electron donors. Methyl viologen (MV^{2+}), N-methylpyridinium iodide ($MePy^{+}$) and Pyridinium trifluoromethane sulfonate (Py^{+}) and TiO_2 were chosen as acceptors. Octa acid (OA) was used as host and Cucurbit[7]uril (CB[7]) as competitive host.

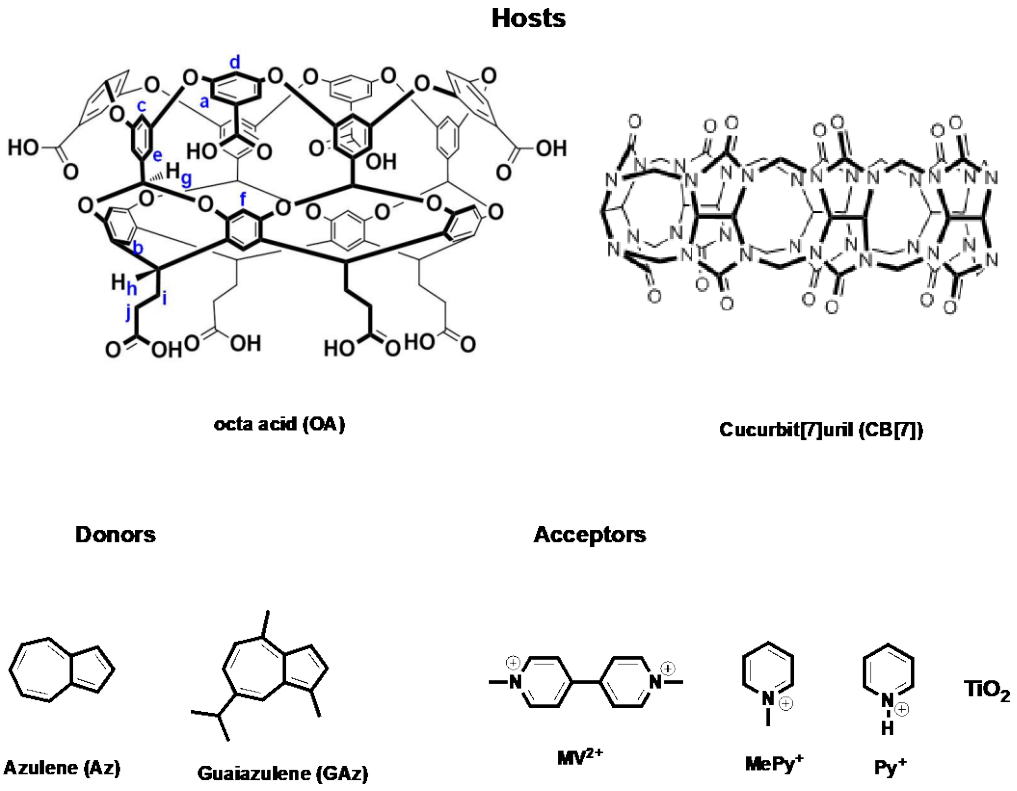

Figure 5.1 Structure of the hosts, donors and acceptors used in this work

5.2.1 NMR studies for the complexation of azulene derivatives

Formation of host-guest complexes between Az, GAz and OA was established from ^{1}H NMR spectra. Since azulene is smaller in size, we expected it would form 2:2 (host : guest) capsuleplex. **Figure-5.2** shows the comparison ^{1}H NMR spectra of host OA, $Az_2@OA_2$ and $GAz@OA_2$. Individual titration spectra are shown in **Figure 5.3 and 5.4.** As we expected, alkyl substituted Guaiazulene (GAz), bigger in size forms 1:2 complex. The appearance of upfield protons confirmed the complexation of GAz with OA (**Figure 5.4**). In case of Az, we could not see any upfield shift of aromatic protons however we could observe shift in host OA protons (**Figure 5.3**) suggesting the complexation of Az with OA. 2D-DOSY spectra provides the diffusion constant values for the complexes, which are 1.45, and 1.50 x 10^{-6} cm^2/s for $Az_2@OA_2$ and $GAz@OA_2$ respectively (**Figure 5.5 and Figure 5.6**). These values also confirmed the complexation of guest molecules with OA capsule. We also checked ^{1}H NMR spectra after the addition of acceptor methylviologen (MV^{2+}) to the $Az_2@OA_2$. We did not observe any significant change in the spectra (**Figure 5.7**). It shows that it did not affect the complex formation between OA and guest molecules. It also indicates that it stays close to the OA capsule. The OA capsule is negatively charged due to the presence of eight carboxylate anion ($-COO^-$) which can bring the positively charged MV^{2+} closer to the wall.

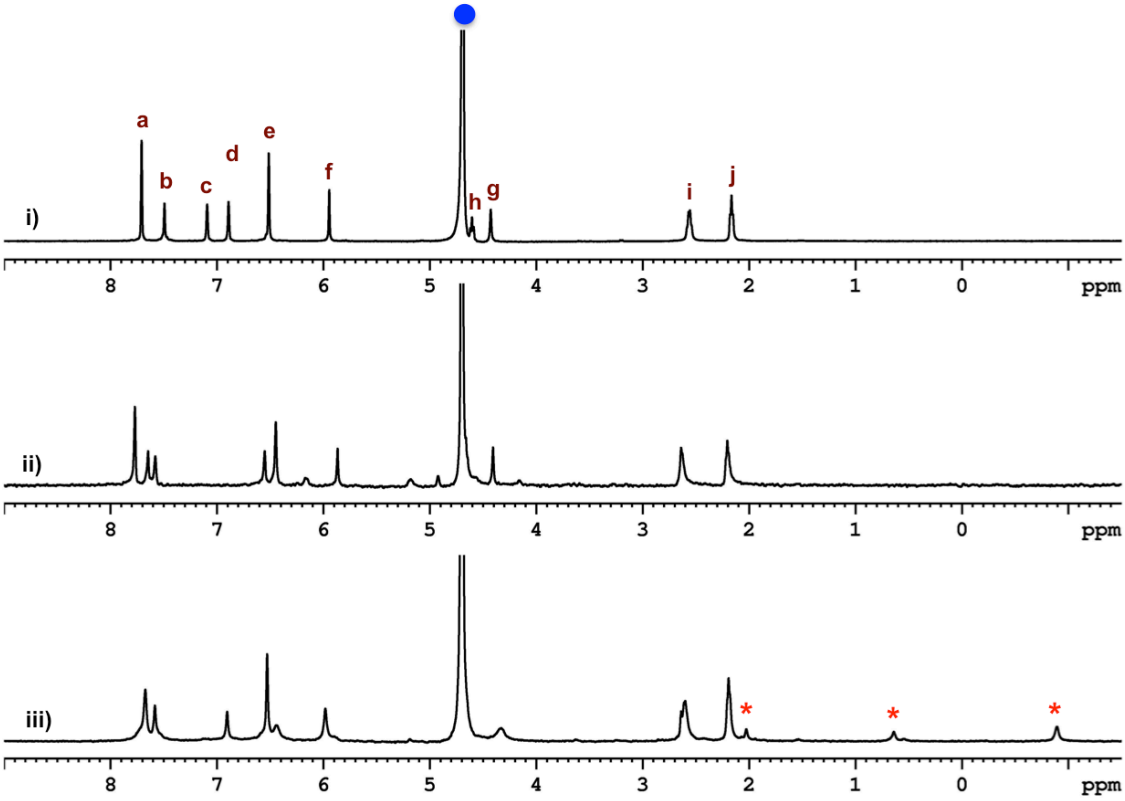

Figure 5.2 ^{1}H NMR (500 MHz) spectra of (i) OA([OA] = 1 mM) in 10 mM $Na_2B_4O_7$ buffer/D_2O; (ii) Az_2@OA_2 ([OA] = 1 mM), [Az] = 1 mM) in10 mM $Na_2B_4O_7$ buffer/D_2O; (iii) Gaz@OA_2 ([OA] = 1 mM), [GAz] = 0.5 mM)in10 mM $Na_2B_4O_7$ buffer/D_2O; "*" "●"represent the bound Guiazulene protons and the residual D_2O respectively.

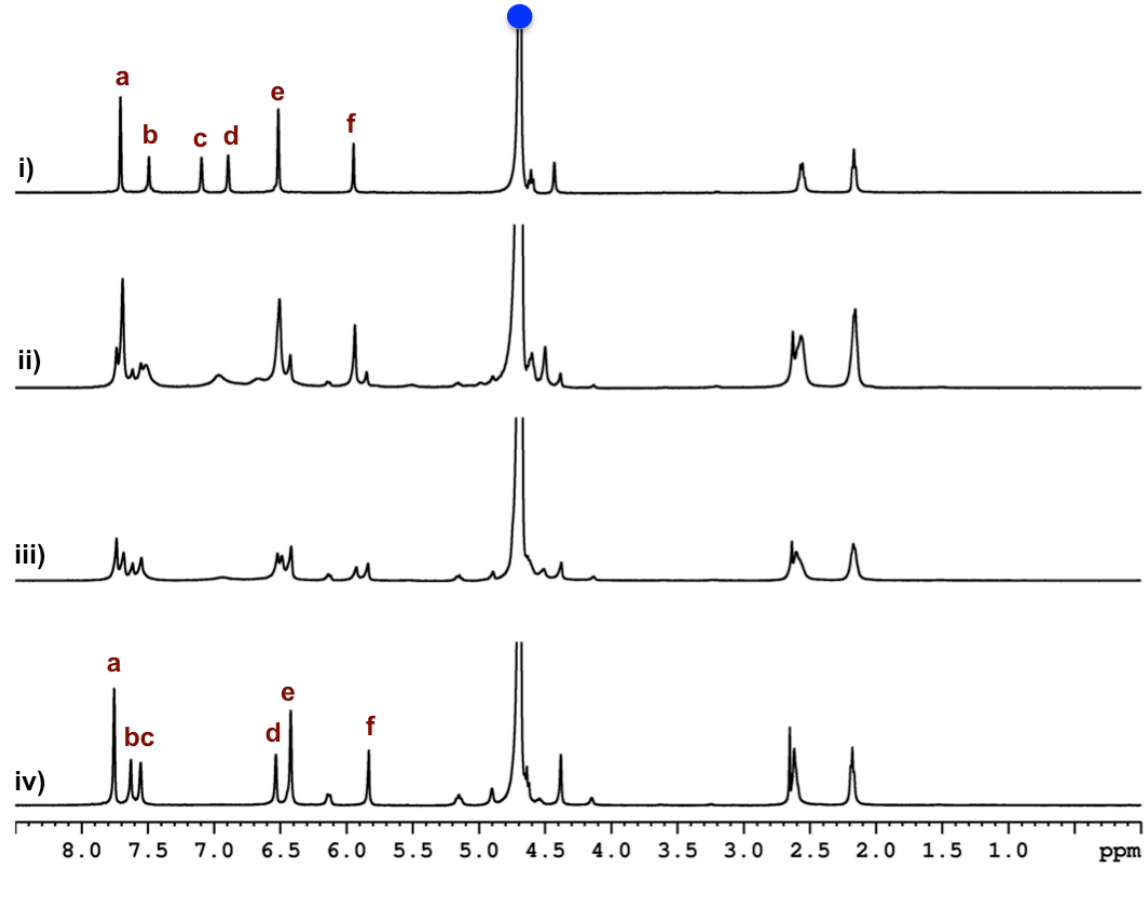

Figure 5.3 ^{1}H NMR (500 MHz) spectra of (i) OA([OA] = 1 mM) in 10 mM $Na_2B_4O_7$ buffer/D_2O; (ii) Az_2@OA_2 ([OA] = 1 mM), [Az] = 0.25 mM); (iii) Az@OA ([OA] = 1 mM), [Az] = 0.5 mM); (iv) Az@OA ([OA] = 1 mM), [Az] = 1 mM) in 10 mM $Na_2B_4O_7$ buffer/D_2O; "●"represent the residual D_2O.

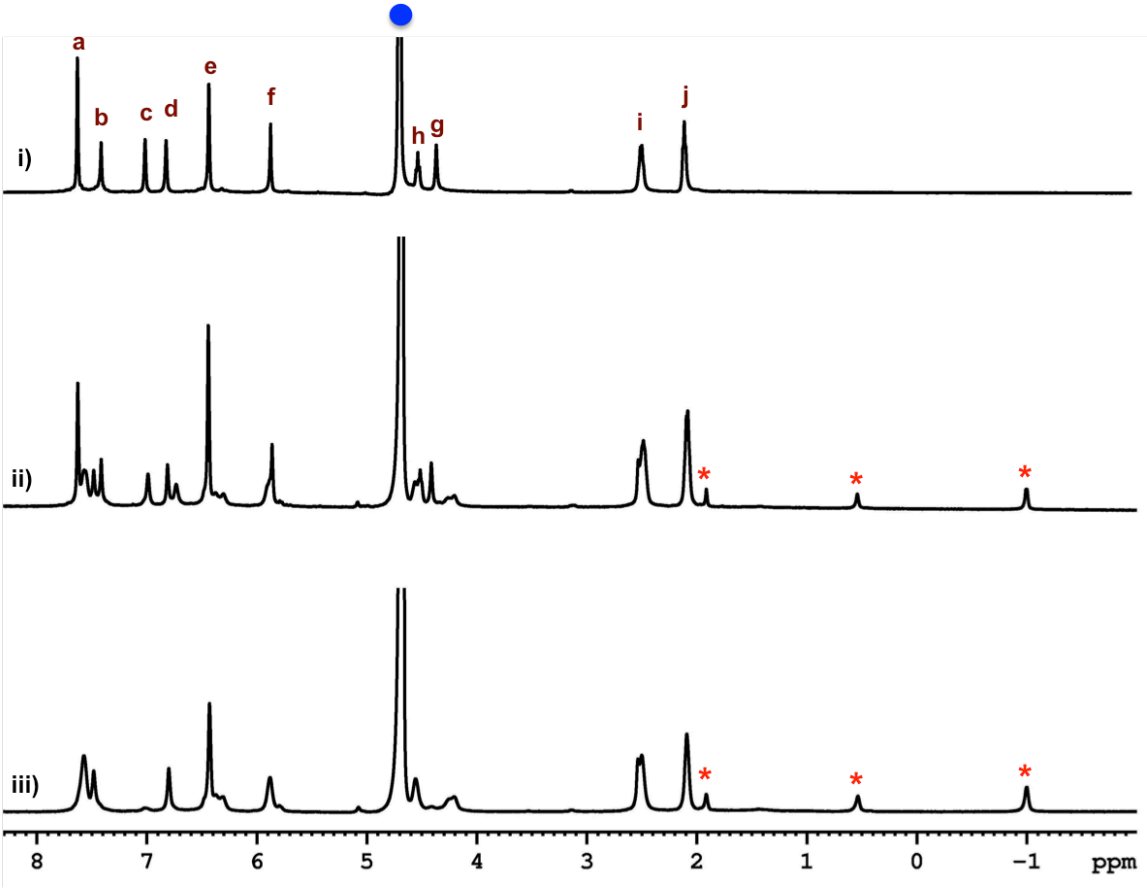

Figure 5.4 ^{1}H NMR (500 MHz) spectra of (i) OA([OA] = 1 mM); (ii) GAz@OA_2 ([OA] = 1 mM), [GAz] = 0.25 mM (iii) GAz@OA_2 ([OA] = 1 mM), [GAz] = 0.5 mM) in 10 mM $Na_2B_4O_7$ buffer/D_2O; "*" and "●"represent the bound Guiazulene protons and the residual D_2O respectively.

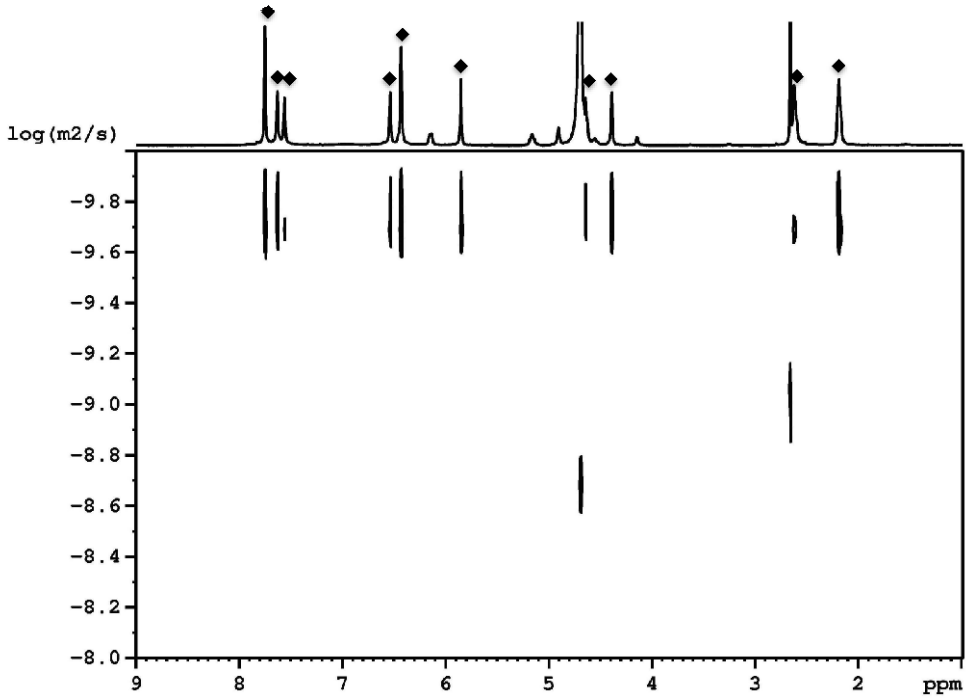

Figure 5.5 2D DOSY (500 MHz, D_2O) spectra of $Az_2@OA_2$; [OA] = 1 mM,[Az] = 1 mM in $Na_2B_4O_7$ buffer/D_2O, diffusion constant of $Az_2@OA_2$ is 1.48 x 10^{-6} cm^2/s. ;
◆ " " represents the shifted host protons.

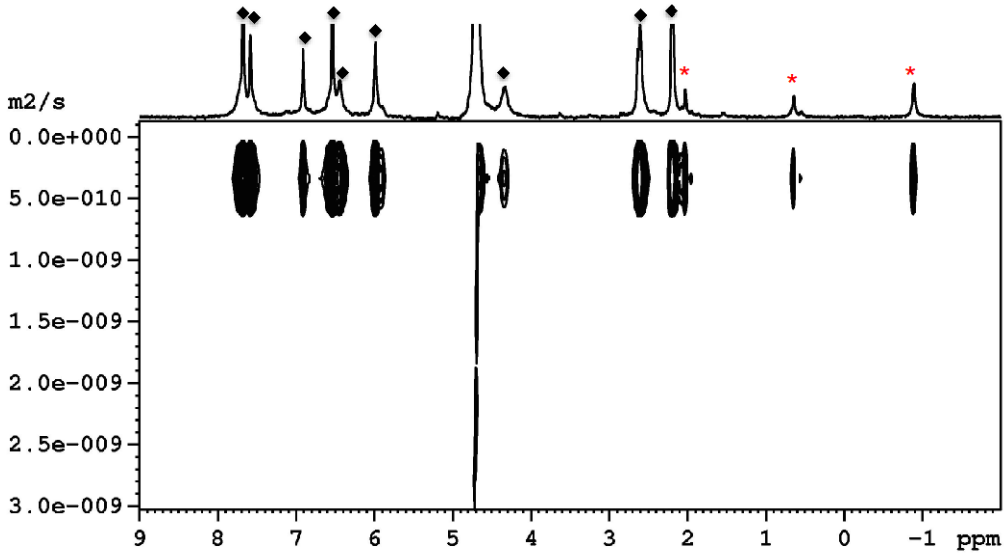

Figure 5.6 2D DOSY (500 MHz, D_2O) spectra of GAz@OA_2; [OA] = 1 mM, [GAz] = 0.5 mM, diffusion constant of GAz@OA_2 is 1.50 x 10^{-6} cm^2/s.; " " ◆ and " * " represent the host and bound guaiazulene protons respectively.

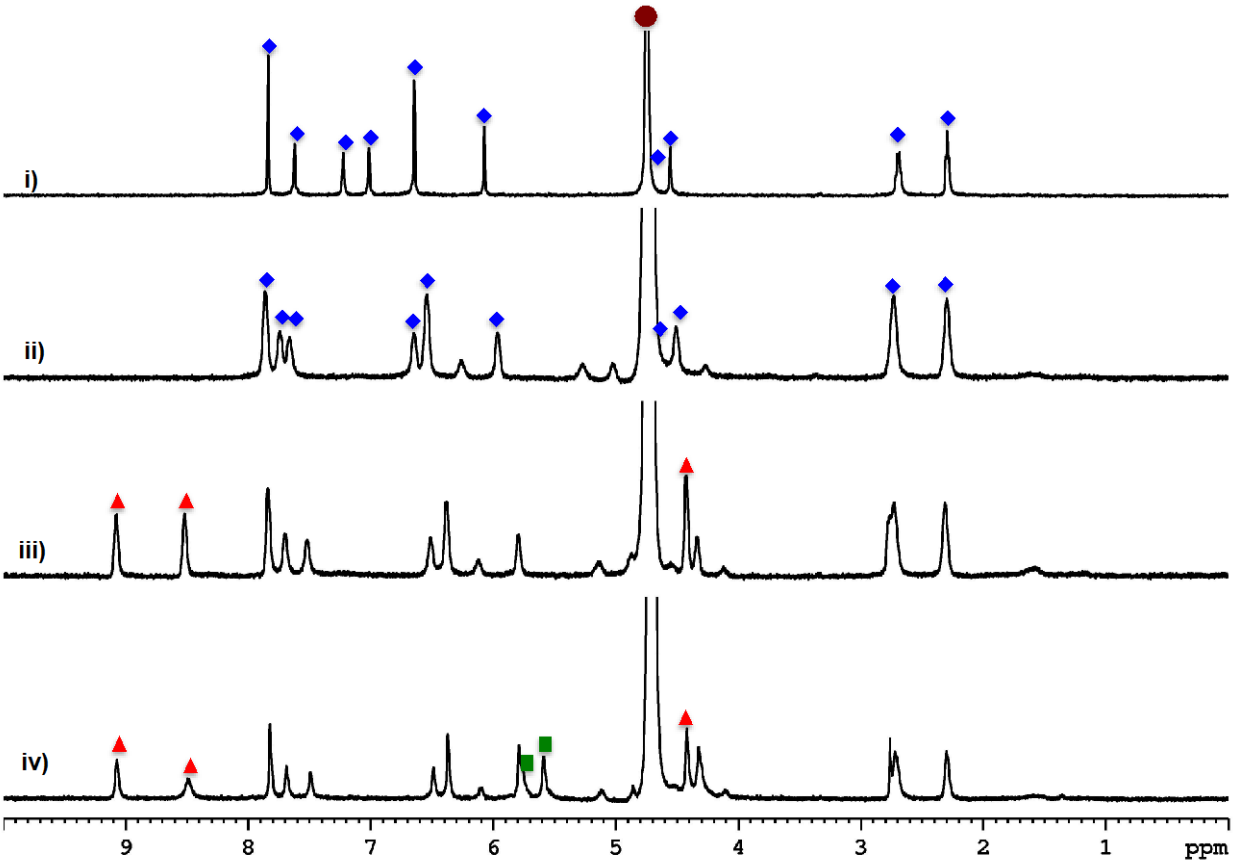

Figure 5.7 ^{1}H NMR (500 MHz) spectra of (i) OA([OA] = 1 mM) (ii) $Az_2@OA_2$ ([OA] = 1 mM), [Az] = 1 mM) ; (iii $Az_2@OA_2$ + MV^{2+} ([OA] = 1 mM), [Az] = 1 mM, [MV^{2+}] = 1 mM) ; (iv) $Az_2@OA_2$ + MV^{2+} + CB[7] ([OA] = 1 mM), [Az] = 1 mM, [MV^{2+}] = 1 mM, [CB-7] = 3 mM) in 10 mM $Na_2B_4O_7$ buffer/D_2O; " ● ", " ◆ ", " ▲ " and " ■ " represent residual D_2O , host OA, MV^{2+} and host CB-7 protons respectively.

5.2.2 Electron transfer of encapsulated azulene derivatives

The feasibility of PET process between donor and acceptor can be predicted using Rehm-Weller equation (**Equation-5.1**). According to **equation 5.1**, if the Gibb's free energy is exergonic (negative), the electron transfer is possible between donor and acceptors. The oxidation potential of Azulene and Guaiazulene are +0.71 V and +0.65 V respectively. The reduction potential of MV^{2+} and Py^{+} are -0.45 and -0.58 V respectively. When these values are incorporated in **equation-5.1**, it shows that electron transfer from azulene derivatives to the acceptors are feasible. Our group had earlier demonstrated the electron transfer from excited coumarins and *trans*-stilbene encapsulated within the OA capsule to MV^{2+}, $MePy^{+}$ and Py^{+} present outside in aqueous media.[36, 125]

The absorbance and emission spectra of both Az and GAz is shown in **Figure-5.8 and 5.9**. The absorbance spectra of Azulene complex with OA clearly has the characteristic S_0-S_2 absorption around 375 nm and S_0-S_1 absorption around 600 nm. The intense fluorescence from S_2-S_0 around 390 nm was observed **Figure 5.8b.** Absorption and emission spectra of GAz complex with OA is shown in **Figure 5.9.**

$$\Delta G = E^{ox}(D) - E^{red}(A) - E_{0-0} - \frac{e^2}{\varepsilon r} \qquad \text{(5.1)}$$

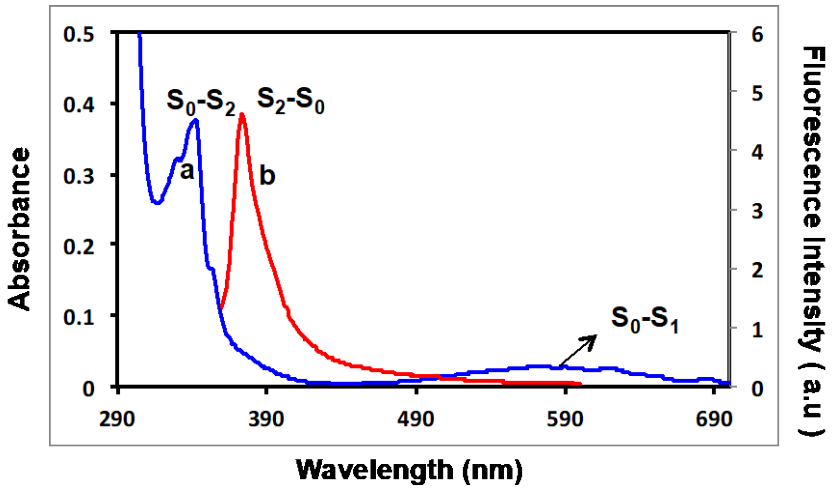

Figure 5.8 a) Absorption spectrum of $Az_2@OA_2$, [OA] = 1 x 10^{-4} M, [Az] = 1 x 10^{-4} M b) Fluorescence spectrum of $Az_2@OA_2$ [OA] = 1 x 10^{-5} M, [Az] = 1 x 10^{-5} M. in borate buffer.

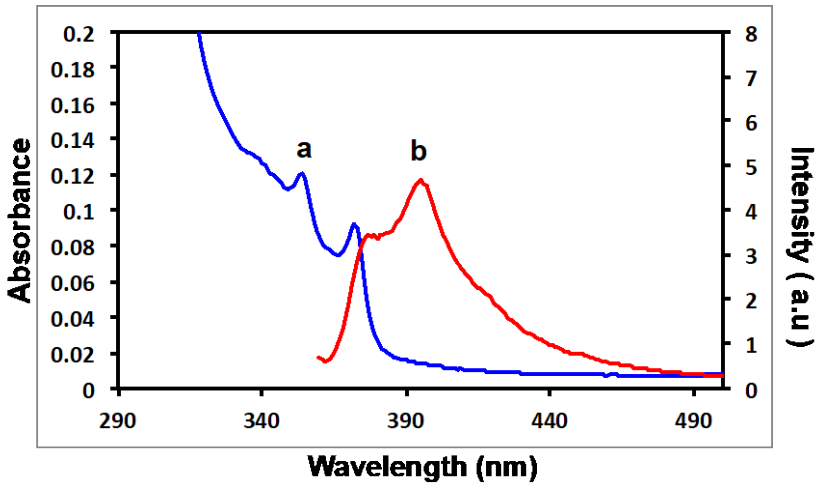

Figure 5.9 a) Absorption spectrum of $GAz@OA_2$, [OA] = 1 x 10^{-4} M, [GAz] = 0.5 x 10^{-4} M b) Fluorescence spectrum of $GAz@OA_2$ [OA] = 2x 10^{-5} M, [GAz] = 1 x 10^{-5} M in borate buffer (λ_{exc} = 350 nm).

The PET from azulene derivatives was monitored by quenching of fluorescence with addition of acceptors. Az shows strong fluorescence from upper excited state when we excite the **Az_2@OA_2** complex at 340 nm. Addition of acceptors to this solution gradually quenches the fluorescence (**Figure 5.10 a, b, & c**). This quenching of fluorescence is due to the electron transfer upper excited state of encapsulated Azulene to acceptors outside the wall. To probe this observation further we used a second host molecule, Cucurbit[7]ruil CB[7], well-known to bind cationic guest molecules like MV^{2+}, $MePy^{+}$ and Py^{+}. We anticipated a disruption of the Coulombic attraction between cationic acceptors and OA from the addition of CB[7] to a solution containing **Az_2@OA_2** and $MV^{2+}$by binding of MV^{2+} to CB[7]. This we envisoned would lead to an increased distance between the excited Az and the quencher MV^{2+} that would ultimately result in reduced quenching. As expected the addition of CB[7] to the solution restored S_2 fluorescence from Az(**Figure 5.11 a**). Similar observations were made with $MePy^{+}$ and PY^{+} (**Figure 5.11 b & c**). We performed quenching experiments with GAz complex and we observed similar results. The quenching of fluorescence with acceptors and competitive addition of CB[7] are shown in (**Figure 5.12 & 5.13**).

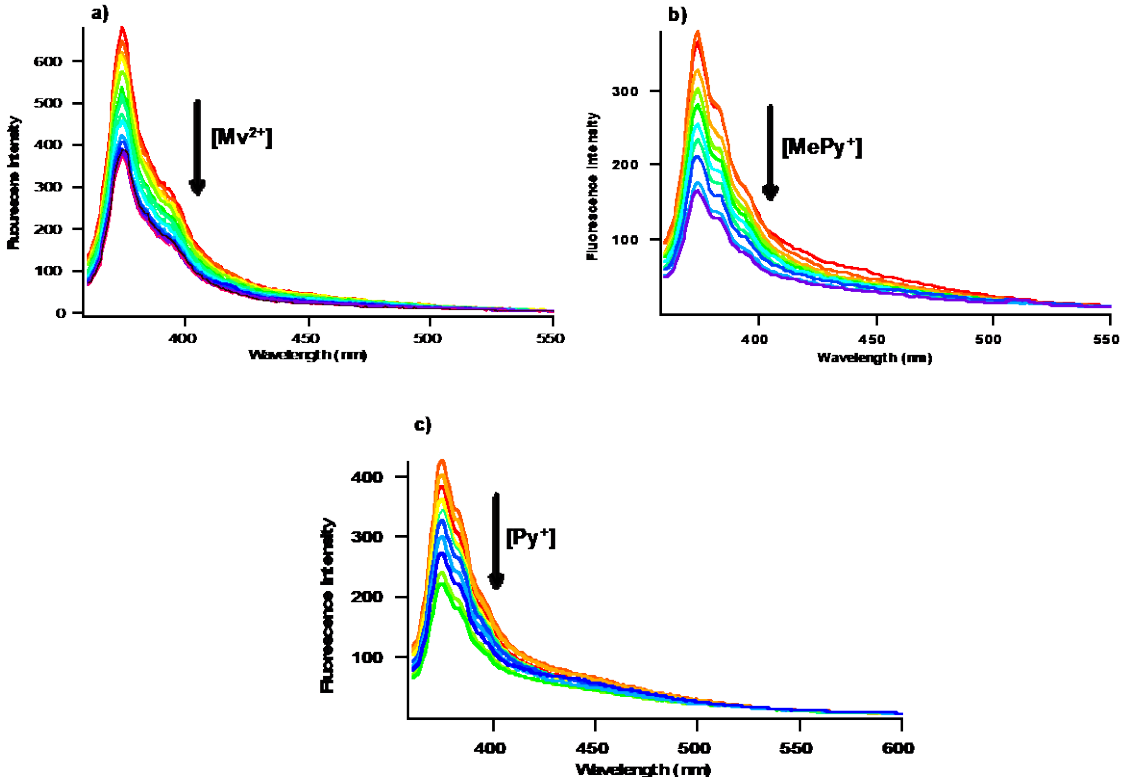

Figure 5.10 a) Fluorescence titration spectra of $Az_2@OA_2$ with MV^{2+} , [OA] = 2 x 10^{-5} M, [Az] = 2 x 10^{-5}M , [MV^{2+}] = 0 to 2.5 x 10^{-5} M ; b) Fluorescence titration spectra of $Az_2@OA_2$ with $MePy^+$,[OA] = 4 x 10^{-5} M, [Az] = 4 x 10^{-5}M ,[$MePy^+$] = 0 to 8.5 x 10^{-5}M; c) Fluorescence titration spectra of $Az_2@OA_2$ with Py^+,[OA] = 4 x 10^{-5} M, [Az] = 4 x 10^{-5}M ,[Py^+] = 0 to 7.5 x 10^{-5}M; λ_{exc} = 340 nm.

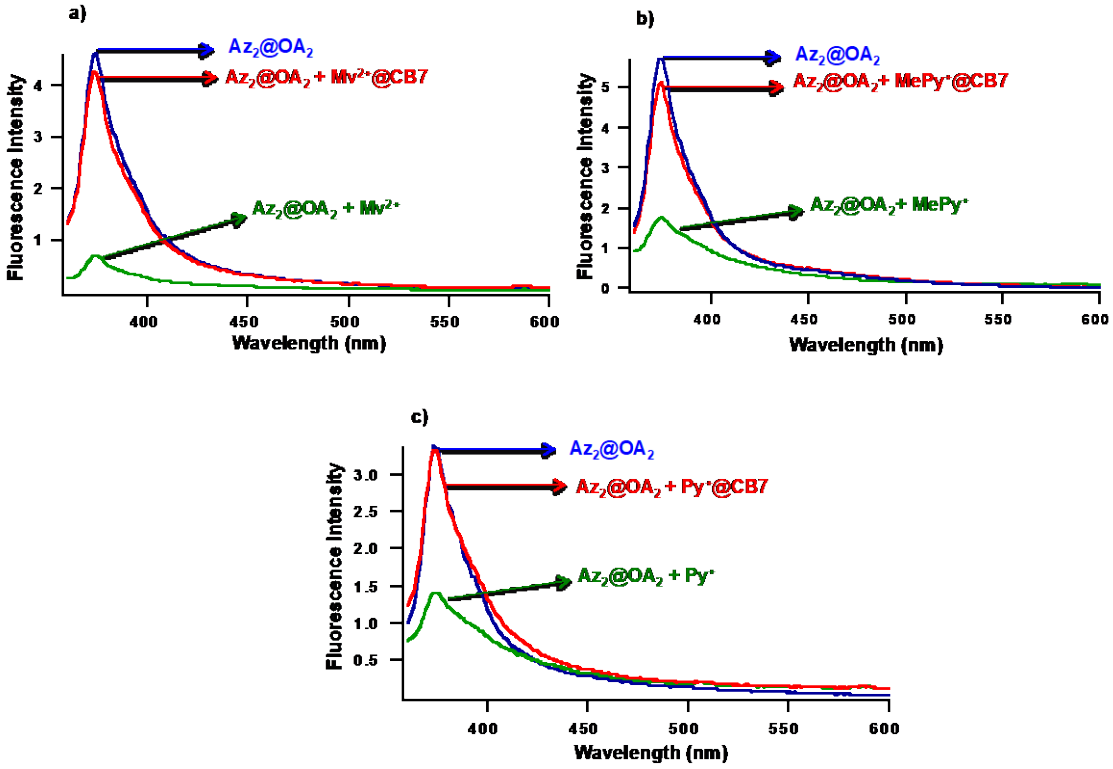

Figure 5.11 a) Fluorescence recovery spectra of $Az_2@OA_2$ [OA] = 4 x 10^{-5} M, [Az] = 4 x 10^{-5}M , [MV^{2+}] = 3 x 10^{-4} M, CB[7] = 1 mM; b) Fluorescence recovery spectra of $Az_2@OA_2$ [OA] = 4 x 10^{-5} M, [Az] = 4 x 10^{-5}M , [$MePy^{+}$] = 6 x 10^{-4} M, CB[7] = 1 mM; c) Fluorescence recovery spectra of $Az_2@OA_2$ [OA] = 4 x 10^{-5} M, [Az] = 4 x 10^{-5}M , [Py^{+}] = 6 x 10^{-4} M, CB[7] = 1 mM; λ_{exc} = 340 nm.

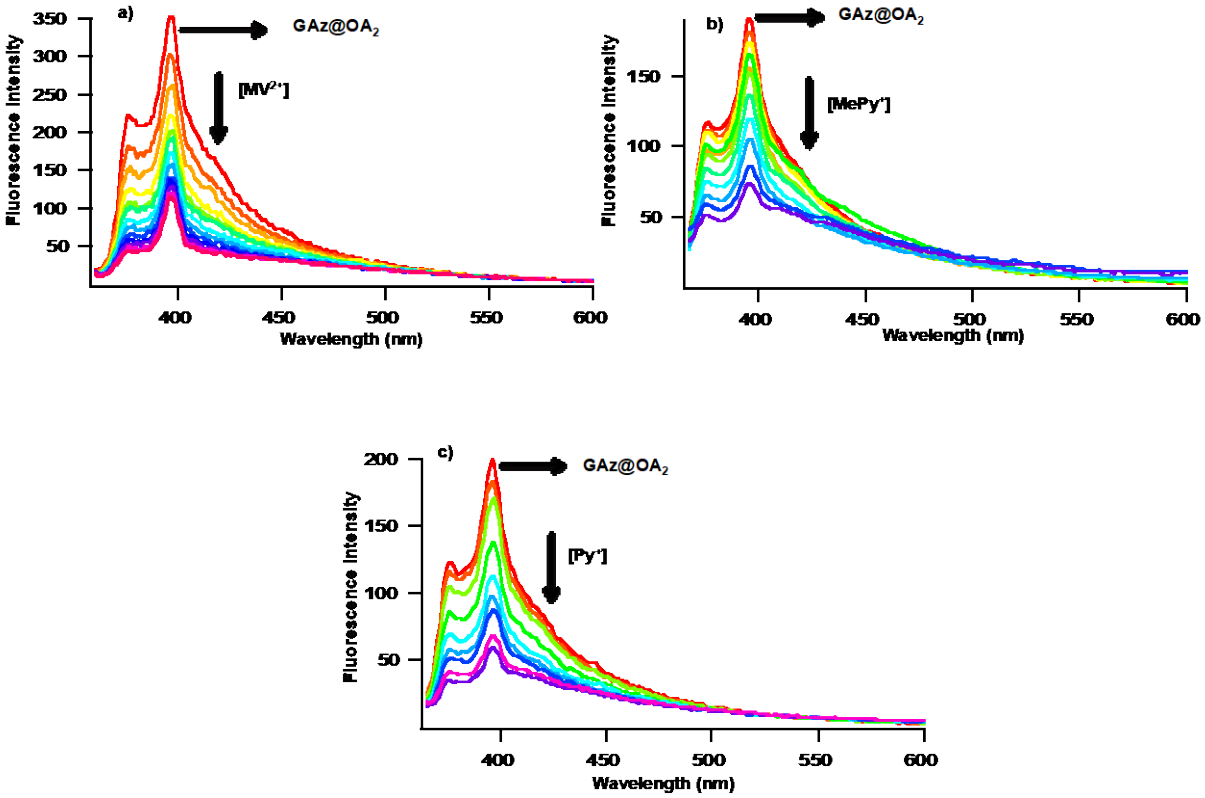

Figure 5.12 a) Fluorescence titration spectra of GAz@OA_2 with MV^{2+} , [OA] = 4 x 10^{-5} M, [GAz] = 2 x 10^{-5}M , [MV^{2+}] = 0 to 3.5 x 10^{-5} M ; b) Fluorescence titration spectra of GAz@OA_2 with $MePy^{+}$,[OA] = 4 x 10^{-5} M, [GAz] = 2 x 10^{-5}M ,[$MePy^{+}$] = 0 to 5 x 10^{-5}M; c) Fluorescence titration spectra of GAz@OA_2 with Py^{+},[OA] = 4 x 10^{-5} M, [GAz] = 2 x 10^{-5}M ,[Py^{+}] = 0 to 4.8 x 10^{-5}M; λ_{exc} = 350 nm.

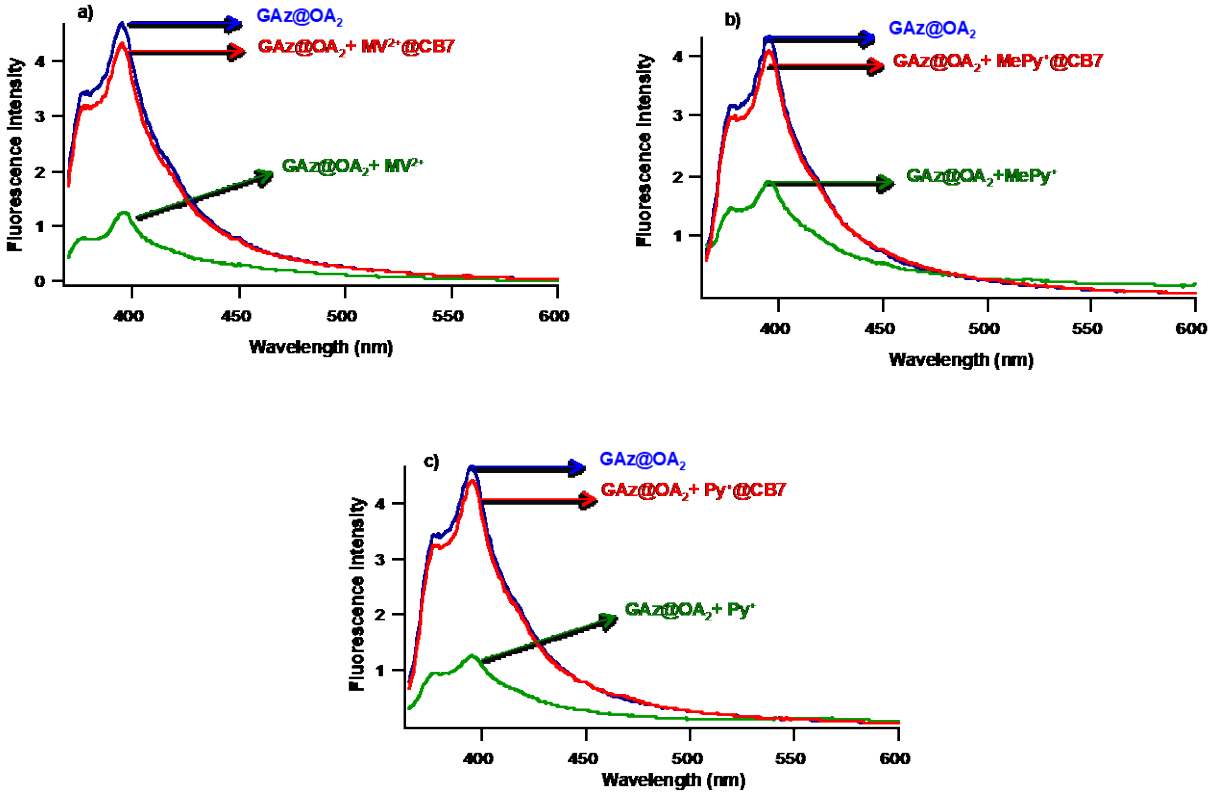

Figure 5.13. a) Fluorescence recovery spectra of GAz@OA_2 [OA] = 1 x 10^{-4} M, [GAz] = 5 x 10^{-5}M , [MV^{2+}] = 3 x 10^{-4} M, CB[7] = 1 mM; b) Fluorescence recovery spectra of GAz@OA_2 [OA] = 1 x 10^{-4} M, [GAz] = 5 x 10^{-5}M , [$MePy^{+}$] = 6 x 10^{-4} M, CB[7] = 1 mM; c) Fluorescence recovery spectra of GAz@OA_2 [OA] = 1 x 10^{-4} M, [GAz] = 5 x 10^{-5}M , [Py^{+}] = 6 x 10^{-4} M, CB[7] = 1 mM; λ_{exc} = 350 nm.

5.2.3 Ultrafast transient absorption studies

We monitored the PET process by time-resolved fluorescence spectroscopy. We used Single Photon Counting (SPC) (nanosecond time regime) to monitor the change in fluorescence lifetime of the Az during the quenching process. We did not see any change in S_2 lifetime of the emitting species. This might be due to the static quenching, suggested the close proximity of the donor and acceptor molecules. When there is electron transfer from $Az_2@OA_2$ to MV^{2+}, there should be formation of radical cations ($AZ^{\bullet+}$ and $MV^{\bullet+}$). We collaborated with Professor Pratik Sen (IIT, Kanpur, India) to perform femtosecond studies on our complexes. When we excite the **$Az_2@OA_2$ + MV^{2+}** using 400 nm light, a broad positive absorption band centered around 600 nm was observed (**Figure 5.14a**). This positive absorption band is due to the formation of $MV^{\bullet+}$ as reported in literature.[129] We also carried our control experiment by exciting only **$Az_2@OA_2$** without the MV^{2+}, showed no excited state dynamics feature at 600 nm confirming that the observed positive transient absorption (TA) band is due to the formation of $MV^{\bullet+}$. The kinetic trace at 600 nm is shown in (**Figure 5.14b**), where a rise component of ≈ 4 ps due to formation of $MV^{\bullet+}$ is observed. To ensure there is no wavelength dependence, global fitting was performed in the wavelength region 550-650 nm using Glotaran software.[130] The data were best fitted with a sum of three exponential functions convoluted with a Gaussian function representing the IRF and the time constants are reported in **Table-5.1**. The first time component (τ_1) of ≈ 4 ps is the rate of forward electron transfer and the second time component (τ_2) ≈ 56 ps is the back electron transfer. We also performed the same experiment with G**Az@OA_2 + MV^{2+}** and their time constants tabulated in **Table-5.1.**

To probe the electron transfer from the excited donor Az, fluorescence decay of Az was monitored. We excited the sample **Az_2@OA_2 + MV^{2+}** at 360 nm and followed the fluorescence decay at 400 nm. We were not able to the fluorescence decay due to the ultrafast nature of PET between Az and MV^{2+}. The IRF for SPC measurement is 120 ps. However, we were able to record an ultrafast decay of Az fluorescence with a femtosecond fluorescence upconversion method whose IRF is about 200 fs. The data obtained using this method is shown in (**Figure 5.14c**) and the time constants obtained from these experiments are tabulated in **Table 5.1**. The decay time constant ≈ 2 ps is similar to the time constant(≈ 4 ps) for the formation of $MV^{\bullet+}$ obtained TA study. These results clearly showed that there is upper excited state electron transfer from Az to MV^{2+} through the molecular wall of OA.

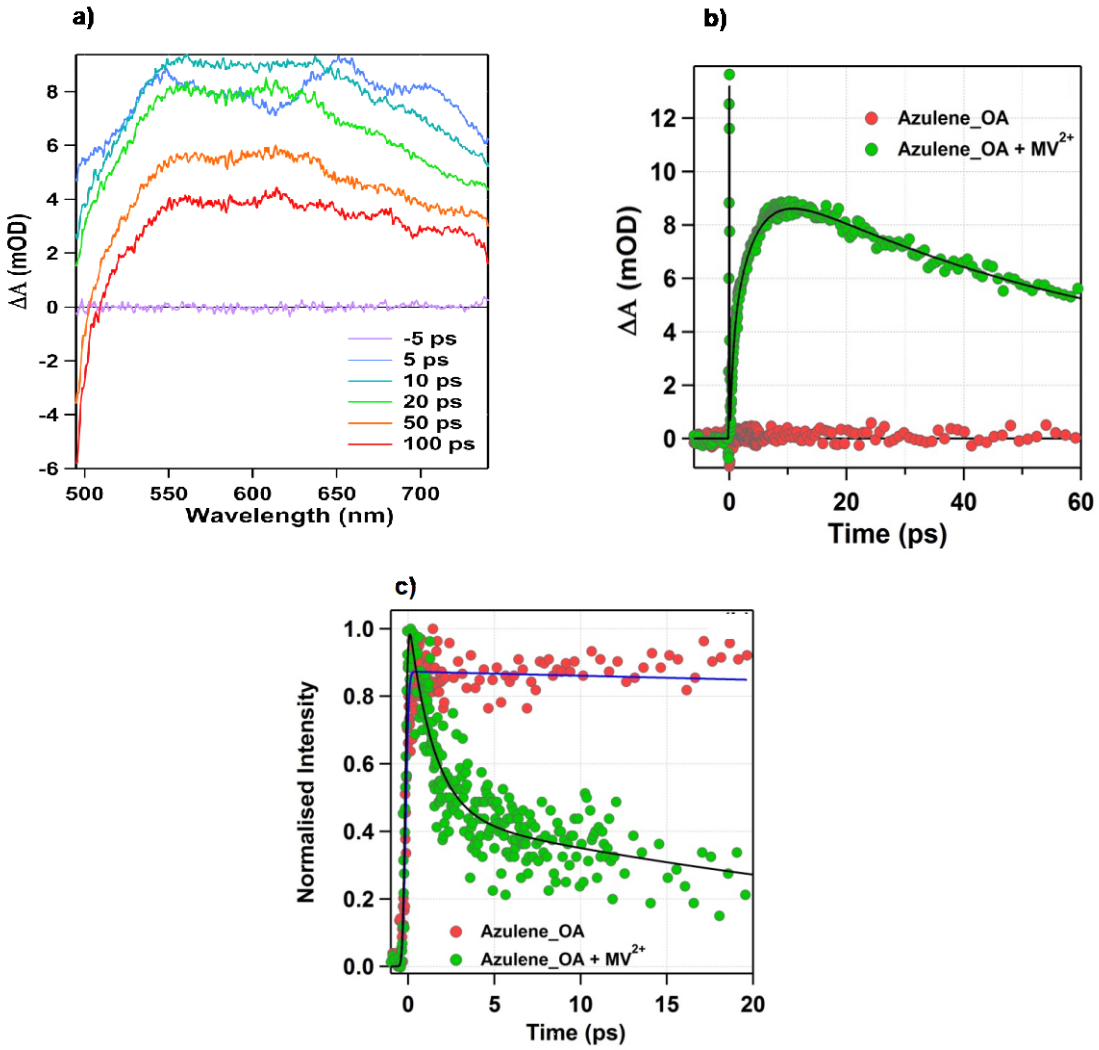

Figure 5.14. a) Femtosecond transient absorption spectra for $Az_2@OA_2$ with 10 mM MV^{2+} at different times; b) Kinetics plot obtained from transient absorption spectroscopy at 600 nm; c) Fluorescence transient obtained from up-conversion study at 400 nm exciting the sample at 360 nm. Concentration of MV^{2+} used is 10mM. The black and blue lines represent the fitting lines.

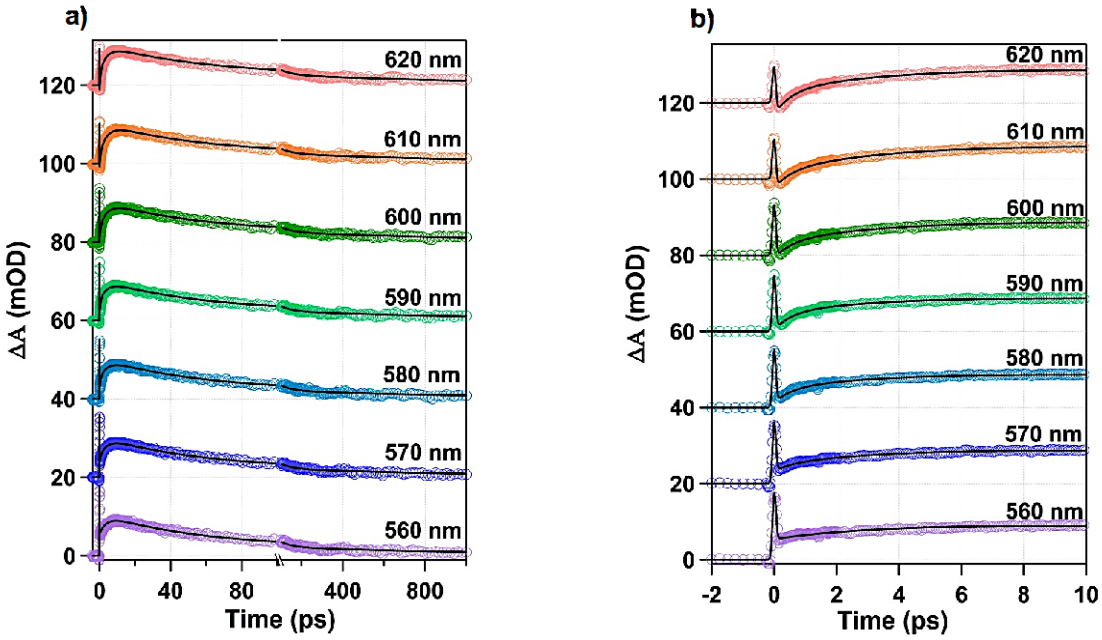

Figure 5.15 Global fitting for wavelength range from 560 to 620 nm.

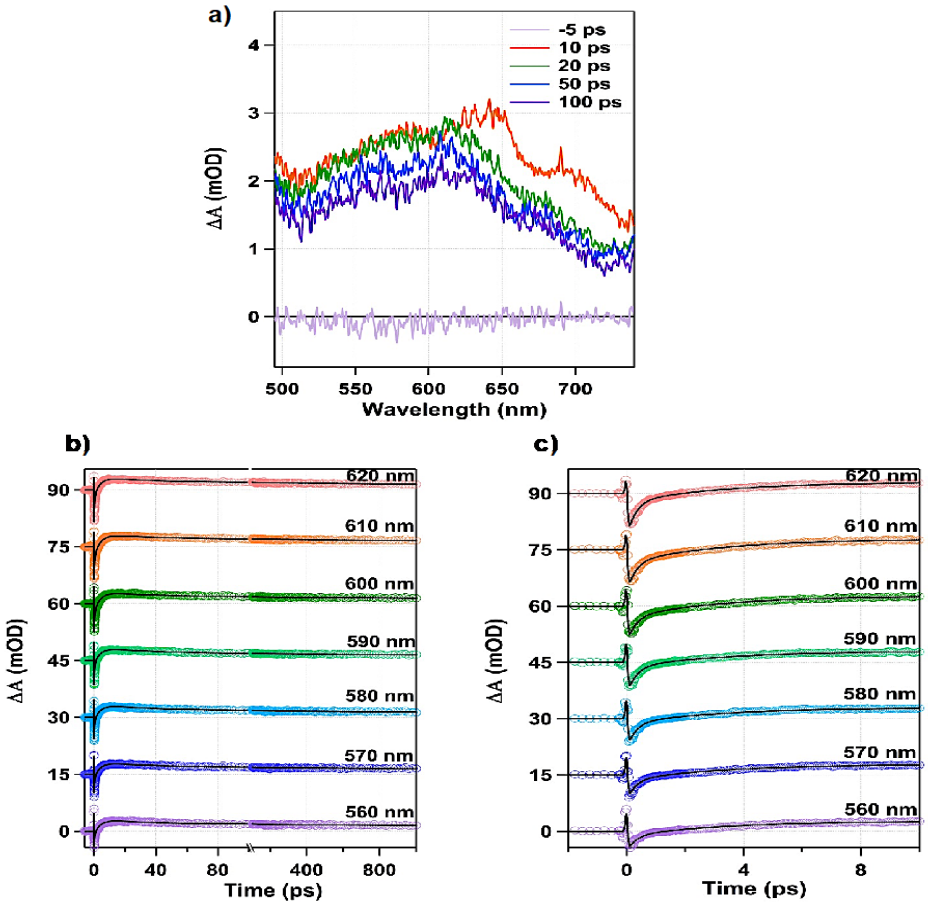

Figure 5.16 a) Femtosecond transient absorption spectra for GAz@OA_2 with 10 mM MV^{2+} at different times λ_{exc} = 400 nm; b) and c) Global fitting for wavelength range from 560 to 620 nm.

Technique	τ_1 (ps)	τ_2 (ps)	τ_3 (ps)
Az$_2$@OA$_2$ + MV^{2+}			
Transient absorption	4.0 (rise)	55.7 (decay)	1000 (fixed)
Fluorescence up-conversion	2.0 (decay)	39.5 (decay)	2000 (fixed)
GAz@OA$_2$ + MV^{2+}			
Transient absorption	3.6 (rise)	36.9 (decay)	4000 (fixed

Table 5.1 Time constants for electron transfer between Azulene and Guaiazulene and Methylviologen measured by Femtosecond time-resolved experiments.

5.2.4 Electron transfer to Nanostructured TiO_2 colloidal solutions and thin film

Since we observed the electron transfer from upper excited state of azulene derivatives, we wanted to expand these studies with semiconductor metal oxides TiO_2. Piotrowick *et al* had already established the PET between encapsulated azulene to TiO_2 nanoparticle solution.[131] They used a water-soluble hemicarcerand synthesized by Yoon and Cram as the host. Their host has small cavity volume and the size of portals limiting to study various guests that are bigger in size. We wanted to use our host OA, which has bigger cavity and forms capsule spontaneously by hydrophobic effect. Our group had already established the binding capacity of OA to TiO_2 metal surface at neutral pH. We had observed electron transfer from Coumarin dyes to TiO_2 colloidal nanoparticles as wells to TiO_2 thin film.[132] It has been demonstrated that the S_2 excited state of azulene derivatives lies above the conduction band of TiO_2.[131, 133] We used wider band gap (5.0 eV) metal oxide ZrO_2 as control experiment.

We checked the fluorescence of $Az_2@OA_2$ and $GAz@OA_2$ at neutral pH (pH~7) and there was no change in the fluorescence (**Figure 5.17**). This condition is suitable for binding with TiO_2 colloidal particles and thin films. Fluorescence spectra of $Az_2@OA_2$ collected following the incremental addition of TiO_2 colloidal aqueous suspension are shown in **Figure 5.18 a.** As expected, the emission intensity showing an inverse relationship to the amount of TiO_2 suspension in solution and the fluorescence was quenched while the emission was not quenched following the addition of aliquots of a colloidal ZrO_2 aqueous solution (**Figure 5.18 b).** A similar behavior was observed with $GAz@OA_2$. To probe the feasibility of eT $Az_2@OA_2$ and $GAz@OA_2$ to the surface of TiO_2 nanostructured thin films, which are more technologically relevant substrates, the capsules were adsorbed on films of

TiO_2 cast on glass (ZrO_2 films were used as the control), by immersing the films in a 1 mM aqueous solution of the host-guest complex at pH~7 overnight. We characterized OA bound to TiO_2 by FT-IR-ATR experiments (**Figure 5.19**). The characterization of bound complex on TiO_2 is shown in (**Figure 5.20)**. The broad, intense bands in the 1500-1650 cm^{-1} region assigned to the *v* (O---C---O) stretching of bound carboxylate groups, with some unbound C=O stretching around *v* 1707 cm^{-1}. The fluorescence spectra of $Az_2@OA_2$ bound to TiO_2 is completely quenched compared to the spectra of $Az_2@OA_2$ bound to ZrO_2 (**Figure 5.21a)**. The quenching in the case of $Az_2@OA_2$ bound to TiO_2 is due to the electron transfer from azulene to TiO_2 metal oxide surface. Similar results were obtained in the case of $GAz@OA_2$ complexes (**Figure 5.21b)**.

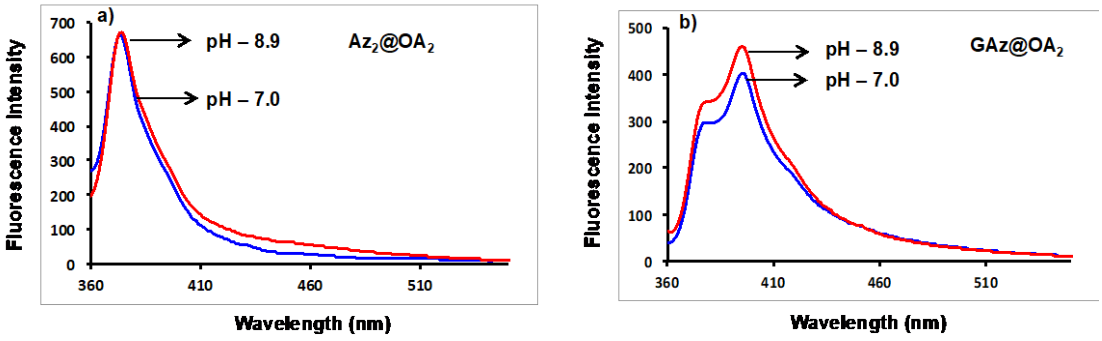

Figure 5.17 a) Fluorescence spectra of Az@OA2 at pH-8.9 and pH-7.0, [OA] = 4 x 10-5 M, [Az] = 4 x 10-5M; b) Fluorescence spectra of GAz@OA2 at pH-8.9 and pH-7.0, [OA] = 4 x 10-5 M, [GAz] = 2 x 10-5M.

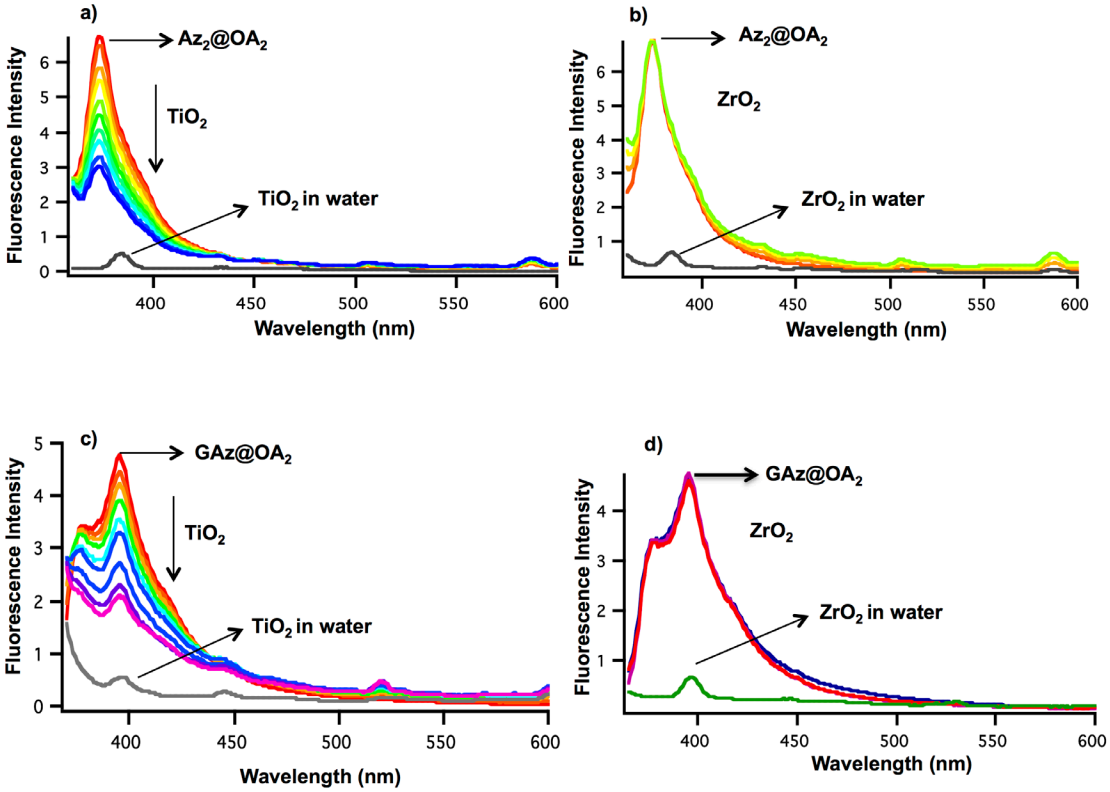

Figure 5.18 Fluorescence titration spectra of a) $Az_2@OA_2$ with TiO_2 nanoparticles b) $Az_2@OA_2$ with ZrO_2 nanoparticles (λ_{exc} = 340 nm); Fluorescence titration spectra of c) $Gaz@OA_2$ with TiO_2 nanoparticles d) $Gaz@OA_2$ with ZrO_2 nanoparticles (λ_{exc} = 350 nm) at pH = 7.

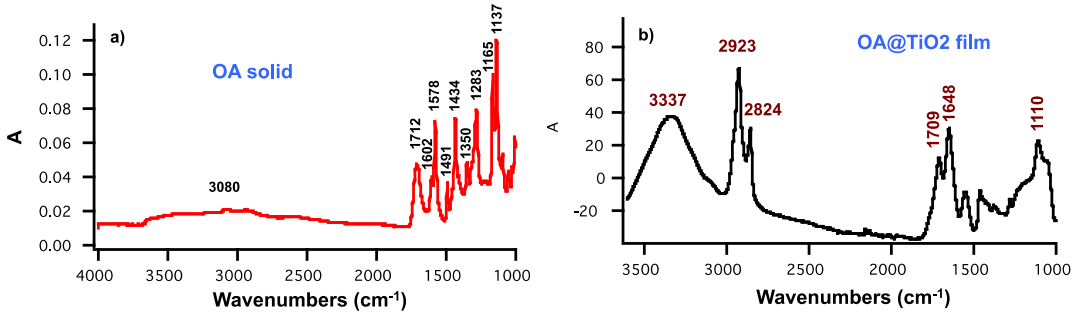

Figure 5.19 a) FT-IR-ATR spectra of OA solid; b) OA@ TiO_2 film.

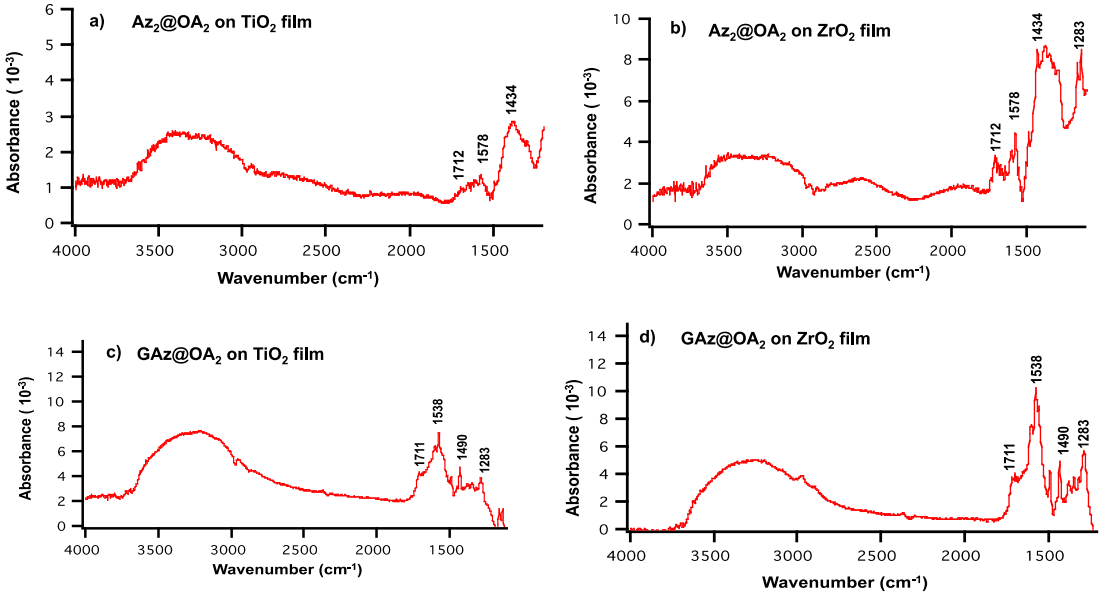

Figure 5.20 a) FT-IR-ATR spectra of a) $Az_2@OA_2$ on TiO_2 film; b) $Az_2@OA_2$ on ZrO_2 film ; c) $GAz@OA_2$ on TiO_2 film, and d) $GAz@OA_2$ on ZrO_2 film

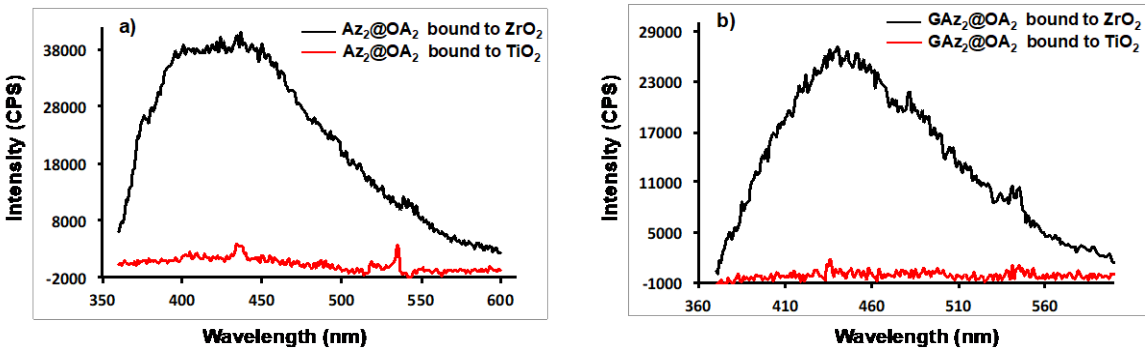

Figure 5.21 a) Fluorescence spectra of $Az_2@OA_2$ bound to TiO_2 and ZrO_2 films (λ_{exc} = 340 nm); b) Fluorescence spectra of $GAz@OA_2$ bound to TiO_2 and ZrO_2 films (λ_{exc} = 350 nm).

5.3. Conclusion

In this chapter we have demonstrated that Az and GAz form 2:2 and 2:1 closed capsules with OA. Upon excitation to the second excited state these molecules transfer electrons to the acceptors present outside the capsule. Femtosecond transient absorption studies used to find the time constant (2-5 ps) for forward electron transfer and 40 ps for the back electron transfer. The fast rate of electron transfer is partially attributable to the proximity of the donor and acceptor molecules. We also observed the PET from azulenes to TiO_2 nanoparticles and thin films.

5.4 Experimental section

Materials and methods

The host octa acid was synthesized following published procedure.[32] Laser grade azulene was purchased and recrystallized with ethanol. Guiazulene , pyridinium trifluoromethanesulfonate (Py^+) and methylviologen(MV^{2+}) were purchased from Sigma-Aldrich and used as received. N-methyl pyridinium iodide ($MePy^+$) was synthesized following reported procedure.[87]

General procedure for guest binding studies probed by NMR

A D_2O stock solution (600 μL) of host OA (1 mM) and sodium borate buffer (10 mM) taken in a NMR tube was titrated with the guest by sequential addition of 0.25 eq of guest (2.5μL of a 60 mM solution in $DMSO_{d6}$). The complexation was achieved by shaking the NMR tube for about five minutes. ^1H NMR spectra were recorded at room temperature under aerated conditions on a Bruker 500 MHz NMR. 1:2 (guest:host) and 2:2 complexes were achieved by adding 5 or 10 μL respectively of guest solution to 600 μL of 1 mM OA host in 10 mM buffer. Completion of complexation was monitored by the disappearance of the free OA signals upon addition of guest.

General protocol for fluorescence study

Fluorescence emission spectra were recorded on a FS920CDT Edinburgh steady-state fluorimeter. The aqueous solution of host OA was prepared in 10 mM sodium tetraborate buffer (1 mM). Stock solutions of the guests were prepared in DMSO. 2:2 and 1:2 complex solutions were prepared by adding required amount of guest solution in a vial. These 2:2 and 1:2 complex were diluted to 10^{-5} M for the experiment. Calculated amounts of acceptor solutions (MV^{2+}, $MePy^+$, Py^+ solutions, TiO_2 and ZrO_2 colloidal solutions)

were added to 2:2 and 1:2 complex solutions and mixed thoroughly and fluorescence spectra recorded. In studies using the host cucurbit[7]uril (1 mM), required amount of it was added to the complex solutions with quenchers, mixed thoroughly and then fluorescence spectra were recorded.

Sample preparation for adsorption on TiO_2 and ZrO_2

Capsular assemblies ($Az_2@OA_2$, $GAz@OA_2$) (in this abbreviation the guest is indicated first, host last and the symbol @ means guest is complexed to host and the number indicates the number of molecules in the complex) were made in sodium tetraborate buffer (pH-8.9) and emission spectra recorded. Aqueous HCl was added dropwise and the pH of the solution was checked. After adjusting to a certain pH, emission of the solution was recorded. It was observed that up to pH ~7, complex emission remained almost the same, which is suitable for binding studies with TiO2 and ZrO_2.

Mesoporous metal oxide (MO) film preparation and binding

Colloidal TiO_2 and ZrO_2 films were prepared by a sol−gel technique that produces mesoporous films of approximately 10 μm thickness and that consist of nanoparticles with an average diameter of ∼20 nm. The TiO_2 films were prepared by casting the colloidal solutions by the doctor-blade technique onto the substrate over an area of 1 × 2 cm^2, followed by sintering at ∼450 °C for 30 min. For absorption and fluorescence studies the films were cast on cover glass slides (VWR).

General protocol for FTIR-ATR study of the films

All FTIR-ATR spectra for OA (neat solid) and host@guest (at pH=7) on TiO_2/ZrO_2 films were collected on a Thermo Electron Corporation Nicolet 6700 FTIR utilizing the SMART MIRacle-single bounce ATR accessory (ZnSe crystal, with 128 scans and spectral resolution of 8 cm^{-1}) The films were dried in the oven to 110 ºC for 30 minutes for further use.

General protocol for emission studies of the films

Fluorescence emission spectra of the host@guest (at pH 7) binding on TiO_2/ ZrO_2 films were recorded on a Horiba Fluorolog-3 instrument equipped with a Xenon short-arc lamp source for films at room temperature. The fluorescence spectra were recorded at 340 nm and 350 nm for $Az_2@OA_2$ and $GAz@OA_2$ respectively.

General protocol for transient absorption and up-conversion studies

Since the details of our femtosecond transient absorption spectroscopy setup (FemtoFrame-II, IB Photonics, Bulgaria) and fluorescence up-conversion setup (FOG-100, CDP Corp., Russia) have been discussed earlier we present here a brief overview. For transient absorption measurements the fundamental 800 nm light obtained from a Spitfire Pro (Spectra Physics, USA) amplifier was split into 2 parts. One part was focused on a BBO crystal to generate 400 nm light, which was used as the pump beam and the other part was focus on a sapphire plate after passing through a delay stage to generate the white light continuum (450 nm to 750 nm), which was used as the probe light. The instrument response function has a FWHM of 120 fs. For fluorescence up-conversion setup the fundamental 720 nm light was obtained from a MaiTai HP (Spectra Physics, USA), which was frequency doubled in a 0.2 mm BBO crystal to obtain 360 nm pump light. The pump beam

was focused onto a rotating sample and the fluorescence was collected and up-converted with the residual fundamental light in another 0.5 mm BBO crystal. This was focused onto a monochromator and then to a photon counting device to obtain the fluorescence transient. The FWHM of the instrument response function is 200 fs. The ps-ns time resolved fluorescence transients were collected using a commercial TCSPC setup (Life Spec II, Edinburgh Instruments, UK). All samples were excited at 375 nm and the FWHM of the instrument response function is 120 ps.

Chapter 6. Trapping of Photoproducts of Nitro Triggers Using Supramolecular Approach.

6.1 Overview

Caging and releasing molecules of interest at a given location and time have been an active area of research. Photocleavage of a specific bond facilitates biomolecule uncaging, fluorescence activation and drug release with spatial and temporal precision. This process is called 'phototriggering' and the molecules are called 'phototriggers'.[134] Phototriggers have been recognized as a powerful tool in biomedical applications and biotechnologies.[135-138] Most of the biomedical applications, including drug release need to be carried out in aqueous medium. Commonly used phototriggers are 2-nitrobenzyls, coumarins, benzoins, and phenacyl derivatives. Molecules to be released are covalently attached to these triggers and released under the exposure of light.[139] Our group used supramolecular approach to encapsulate phototriggers such as p-methoxy phenacylesters, p-hydroxy phenacyl ester, 7-methoxy coumaryl-4-methyl esters and 7-diethylamino coumaryl-4-methy esters.[140-143] We have demonstrated release of small molecules of interest in aqueous media. 2-Nitrobenzyl derivatives are the most widely used phototriggers. Photochemical reaction mechanisms and ultrafast studies of 2-Nitro benzyl derivatives have been established by various groups.[139] General mechanism of photoreaction 2-Nitrobenzyl deriviative is shown in **Scheme-6.1**. One of the main deficiencies of the 2-Nitro benzyl derivatives is that the product from the trigger part namely nitroso benzaldehyle is toxic. Usage of nitrotrigger as drug delivery system in the body would leave the toxic photoproduct 2-nitroso benzaldehyde after the release of drug to the desired location. Hence release of desired drug molecule in the environment and

safe trapping of the photoproduct is very important. In this chapter, we wanted to study the phototriggering of nitro derivatives and trapping of toxic nitroso products by supramolecular approach.

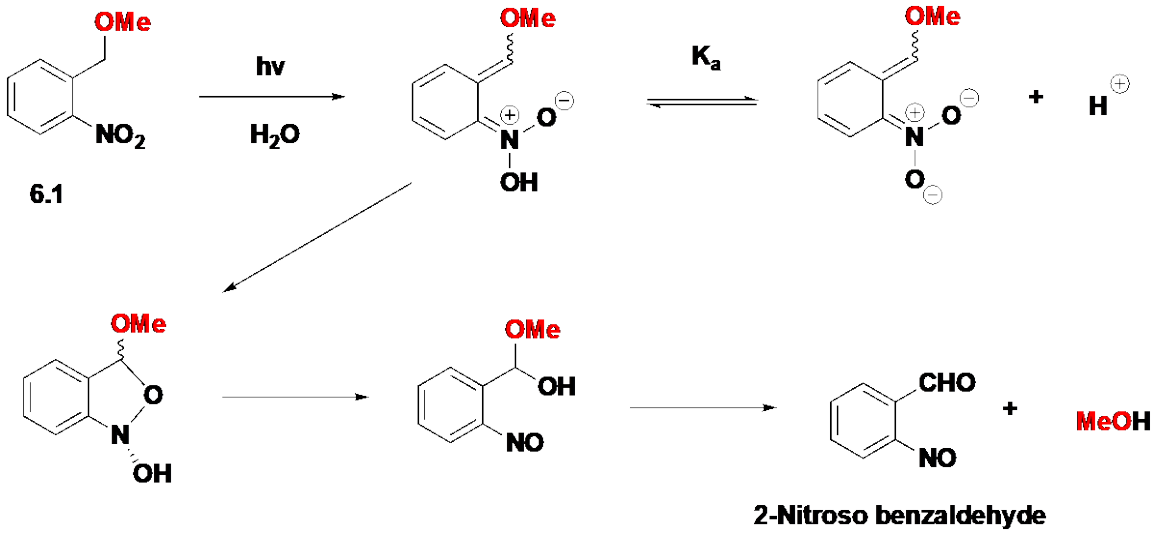

Scheme 6.1 Mechanism of compound 6.1 photoreaction.[139]

6.2. Results and discussion

We chose OA as host and model compounds **6.1, 6.2** and **6.3** are as guest molecules in this chapter (**Figure 6.1**).

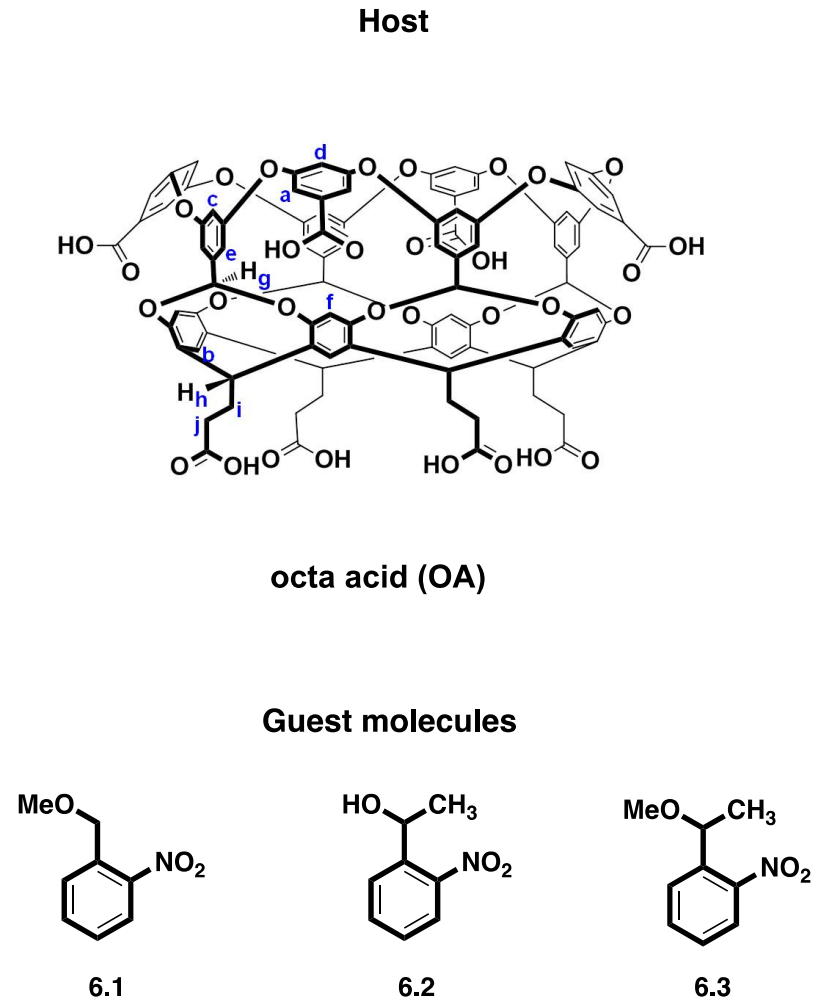

Figure 6.1 Structure of the host OA and guest molecules used in this study.

6.2.1 Absorption spectra of 2-Nitrobenzyl compounds

The model compounds used in this study were synthesized by reported literature.[144] Wirz *et al* have studied these compounds extensively.[145-146] They explained the photochemical reaction mechanisms and formation of intermediates by laser flash photolysis and time-resolved infrared (TRIR) measurements. Irradiation of compound **6.1** and **6.3** releases methanol along with the photoproducts 2-Nitrosobenzaldehyde and 2-Nitroso acetophenone. Compound **6.2** under photoirradiation releases 2-Nitrosoaceotphenone as photoproduct and water as by product. The formation of photoproduct after irradiation with 365 nm light was monitored by UV-Vis absorption spectra. The spectra collected by Wirz group were shown in **Figure 6.2**. We also tried the photoirradition of the model compounds in water and absorption spectra were recorded shown in **Figure 6.3**

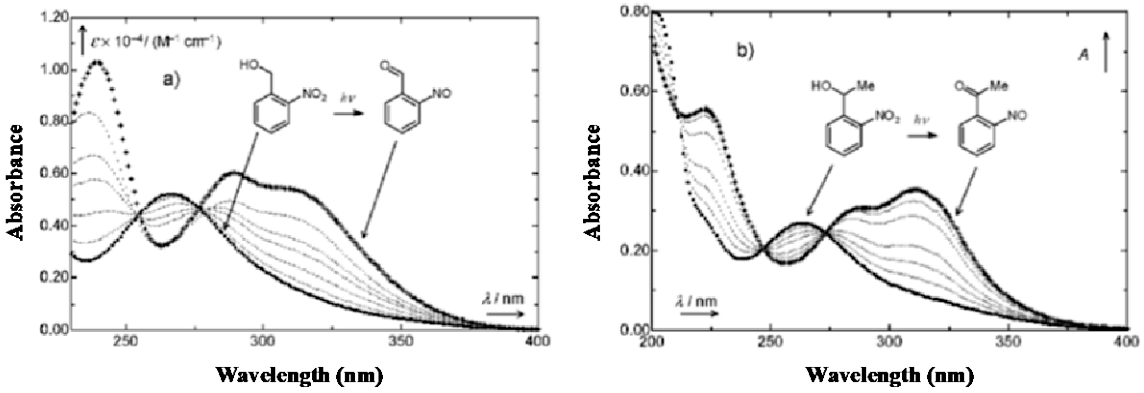

Figure 6.2 Absorption spectra of UV irradiation of ortho-nitro benzyl derivatives.[145]

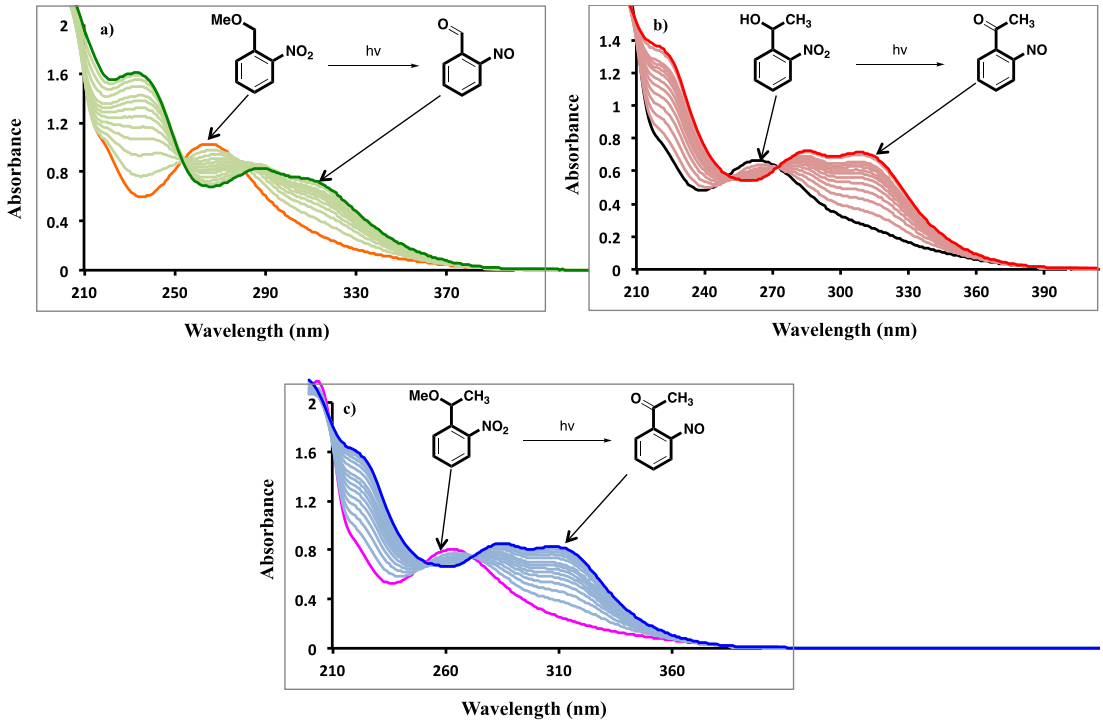

Figure 6.2 Absorption spectra of UV irradiation of synthesized compounds (**6.1,6.2 & 6.3**) in water.

Absorption spectra for our synthesized compounds look exactly similar to reported spectra in literatures.

6.2.2 NMR studies for the complexation of guest molecules

The guest molecules used in this study are smaller in size and we expected it would form 2:2 complex with our host OA. ^{1}H NMR titration spectra of guest molecules are shown in **Figure 6.3, 6.4 & 6.5.** NMR spectra show that all the guest molecules form 2:2 complex with OA. Since the guest molecules are smaller, their dynamics is very fast inside the OA cavity. **Figure 6.4** shows that initial addition of **6.2** shows broad peak in the upfield region (δ -0.2 ppm). This broad peak slowly shifted to downfield from (δ -0.2 to 0.6 ppm) with addition of the guest molecule **6.2** from 0.25 eq to 1.0 eq with respect to 1.0 equiv of OA. We did not observe any shift or change in the host region. This might be due to the equilibrium between 2:1 and 2:2 complexes of 6.2@OA in NMR time scale. **Figure 6.5**

shows that compound **6.3** forms much stronger and cleaner complex than compound **6.1** and **6.2**. We could see sharp peaks in the upfield field region (δ -1.0 ppm) and also sharp OA peaks. 2D-DOSY spectra were also done for the complexes and the corresponding diffusion constants are tabulated in Table 6.1. The values suggested the compounds **6.1,6.2** and **6.3** forms 2:2 complex with OA.

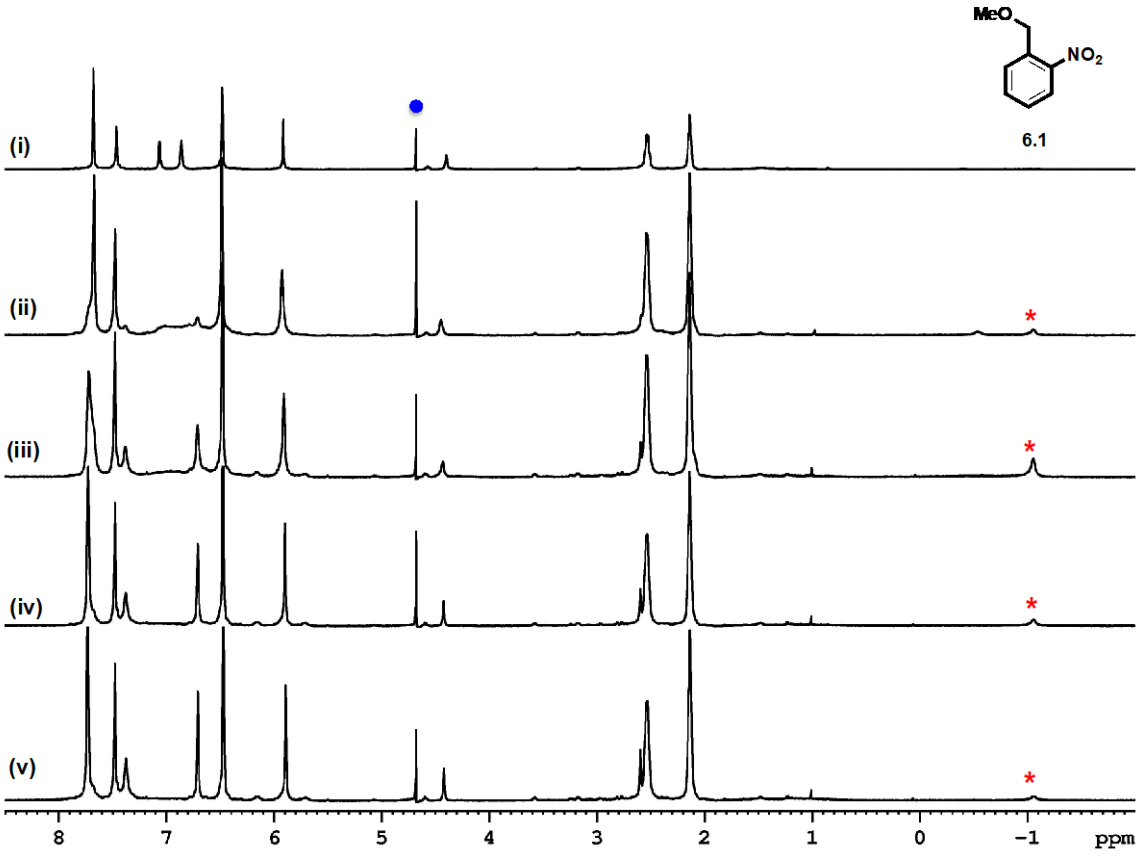

Figure 6.3 ^{1}H NMR (500 MHz) spectra of (i) OA(1 mM) in 10 mM $Na_2B_4O_7$ buffer/D_2O; (ii) **6.1**@OA ([OA] = 1 mM), [**6.1**] = 0.25 mM); (iii) **6.1**@OA ([OA] = 1 mM), [**6.1**] = 0.5 mM); (iv) **6.1**@OA ([OA] = 1 mM), [**6.1**] = 0.75 mM); (v) **6.1**@OA ([OA] = 1 mM), [**6.1**] = 1 mM); "*" indicates the bound guest proton peak and "●"represent the residual D_2O.

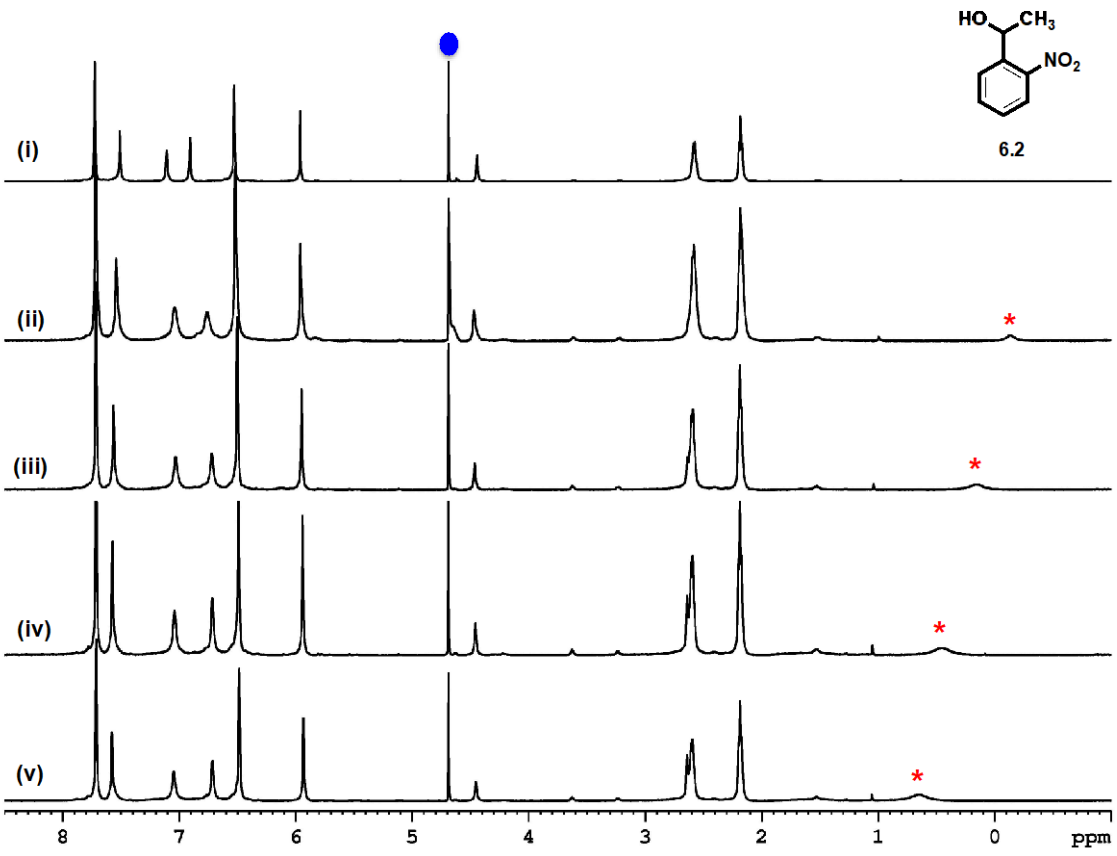

Figure 6.4 ^{1}H NMR (500 MHz) spectra of (i) OA(1 mM) in 10 mM $Na_2B_4O_7$ buffer/D_2O; (ii) **6.2**@OA ([OA] = 1 mM), [**6.2**] = 0.25 mM); (iii) **6.2**@OA ([OA] = 1 mM), [**6.2**] = 0.5 mM); (iv) **6.2**@OA ([OA] = 1 mM), [**6.2**] = 0.75 mM); (v) **6.2**@OA ([OA] = 1 mM), [**6.2**] = 1 mM); "*" indicates the bound guest proton peak and "●"represent the residual D_2O.

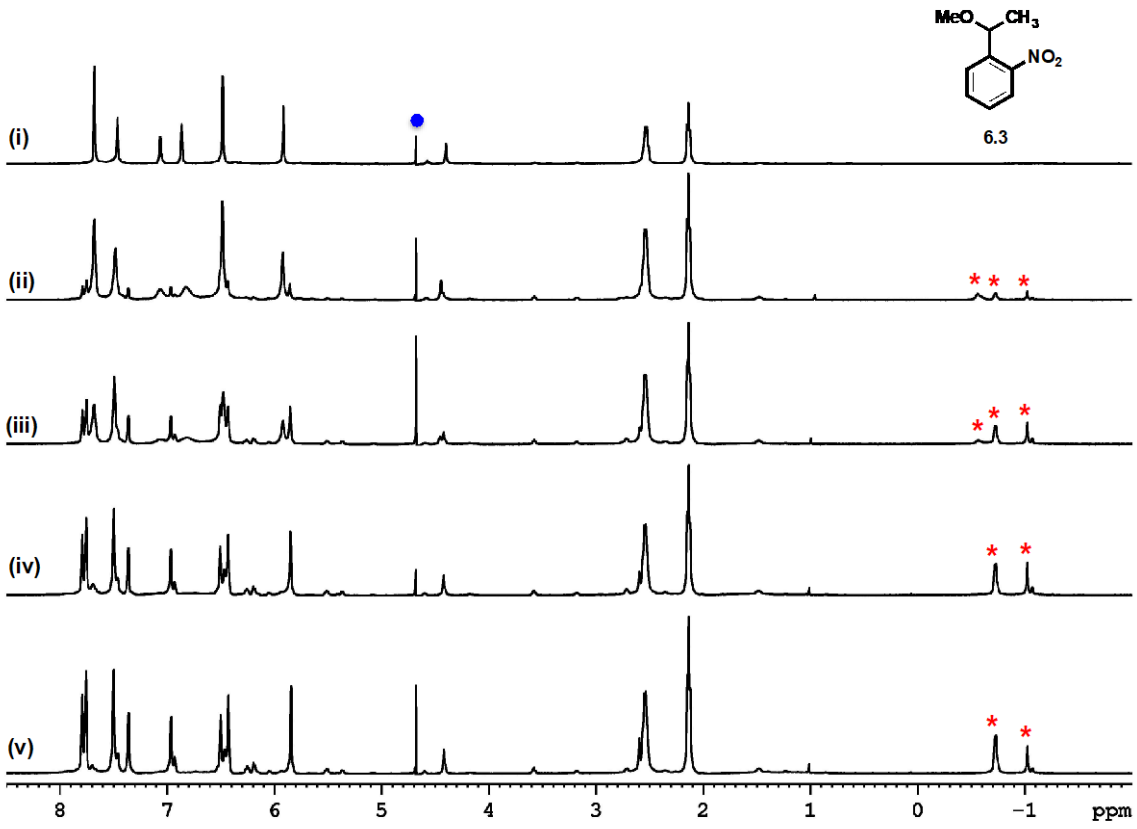

Figure 6.5 ^{1}H NMR (500 MHz) spectra of (i) OA(1 mM) in 10 mM $Na_2B_4O_7$ buffer/D_2O; (ii) **6.3**@OA ([OA] = 1 mM), **[6.3]** = 0.25 mM); (iii) **6.3**@OA ([OA] = 1 mM), [**6.3**] = 0.5 mM); (iv) **6.3**@OA ([OA] = 1 mM), [**6.3**] = 0.75 mM); (v) **6.3**@OA ([OA] = 1 mM), [**6.3**] = 1 mM); "*" indicates the bound guest proton peak and "●"represent the residual D_2O.

Compound	**Diffusion constant (cm^2/s)**
Only OA	1.88×10^{-6}
***Compd-6.1*$_2$@OA_2**	1.30×10^{-6}
***Compd-6.2*$_2$@OA_2**	1.46×10^{-6}
***Compd-6.3*$_2$@OA_2**	1.32×10^{-6}

Table 6.1 Diffusion constant of the complexes.

6.2.3 Photochemistry of complexes by NMR

Photoirradiation of the complexes were done using Luzchem reactor under UV light (360 ± 20 nm) and the formation of the photoproducts were monitored by NMR spectra. ^{1}H NMR spectra were recorded before and after irradiation over a period to see the changes in the complex. **Figure 6.6** shows that there are significant changes observed before and after 30 minutes irradiation and we could also see formation of methanol by NMR spectra. **Figure 6.7** shows slow monitoring of the photoirradition of **6.1$_2$@OA$_2$** under UV light (360 ± 20 nm). We were able to see the disappearance of the encapsulated methoxy proton of the compound **6.1** during the process. Since the photoirradiation would release methanol as the photoproduct along with 2-Nitroso benzaldehyde, we did observe the formation of methanol slowly (**Figure 6.8)**. **Figure 6.9** shows the change in host protons during the photoirradiation. But unfortunately, we could not identify the location of 2-Nitrosobenzaldehyde by NMR.

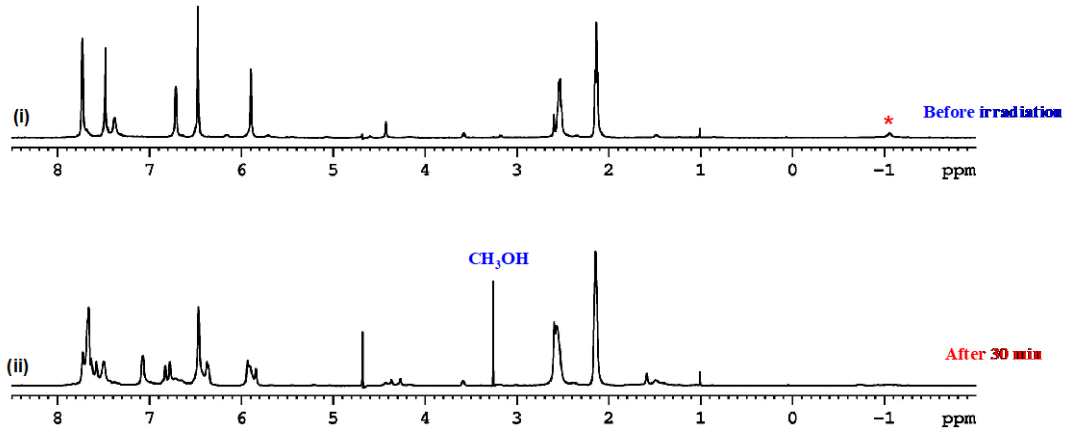

Figure 6.6 ^{1}H NMR (500 MHz) spectra of (i) **6.1$_2$@OA$_2$** before irradiation; (ii) **6.1$_2$@OA$_2$** after 30 min irradiation.

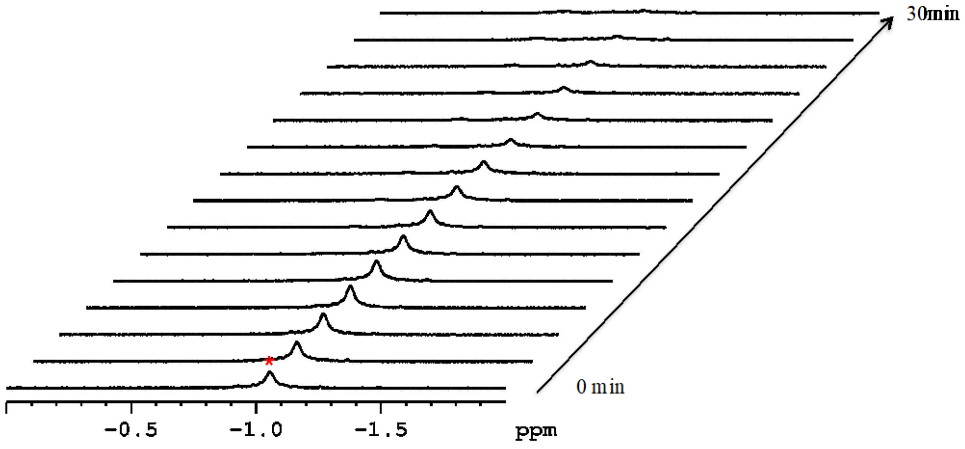

Figure 6.7 Partial ^{1}H NMR (500 MHz) spectra of photoirradiation of **6.1$_2$@OA$_2$** with respect to disappearance of encapsulated proton peak over time.

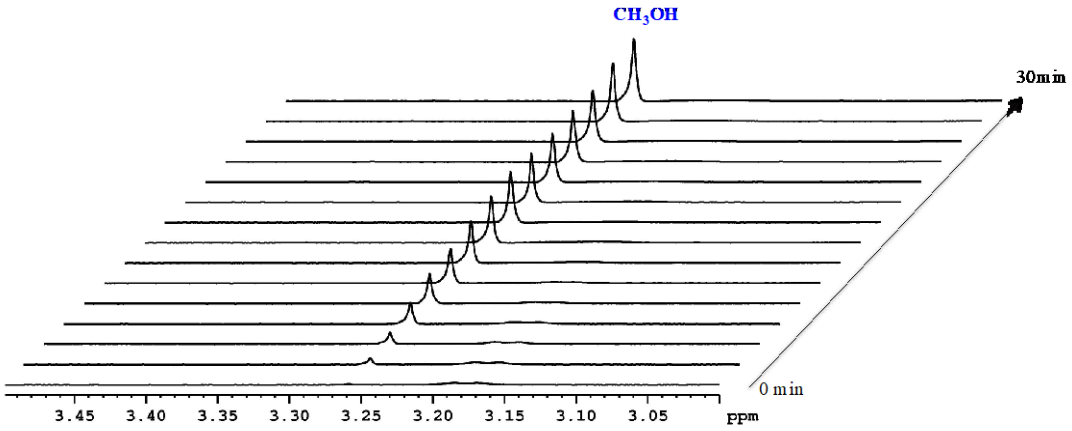

Figure 6.8 Partial ^{1}H NMR (500 MHz) spectra of formation of methanol during photoirradiation of **6.1$_2$@OA$_2$**

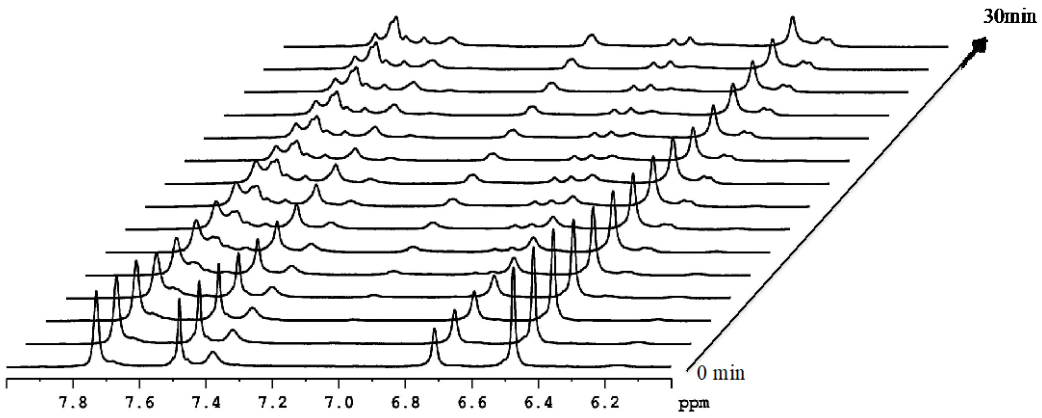

Figure 6.9 Partial ^{1}H NMR (500 MHz) spectra of aromatic region (host peaks) during photoirradiation of **6.1$_2$@OA$_2$**

Complex 6.2_2@OA_2 was also irradiated and monitored by NMR. **Figure 6.10** indicates that there is new peak around (δ -1.0 ppm) was observed after irradiation along with disappearance of the encapsulated peak corresponding to the complex before irradiation. Slow monitoring of the photoirradiation of the complex **6.2_2@OA_2** (**Figure 6.11**) clearly shows that disappearance of the methyl peak and gradual formation of two distinctive peaks initially. At this stage, we were not able to identify the two peaks. However, at the end of irradiation of process, we observed only one broad peak around (δ -1.0 ppm). We believe that this new peak corresponds to methyl proton of 2-Nitroso acetophenone. Since the byproduct for photoirradiation of this complex 6.2_2@OA_2 is water, we did not observe any other peaks by NMR.

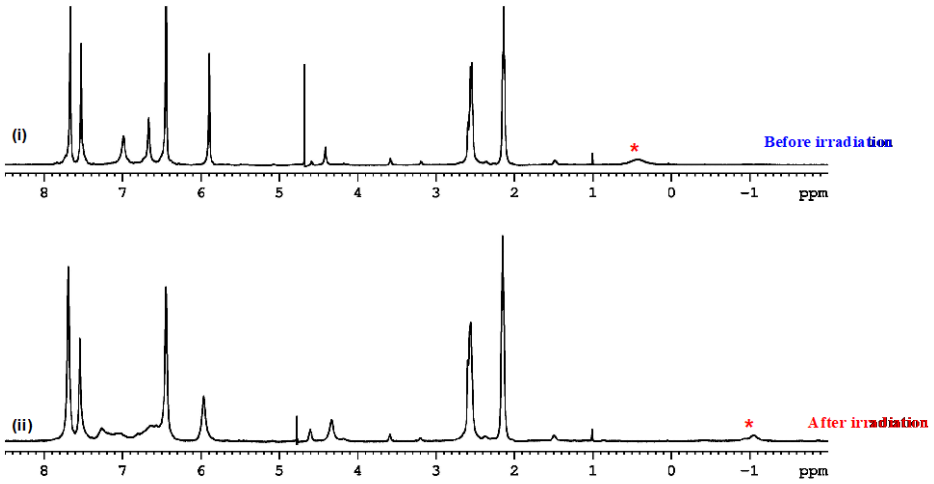

Figure 6.10 ^{1}H NMR (500 MHz) spectra of (i) **6.2_2@OA_2** before irradiation; (ii) **6.2_2@OA_2** after 30 min irradiation.

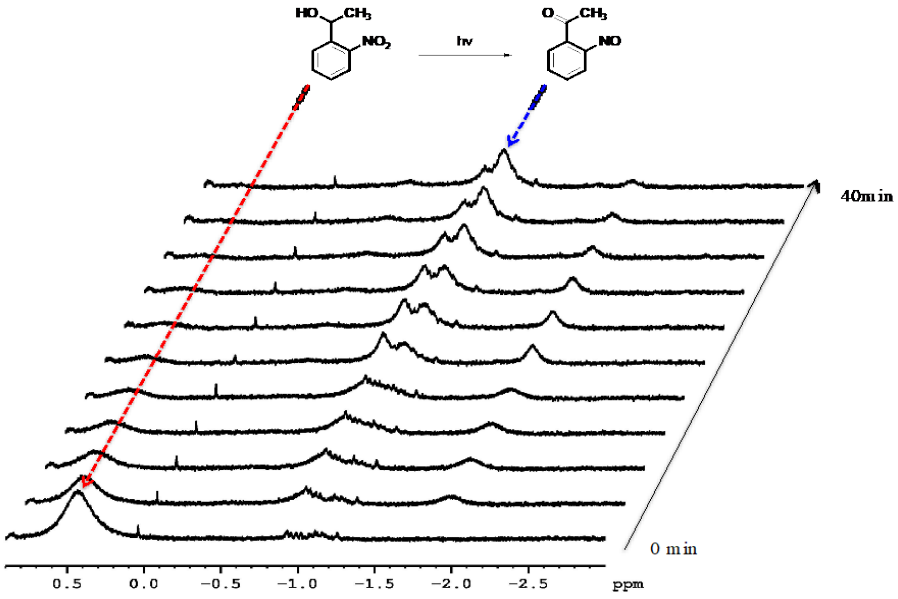

Figure 6.11 Partial ^{1}H NMR (500 MHz) spectra of photoirradiation of **6.2$_2$@OA$_2$**

When we irradiate the **6.2$_2$@OA$_2$** complex, NMR shows disappearance of sharp encapsulated peak and appear of very weak broad peak in the upfield region (δ -1.6 ppm) (**Figure 6.12).** Slow monitoring by partial NMR spectra clearly shows the appearance of broad peaks (**Figure 6.13**). We were also able to monitor the formation of photoproduct methanol during the irradiation process by NMR. The new peak observed in the upfield region might be encapsulated 2-Nitroso acetophenone photoproduct.

NMR studies clearly shows the photoproducts formed during the phototriggering 2-Nitro benzyl model compounds within OA remains inside the cavity. But we could not characterize the observed new peaks. We did mass spectrometry studies to identify whatever the product formed is our expected nitroso derivative or not. LCMS experiment and the details are discussed in the later section.

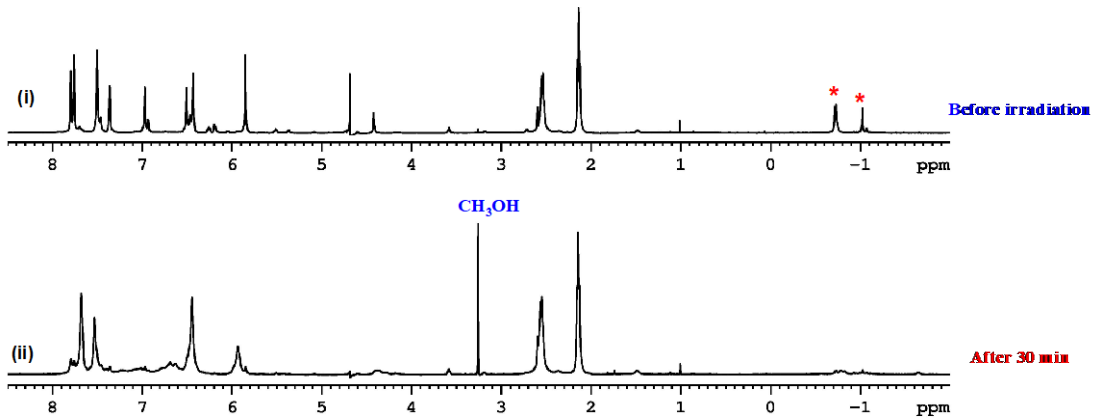

Figure 6.12 ^{1}H NMR (500 MHz) spectra of (i) **6.3$_2$@OA$_2$** before irradiation; (ii) **6.3$_2$@OA$_2$** after 30 min irradiation.

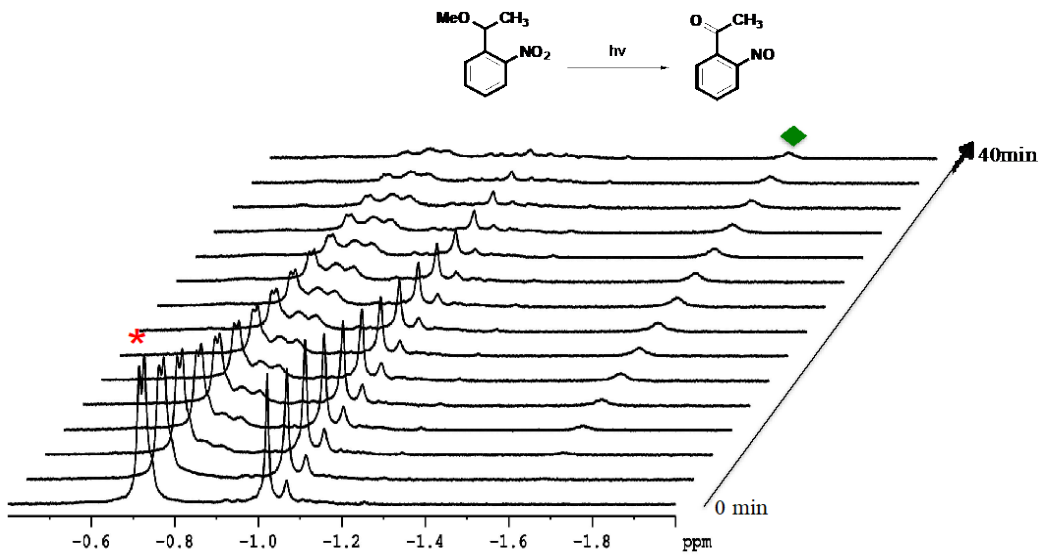

Figure 6.13 Partial ^{1}H NMR (500 MHz) spectra of photoirradiation of **6.3$_2$@OA$_2$**

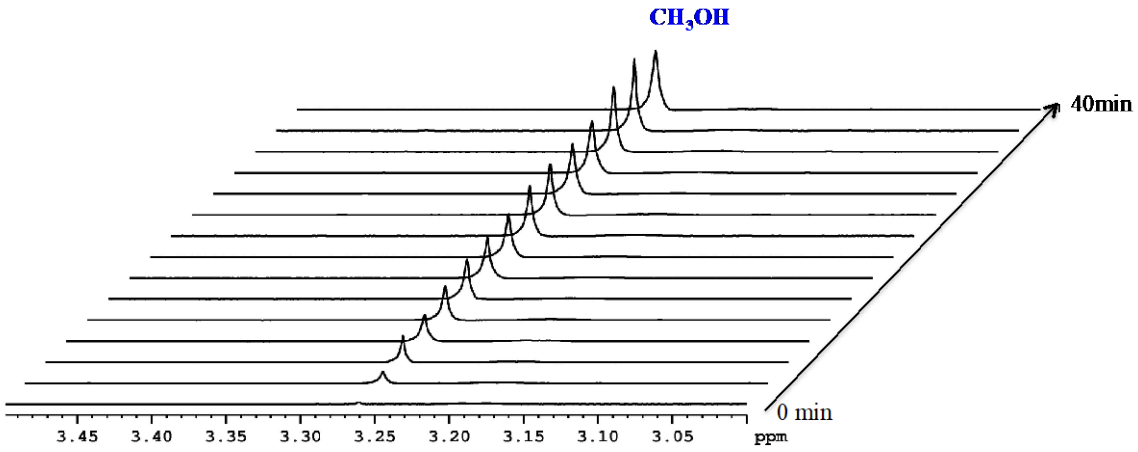

Figure 6.14. Partial ^{1}H NMR (500 MHz) spectra of formation of methanol during photoirradiation of **6.3$_2$@OA$_2$**

6.2.4 Photoirradiation monitored by absorption spectra

We carried out absorption studies to follow the photoirradiation of complexes. Absorption spectra recorded for the complexes before irradiation and irradiated at regular interval using UV light (360 ± 20 nm). The absorption spectra for each radiation is recorded and shown in **Figure 6.15**. **Figure 6.15b and 6.15 c** insets clearly showed that increase of absorbance band around 320 nm, which is due to the formation of nitroso photoproduct inside the cavity. We also observed slight red shift of OA peaks which also indicates there is formation of new product inside the cavity.

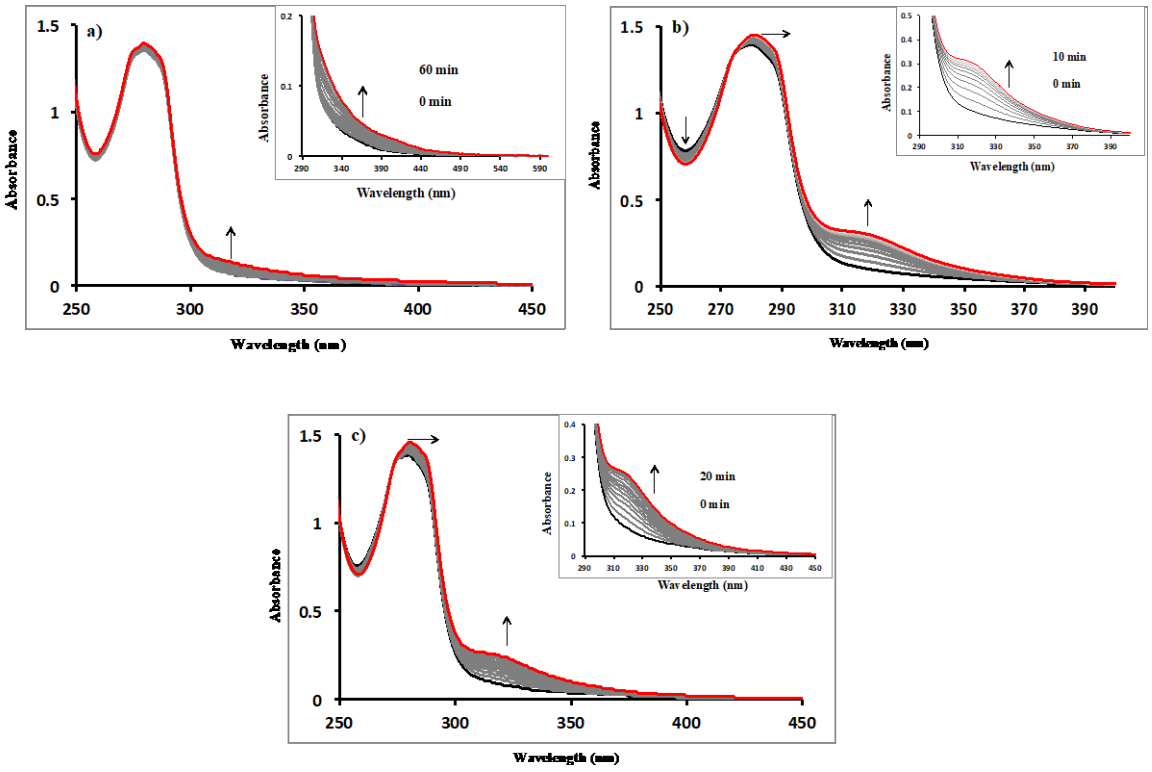

Figure 6.15 Absorption spectra for the photoirradiation of the complexes a) **6.1**$_2$**@OA**$_2$; b) **6.2**$_2$**@OA**$_2$**;** c) **6.3**$_2$**@OA**$_2$.

6.2.5 Analysis of photoproducts by mass spectroscopy

We analyzed the photoreaction and formation of photoproducts using Liquid chromatography (LC) coupled with a diode array detector (DAD). The nitroso photoproducts were confirmed by LC-MS , GC-MS spectra and UV-Vis spectra. Upon UV irradiation, LC traces were recorded and corresponding LC –MS were analyzed. The LC-DAD and LC-MS traces for **6.2@OA$_2$** is shown in **Figure 6.17**. The nitroso photoproduct (2-nitroso acetophenone) formed during the photoirradiation was clearly observed in LC-DAD traces. LC-MS corresponding the new peak (6.67 min) formed after irradiation matches with $[M+H]^+$ of the nitroso product **Figure 6.17**. The UV-Vis spectrum extracted for the new peak (6.67 min) matches with the reported 2-nitroso acetophenone photoproduct **Figure 6.17**. This result confirmed that the formation of nitroso photoproducts of nitro triggers inside OA. Similarly, we observed the formation of 2-nitroso acetophenone when **6.3@OA$_2$** undegoes photoreaction with UV light. The results LC-DAD and LC-MS traces are shown in **Figure 6.18.** Electron impact (EI) and ESI-MS^2 spectra for the nitroso photoproduct (2-nitros acetophenone) shown in **Figure 6.20.** Irradiation of **6.3@OA$_2$** forms new peak in the very low intensity LC-traces and the corresponding mass show m/Z peak of 271 which is the dimer of formed 2-nitroso benzaldehyde. We were not able to see any distinct peak for 2-nitrosobenzaldehyde by LC-DAD trace and UV-Vis spectrum **Figure 6.16**. We believe that there is formation of 2-nitroso benzaldehyde during photoirradiation which is unstable and reactive in this condition. 2-nitroso benzaldehyde immediately reacts to form dimer inside the cavity. At this stage, we are not able to confirm our prediction. We performed the irradiation of **6.1**

in acetonitrile and confirmed the formation of 2-nitrosobenzaldehyde by Electron impact and ESI-MS^2 spectra (**Figure 6.19).**

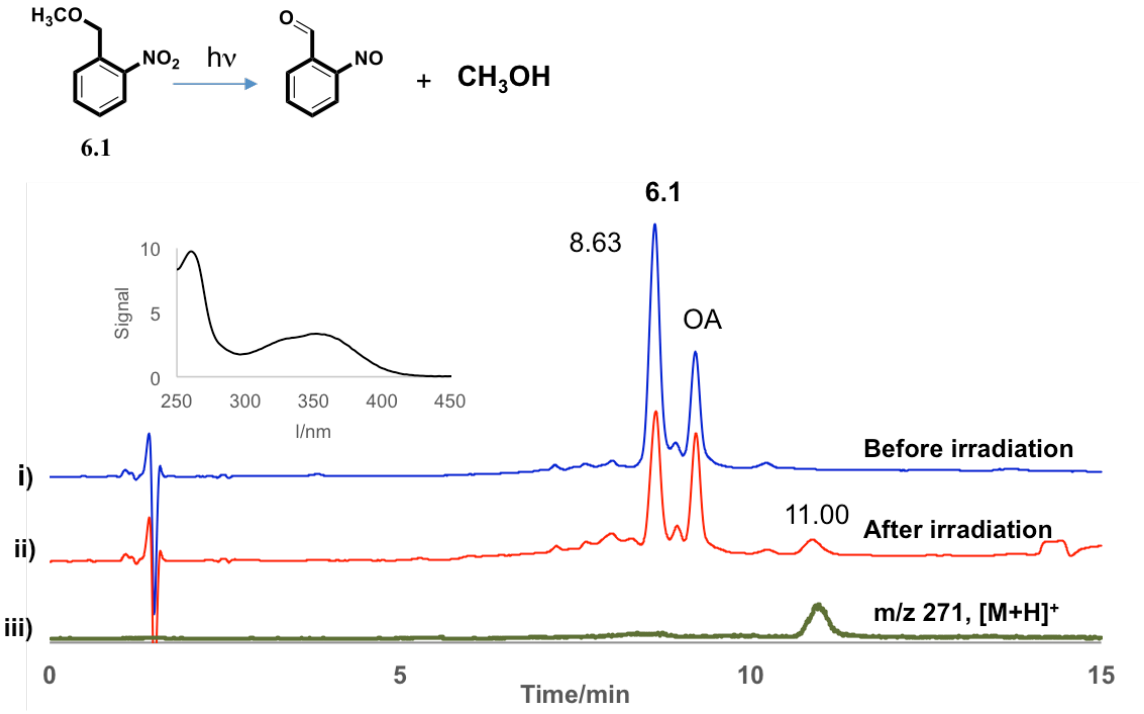

Figure 6.16 LC−DAD and LC−MS traces of **6.1**@OA (0.5 mM : 1 mM) in borate buffer (10 mM). (i) LC−DAD trace at 320 nm before irradiation, (ii) LC−DAD trace at 320 nm after 2 minutes irradiation (λ > 300 nm), (iii) single ion trace at m/z 271, assigned to $[M + H]^+$ of dimer of 2-nitrosobenzaldehyde. The insert shows the UV spectrum of compound with 11.00 minutes retention time.

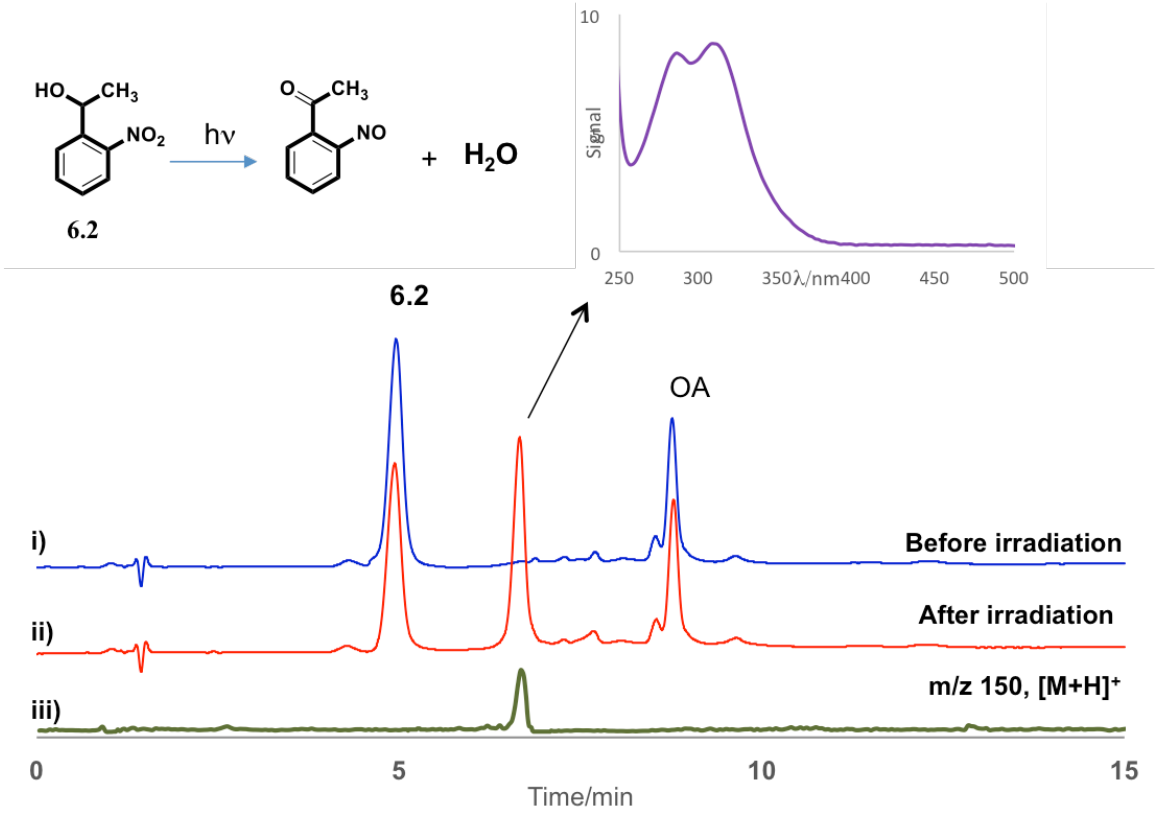

Figure 6.17 LC−DAD and LC−MS traces of **6.2**@OA (0.5 mM : 1 mM) in borate buffer (10 mM). (i) LC−DAD trace at 320 nm before irradiation, (ii) LC−DAD trace at 320 nm after 2 minutes irradiation (λ > 300 nm), (iii) single ion trace at m/z 150, assigned to $[M + H]^+$ of 2-nitroso acetophenone. The insert shows the UV spectrum of compound with 6.67 minutes retention time.

.

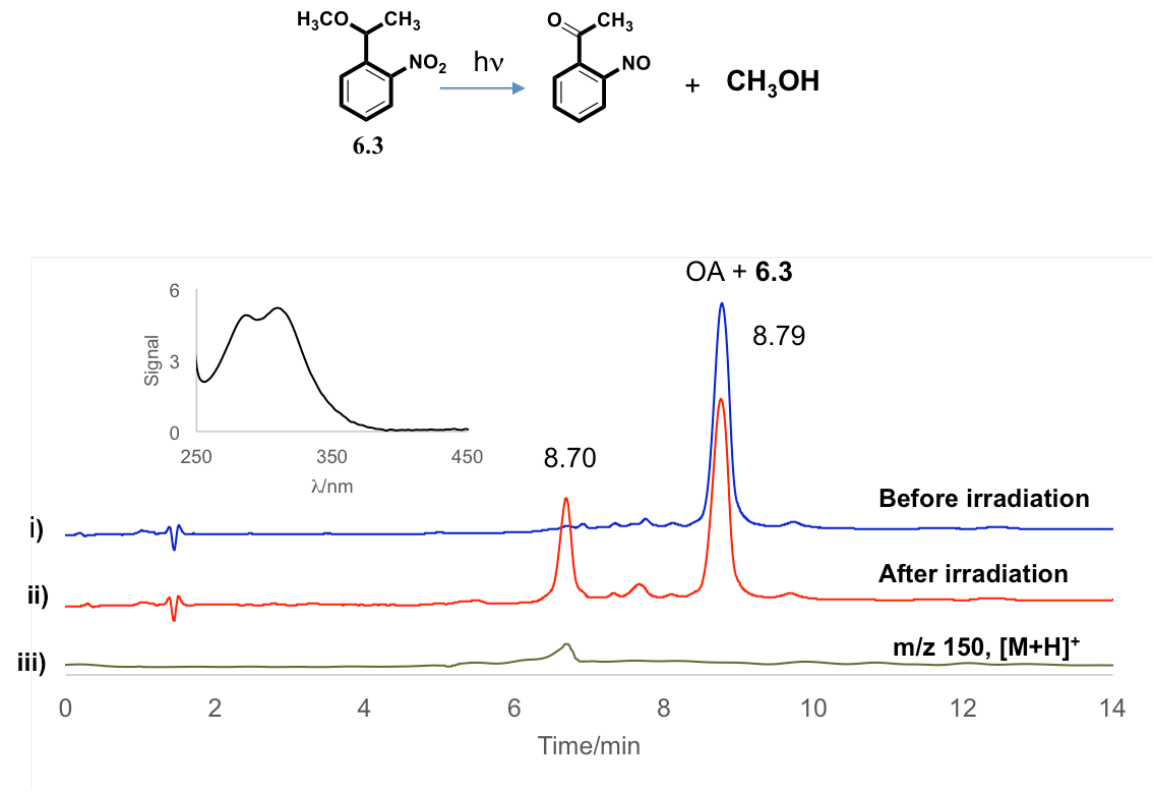

Figure 6.18 LC−DAD and LC−MS traces of **6.3**@OA (0.5 mM : 1 mM) in borate buffer (10 mM). (i) LC−DAD trace at 320 nm before irradiation, (ii) LC−DAD trace at 320 nm after 2 minutes irradiation (λ > 300 nm), (iii) single ion trace at m/z 150, assigned to $[M + H]^+$ of 2-nitroso acetophenone. The insert shows the UV spectrum of compound with 8.70 minutes retention time.

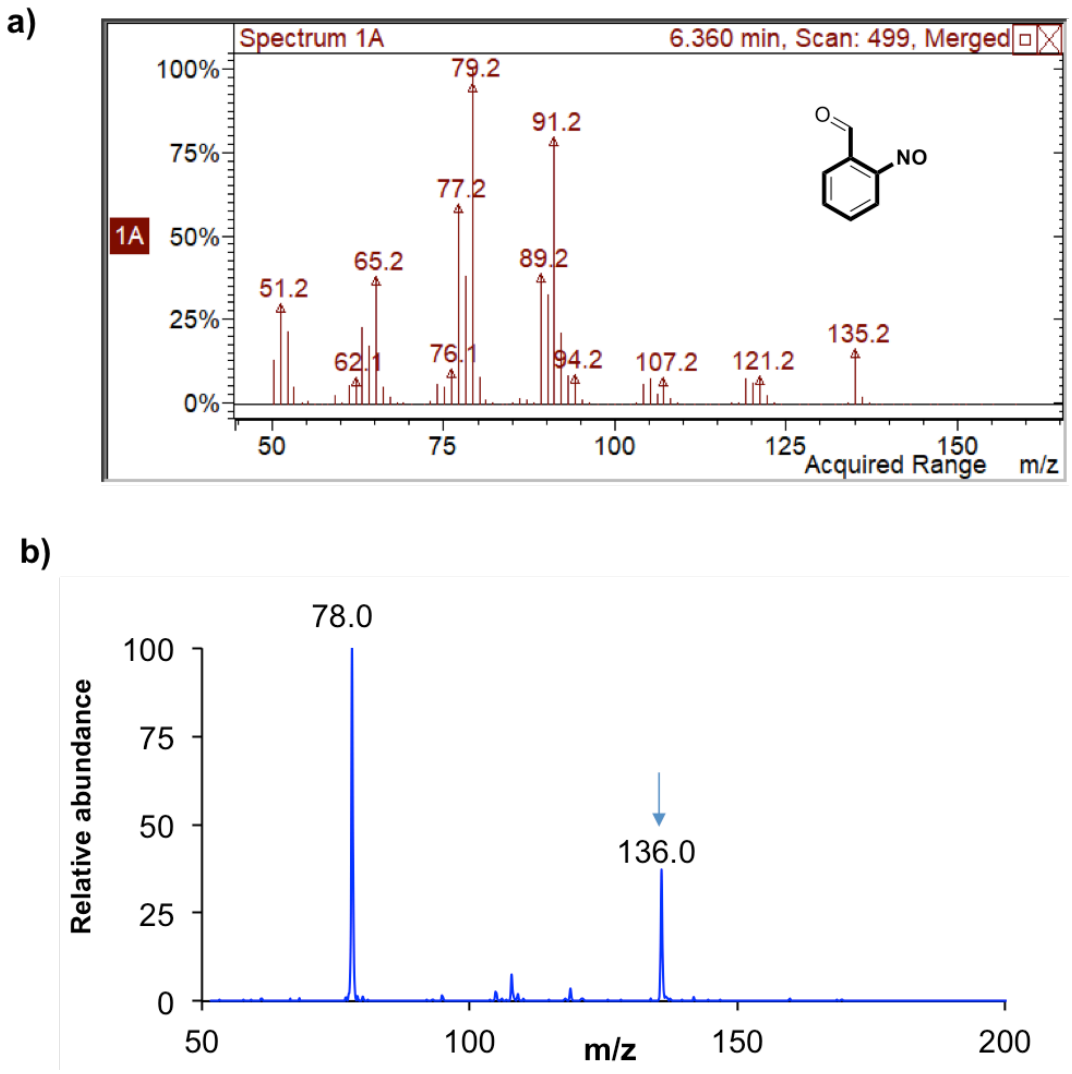

Figure 6.19. EI (electron impact), a), and ESI-MS^2, b), of 2-nitrosobenzaldehyde.

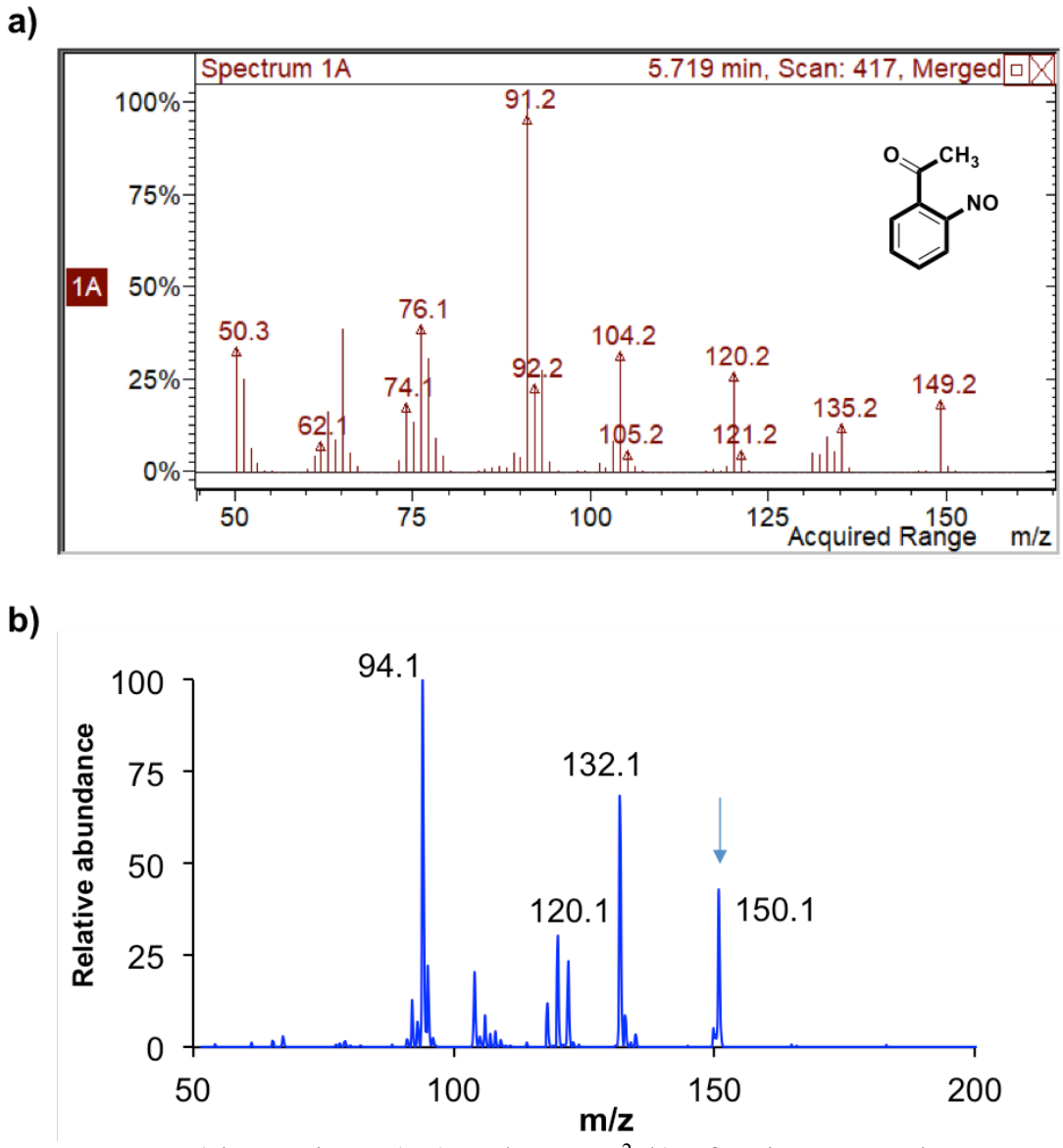

Figure 6.20. EI (electron impact), a), and ESI-MS^2, b), of 2-nitrosoacetophenone.

6.3 Conclusion

In this chapter, we have explained the photoirradiation of 2-Nitrobenzyl derivatives inside OA cavity. NMR studies showed that toxic nitroso photoproducts during the irradiation process were trapped inside OA capsule. We also able to monitored the formation of other biproducts like methanol by NMR. Liquid chromatography studies also confirmed the formation of nitrosoproduct during the photoirradiation. We believe that our supramolecular approach would be useful to release the wanted drug molecule to the target and trap the unwanted or toxic photoproducts.

6.4. Experimental section

Materials and Methods

The host Octa acid was synthesized following published procedure.[32] Guest molecules 6.1, 6.2 and 6.3 were synthesized using the following literature procedure.

General Procedure for guest binding studies probed by NMR

A D_2O stock solution (600 μL) of host OA (1 mM) and sodium borate buffer (10 mM) taken in a NMR tube was titrated with the guest by sequential addition of 0.25 eq of guest (2.5 μL of a 60 mM solution in $DMSOd_6$). The complexation was achieved by shaking the NMR tube for about five minutes. ^1H NMR spectra were recorded at room temperature under aerated conditions on a Bruker 500 MHz NMR. 2:2 complex was achieved by 10 μL of guest solution to 600 μL of 1 mM OA host in 10 mM buffer. This complexes were irradiated with a Luzchem research reactor, UV(Hitachi-FL-8BL-B, 365 nm).

Sample preparation for the photochemical reactions

600 μL of the complex solution was diluted to 6 mL to give the stock solution. The concentration of host and the guest molecules are [OA = 10^{-4} M], [guest = 5 x 10^{-5} M] respectively. For UV-Vis studies, the samples were irradiated with a Luzchem research reactor , UV(Hitachi-FL-8BL-B, 365 nm).

Sample preparation for photochemical studies of products by liquid chromatography (LC) coupled to a diode array detector (DAD) and to a mass spectrometer (MS), LC-DAD-MS and ESI-MS^2

Irradiation of **6.1-6.3** @OA complexes was carried out in air equilibrated aqueous solutions of Na_2B4O_7 (10 mM, pH = 8.7) containing 100 μM of the guest and 200 μM of the host. Other concentrations of guest and host, specifically 250 μM:500 and 500 μM:1000 μM (guest-host) were also tested. Compounds **6.1-6.3** were also irradiated in acetonitrile (100 μM). For comparison purposes **6.1**(250 □M) was also irradiated an acetonitrile-buffer solution (50:50). The irradiations were performed using a high-pressure xenon lamp in conjunction with a water filter to prevent heating of the sample solution. An additional Pyrex filter was inserted to remove UV light below 300 nm.

Identification and quantification studies of non-irradiated and irradiated samples by LC-DAD-MS and ESI-MS^2

Photoproducts of compounds **6.1-6.3** in acetonitrile and **6.1-6.3** @OA complexes were followed by LC-DAD with UV analysis at 280, 320, 350, 380 nm and by LC-MS under positive polarity. The identification of nitroso products was based on the UV absorbance spectra, on the m/z value under positive polarity (LC-MS traces) and on the fragmentation patterns obtained under ESI-MS^2. ESI-MS^2 spectra were obtained by infusing (direct

injection) the irradiated solutions in acetonitrile. The presence of nitroso compounds was further confirmed by GC-MS and analysis of the obtained electron impact (EI) spectra. Quantitative analyses of trigger compounds **6.1-6.3** was performed using calibrations curves prepared from DAD traces obtained at 280 nm. The non-irradiated and irradiated solutions were directly analyzed by LC-DAD-MS without further processing.

LC-DAD-MS analysis conditions

The LC-DAD-MS analyses were performed using an Agilent Technologies 1200 Series LC, equipped with a diode array detector and coupled to a Bruker Daltonics HCT ultra. The mobile phase comprises acetonitrile (A) and water (B), both with 0.1 % of formic acid, and ethyl acetate (C). The gradient started with 52 % of A, 38 % of B and 10 % of C. The mobile phase composition was changed to 2 % of A, 73 % of B and 25 % of C in 5 minutes and kept at this composition for an additional 7 minutes. Finally, the system was allowed to return to the initial mobile phase composition (52 % of A, 38 % of B and 10 % of C) in 1 min and then stabilized for additional 5 minutes before the next run. The flow was 0.35 ml/min. An Agilent PLRP-S LC column (15.0 cm length, 2.1 mm internal diameter, 5 µm), stabilized at 25 °C was used. Typical mass spectral conditions used under LC-DAD-MS were as follows: capillary voltage, -4.0 kV; capillary exit voltage (CE), 75 V; skimmer voltage, 40 V; drying gas, 320 ºC at 8 L/min; nebulizer gas pressure, 45 psi.

The ESI-MS^2 spectra were obtained using the above described mass spectrometer by infusing the acetonitrile solutions using a syringe pump (KdScientific, model 781100, USA). Typical experimental conditions were as follows: capillary voltage, -3.5 kV;

capillary exit voltage (CE), 75 V; skimmer voltage, 40 V; drying gas, 300 ºC at 5 L/min; nebulizer gas pressure, 20 psi.

GC-MS analysis conditions

The GC-MS analyses were performed using a Bruker SCION 456 GC TQ (Triple Quadrupole) system. A ZB-5MS capillary column with 30 m length, 0.25 mm internal diameter and 0.25 □m of film thickness was used. The program of temperatures started at 45 ºC, hold for 1 min, and then raised at 25 ºC/min up to 250 ºC, which was kept for additional 4.8 min. The injection temperature was 250 ºC and the ion source was kept at 200 ºC. The injected volume was 1 □L

References

1. Pedersen, C. J., *J. Am. Chem. Soc.* **1967,** *89*, 2495-2496.

2. Pedersen, C. J., *J. Am. Chem. Soc.* **1967,** *89*, 7017-7036.

3. Cram, D. J.; Cram, J. M., *Science* **1974,** *183*, 803-809.

4. Lehn, J.-M., *Supramolecular Chemistry: Concepts and Perspectives*. VCH: Weinheim, 1995.

5. Lehn, J. M., *Acc. Chem. Res.* **1978,** *11*, 49-57.

6. Lehn, J. M., *Pure Appl. Chem.* **1994,** *66*, 1961-1966.

7. Lehn, J. M., *Angew. Chem. Int. Ed.* **1988,** *27*, 89-112.

8. Lehn, J. M., *Science* **1985,** *227*, 849-856.

9. Cram, D. J., *Science* **1983,** *219*, 1177-1183.

10. Cram, D. J., *Angew. Chem. Int. Ed.* **1986,** *25*, 1039-1057.

11. Cram, D. J., *Angew. Chem. Int. Ed.* **1988,** *27*, 1009-1020.

12. Cram, D. J.; Cram, J. M., In *Container Molecules and Their Guests*, Cram, D. J.; Cram, J. M., Eds. The Royal Society of Chemistry: 1997; pp 20-48.

13. Varshey, D. B.; Sander, J. R.; Friščić, T., *Supramolecular Interactions*. John Wiley & Sons, Ltd.,: 2012.

14. Steed, J. W.; Atwood, J. L., *Supramolecular Chemistry*. 2nd ed.; Wiley: 2009.

15. Ghadiri, M. R.; Granja, J. R.; Milligan, R. A.; McRee, D. E.; Khazanovich, N., *Nature* **1993,** *366*, 324-327.

16. Anslyn, E. V.; Dougherty, D. A., *Modern Physical Organic Chemisry*. University Science Books: 2006.

17. Ben-Amotz, D., *Annu. Rev. Phys. Chem.* **2016,** *67*, 617-638.

18. Bakker, H. J., *Nature* **2012,** *491*, 533-534.

19. Blokzijl, W.; Engberts, J. B. F. N., *Angew. Chem. Int. Ed.* **1993,** *32*, 1545-1579.

20. Szejtli, J., *Chem. Rev.* **1998,** *98*, 1743-1754.

21. Villalonga, R.; Cao, R.; Fragoso, A., S.*Chem. Rev.* **2007,** *107*, 3088-3116.

22. Hu, Q.-D.; Tang, G.-P.; Chu, P. K., *Acc. Chem. Res.* **2014,** *47*, 2017-2025.

23. Freeman, W. A.; Mock, W. L.; Shih, N. Y., *J. Am. Chem. Soc.* **1981,** *103*, 7367-7368.

24. Barrow, S. J.; Kasera, S.; Rowland, M. J.; del Barrido, J.; Scherman, O. A., *Chem. Rev.* **2015,** *115*, 12320-12406.

25. Timmerman, P.; Verboom, W.; Reinhoudt, D. N., *Tetrahedron* **1996,** *52*, 2663-2704.

26. MacGillivray, L. R.; Atwood, J. L., *Nature* **1997,** *389*, 469-472.

27. Shivanyuk, A.; Rebek Jr, J., *Proc. Natl. Acad. Sci. U. S. A.* **2001,** *98*, 7662-7665.

28. Palmer, L. C.; Shivanyuk, A.; Yamanaka, M.; Rebek Jr, J., *Chem. Commun.* **2005**, 857-858.

29. Evan-Salem, T.; Baruch, I.; Avram, L.; Cohen, Y.; Palmer, L. C.; Rebek Jr, J., *Proc. Natl. Acad. Sci. U. S. A.* **2006,** *103*, 12296-12300.

30. Avram, L.; Cohen, Y., *J. Am. Chem. Soc.* **2002,** *124*, 15148-15149.

31. Cram, D. J.; Karbach, S.; Kim, Y. H.; Baczynskyj, L.; Kallemeyn, G. W., *J. Am. Chem. Soc.* **1985,** *107*, 2575-2576.

32. Gibb, C. L. D.; Gibb, B. C., *J. Am. Chem. Soc.,* **2004,** *126*, 11408-11409.

33. Ramamurthy, V., *Acc. Chem. Res.* **2015,** *48*, 2904−2917.

34. Porel, M.; Jayaraj, N.; Kaanumalle, L. S.; Maddipatla, M. V. S. N.; Parthasarathy, A.; Ramamurthy, V., *Langmuir* **2009,** *25*, 3473-3481.

35. Parthasarathy, A.; Kaanumalle, L. S.; Ramamurthy, V., *Org. Lett.* **2007,** *9* (24), 5059-5062.

36. Porel, M.; Jockusch, S.; Parthasarathy, A.; Rao, V. J.; Turro, N. J.; Ramamurthy, V., *Chem. Commun.,* **2012,** *48* (21), 2710-2712.

37. Ramamurthy, V.; Jockusch, S.; Porel, M., *Langmuir* **2015,** *31*, 5554-5570.

38. Kamatham, N.; Da Silva, J. P.; Givens, R. S.; Ramamurthy, V., *Org, Lett.* **2017,** *19*, 3588-3591.

39. Jagadesan, P.; Da Silva, J. P.; Givens, R. S.; Ramamurthy, V., *Org, Lett.* **2015,** *17*, 1276-1279.

40. Jayaraj, N.; Jagadesan, P.; Samanta, S. R.; Da Silva, J. P.; Ramamurthy, V., *Org, Lett.* **2013,** *15*, 4374-4377.

41. Vriezema, D. M.; Aragones, M. C.; Elemans, J.; Cornelissen, J.; Rowan, A. E.; Nolte, R. J. M., *Chem. Rev.* **2005,** *105*, 1445-1489.

42. Kolbenz, T. S.; Wassenaar, J.; Reek, J. N. H., *Chem. Soc. Rev.* **2008,** *37*, 247-262.

43. Catti, L.; Zhang, Q.; Tiefenbacher, K., *Synthesis* **2016**, 313-328.

44. Liu, S.; Gibb, B. C., *Chem. Commun.* **2008**, 3709.

45. Mal, P.; Breiner, B.; Rissanen, K.; Nitschke, J. R., *Science* **2009,** *324*, 1697-1699.

46. Riddell, I. A.; Smulders, M. M. J.; Clegg, J. K.; Nitschke, J. R., *Chem. Commun.* **2011,** *47*, 457-459.

47. Meng, W. J.; Breiner, B.; Rissanen, K.; Thoburn, J. D.; Clegg, J. K.; Nitschke, J. R., *Angew. Chem. Int. Ed.* **2011,** *50*, 3479-3483.

48. Ma, Z. B.; Moulton, B., *Coord. Chem. Rev.,* **2011,** *255*, 1623-1641.

49. Tong, R.; Hemmati, H. D.; Langer, R.; Kohane, D. S., *J. Am. Chem. Soc.* **2012,** *134*, 8848-8855.

50. Kammona, O.; Kiparissides, C., *J. Controlled Release* **2012,** *161*, 781-794.

51. Wu, Z. L.; Song, N.; Menz, R.; Pingali, B.; Yang, Y. W.; Zheng, Y. B., *Nanomedicine* **2015,** *10*, 1493-1514.

52. Wang, M.; Vajpayee, V.; Shanmugaraju, S.; Zheng, Y. R.; Zhao, Z. G.; Kim, H.; Mukherjee, P. S.; Chi, K. W.; Stang, P. J., *Inorg. Chem.,* **2011,** *50*, 1506-1512.

53. Davis, A. P., *Org. Biomol. Chem.,* **2009,** *7*, 3629-3638.

54. Clement, P.; Korom, S.; Struzzi, C.; Parra, E. J.; Bittencourt, C.; Ballester, P.; Llobet, E., *Adv. Funct. Mater.,* **2015,** *12*, 4011-4020.

55. Dube, H.; Ajami, D.; Rebek, J., Jr., *Angew. Chem. Int. Ed.* **2010,** *49*, 3192-3195.

56. Dube, H.; Ams, M. R.; Rebek, J., Jr., S*J. Am. Chem. Soc.,* **2010,** *132* (29), 9984-9985.

57. Furukawa, H.; Cordava, K. E.; O'Keeffe, M.; Yaghi, O. M., *Science* **2013,** *341*, 1-12.

58. Moshoeshoe, M.; Nadiye-Tabbiruka, M. S.; Obuseng, V., *American Journal of Materials Science* **2017,** *7*, 196-221.

59. Del Valle, E. M. M., *Process Biochemistry* **2004,** *39* (9), 1033-1046.

60. Barrwo, S. J.; Kasera, S.; Rowland, M. J.; del Barrio, J.; Scherman, O. A., *Chem. Rev.* **2015,** *115* (22), 12320-12406.

61. Diaz-Moscoso, A.; Ballester, P., *Chem. Commun.* **2017,** *53*, 4635-4652.

62. Klajn, R., *Chem. Soc. Rev.,* **2014,** *43*, 143-184.

63. Kohl-Landgraf, J.; Braun, M.; Ozcoban, C.; Goncalves, D. P. N.; Heckel, A.; Wachtveitl, J., *J. Am. Chem. Soc.* **2012,** *134*, 14070-14077.

64. Santos, C. S.; Miller, A. C.; Pace, T. C. S.; Morimitsu, K.; Bohne, C., *Langmuir* **2014,** *30* (38), 11319-11328.

65. Sunamoto, J.; Iwamoto, K.; Akutagawa, M.; Nagase, M.; Kondo, H., *J. Am. Chem. Soc.* **1982,** *104* (18), 4904-4907.

66. Ikeda, S.; Saso, Y., *Colloids Surf.* **1992,** *67*, 21-27.

67. Ishiwatari, T.; Kondo, T.; Mitsuishi, M., P*Colloid Polym. Sci.* **1996,** *274* (10), 1000-1005.

68. Iyengar, S.; Biewer, M. C., *Cryst. Growth Des.* **2005,** *5* (6), 2043-2045.

69. Tamaki, T.; Sakuragi, M.; Ichimura, K.; Aoki, K.; Arima, I., *Polym. Bull.* **1990,** *24*, 559-564.

70. Miskolczy, Z.; Biczok, L., *J. Phys. Chem. B* **2011,** *115*, 12577-12583.

71.Miskolczy, Z.; Biczok, L., *Photochem. Photobiol.* **2012,** *88*, 1461-1466.

72. Miskolczy, Z.; Biczok, L., *J. Phys. Chem. B* **2013,** *117*, 648-653.

73. Gorner, H., *Phys. Chem. Chem. Phys.* **2001,** *3*, 416-423.

74. Gorner, H., *Chem. Phys. Lett.* **1998,** *282*, 381-390.

75. Horie, K.; Hirao, K.; Mita, I.; Takubo, Y.; Okamoto, T.; Washio, M.; Tagawa, S.; Tabata, Y., *Chem. Phys. Lett.* **1985,** *119* (6), 499-502.

76. Wohl, C. J.; Kuciauskas, D., *J. Phys. Chem. B* **2005,** *109* (47), 22186-22191.

77. Lenoble, C.; Becker, R. S., *J. Phys. Chem.,* **1986,** *90* (1), 62-65.

78. Holm, A. K.; Mohammed, O. F.; Rini, M.; Mukhtar, E., *J. Phys. Chem. A* **2005,** *109* (40), 8962-8968.

79. Krysanov, S. A.; Alfimov, M. V., *Chem. Phys. Lett.* **1982,** *91* (1), 77-80.

80. Koelsch, C. F.; Workman, W. R., *J. Am. Chem. Soc.* **1952,** *74*, 6288-6289.

81. Berg, J. M.; Tymoczko, J. L.; Stryer, L., *Biochemistry*. 5th ed.; W. H. Freeman: New York, 2002.

82. Liu, R. S.; Asato, A. E., *Proc. Natl. Acad. Sci. U. S. A.* **1985,** *82*, 259-263.

83. Szymanksi, W.; Beierle, J. M.; Kistemaker, H. A. V.; Velema, W. A.; Feringa, B. L., *Chem. Rev.* **2013,** *113*, 6114-6178.

84. Wei, Y.-B.; Tang, Q.; Gong, C.-B.; Lam, M. H.-W., *Analytica Chimica Acta* **2015,** *900*, 10-20.

85. Klajn, R.; Stoddart, J. F.; Grzybowski, B. A., *Chem. Rev.* **2010,** *2039*, 2203-2237.

86. Wildes, P. D.; Pacifici, J. G.; Irick, J., G.; Whitten, D. G., *J. Am. Chem. Soc.* **1971,** *93*, 2004-2008.

87. Lux, J.; Rebek, J., Jr., *Chem. Commun.,* **2013,** *49*, 2127-2129.

88. Parthasarathy, A.; Ramamurthy, V., *Photochem. Photobiol. Sci.* **2011,** *10*, 1455-1462.

89. Yoon, J. H.; Yoon, S., P*Phys. Chem. Chem. Phys.,* **2011,** *13*, 12900-12905.

90. Nachtigall, O.; Kördel, C.; Urner, L. H.; Haag, R., P *Angew. Chem. Int. Ed.,* **2014,** *53*, 9669-9673.

91. Hallett-Tapley, G. L.; D'Alfanso, C.; Pacioni, N. L.; McTiernan, C. D.; González-Béjar, M.; Lanzalunga, O.; Alarcon, E. I.; Scaiano, J. C., *Chem. Commun.,* **2013,** *49*, 10073-10075.

92. Simoncelli, S.; Aramendia, P. F., *Catal. Sci. Technol.,* **2015,** *5*, 2110-2116.

93. Titov, E.; Lysyakova, L.; Lomadze, N.; Kabashin, A. V.; Saalfrank, P.; Santer, S., *J. Phys. Chem. C* **2015,** *119*, 17369-17377.

94. Neta, P.; Levanon, H., *J. Phys. chem.,* **1977,** *81* (24), 2288-2292.

95. Laviron, E.; Mugnier, Y., *J. Electroanal. Chem. Interfacial Electrochem.* **1978,** *93*, 69-73.

96. Mondal, B.; Kamatham, B.; Samanta, S. R.; Jagadesan, P.; He, J.; Ramamurthy, V., *Langmuir* **2013,** *29*, 12703-12709.

97. Turkevick, J.; Stevenson, P. C.; Hillier, J. A., S*Discuss. Faraday, Soc.* **1951,** *11*, 55-75.

98. Dugave, C.; Demange, L., *Chem. Rev.* **2003,** *103*, 2475-2532.

99. Waldeck, D. H., *Chem. Rev.* **1991,** *91*, 415-436.

100. Mizuno, K.; Ichinose, N.; Yoshimi, Y., *J. Photochem. Photobiol. , C* **2000,** *1*, 167-193.

101. Khorana, H. G., *J. Biol. Chem.* **1992,** *267*, 1-4.

102. Rao, V., J, *Organic molecular photochemistry*. Marcel Dekker, Inc.: New York, 1998; Vol. 3.

103. Birge, R. R., *Biochim. Biophys. Acta.* **1990,** *1016*, 293-327.

104. Ramamurthy, V.; Weiss, R. G.; Hammond, G. S., `. *Adv. Photochem.* **1993,** *18*, 67-236.

105. Syamala, M. S.; Devanathan, S.; Ramamurthy, V., *J. Photochem.* **1986,** *34*, 219-229.

106. Zimmerman, H. E.; Zuraw, M. J., *J. Am. Chem. Soc.* **1989,** *111*, 7974-7989.

107. Lakshminarasimhan, P.; Sunoj, R. B.; Chandrasekhar, J.; Ramamurthy, V., *J. Am. Chem. Soc.* **2000,** *122*, 4825-4816.

108. Samanta, S. R.; Choudary, R.; Ramamurthy, V., *J. Phys. Chem. A.* **2014,** *118* (45), 10554-10562.

109. Applequist, D. E.; Gdanski, R. D., *J. Org. Chem.* **1981,** *46*, 2502-2510.

110. Jagadesan, P.; Mondal, B.; Parthasarathy, A.; Rao, V. J.; Ramamurthy, V., *Org, Lett.* **2013,** *15* (6), 1326-1329.

111. Choudhury, R.; Barman, A.; Prabhakar, R.; Ramamurthy, V., *J. Phys. Chem. B* **2012,** *117*, 398-407.

112. Frisch, M.; Trucks, G.; Schlegel, H.; Scuseria, G.; Robb, M.; Cheeseman, J.; Scalmani, G.; Barone, V.; Mennuci, B.; Petersson, G. Gaussian, Inc.,: Wallingford CT, 2009.

113. Wang, J.; Wang, W.; Kollman, P. A.; Case, D. A., *J. Am. Chem. Soc.,* **2001,** *222*.

114. Trott, O.; Olson, A. J., *J. Comput. Chem.* **2010,** *31*, 455-461.

115. Hess, B.; Kutzner, C.; Van Der Spoel, D.; Lindahl, E., *J. Chem. Theory Comput.* **2008,** *4*, 435-447.

116. Case, D. A.; Cheatham, T. E.; Darden, T.; Gohlke, H.; Luo, R.; Merz, K. M.; Onufriev, A.; Simmerling, C.; Wang, B.; Woods, R. J., *J. Comput. Chem.* **2005,** *26*, 1668-1688.

117. Price, D. J.; Brooks III, C. L., *J. Chem. Phys.* **2004,** *121*, 10096-10103.

118. Miyamoto, S.; Kollman, P. A., *J. Comput. Chem.* **1992,** *18*, 952-962.

119. Hess, B.; Bekker, H.; Berendsen, H. J.; Fraaije, J. G., *J. Comput. Chem.* **1997,** *18* (1463-1472), 1463.

120. Krieger, E.; Vriend, G., *Bioinformatics* **2014,** *30*, 2981-2984.

121. Pettersen, E. F.; Goddard, T. D.; Huang, C. C.; Couch, G. S.; Greenblatt, D. M.; Meng, E. C.; Ferrrin, T. E., *J. Chem. Phys.* **2004,** *25*, 1605-1612.

122. Balzani, V., *Electron Transfer Chemistry*. Wiley: New York, 2001; Vol. 1-5.

123. Fox, M. A.; Chanon, M., *Photoinduced Electron Transfer*. Elsevier: Amsterdam, 1988; Vol. 1-4.

124. Piotrowiak, P., *Chem. Soc. Rev.* **1999,** *28*, 143-150.

125. Porel, M.; Chuang, C.-H.; Burda, C.; Ramamurthy, V., *J. Am. Chem. Soc.,* **2012,** *134*, 14718-14721.

126. Kasha, M., *Faraday Discuss Chem. Soc.* **1950,** *9*, 14-19.

127. Turro, N. J.; Ramamurthy, V.; Cherry, W.; Farneth, W., *Chem. Rev.* **1978,** *78* (2), 125-145.

128. Wagner, B. D.; Tittelbach-Helmrich, D.; Steer, R. P., *J. Phys. Chem.* **1992,** *96* (20), 7904-7908.

129. Peon, J.; Tan, X.; Hoerner, J. D.; Xia, C.; Luk, Y. F.; Kohler, B., *J. Phys. Chem. A* **2001,** *105* (24), 5768-5777.

130. Mullen, K. M.; van Stokkum, I. H. M., TIMP: *J. STAT SOFTW* **2007,** *18* (3), 1-8.

131. Pagba, C.; Zordan, G.; Galoppini, E.; Piatnistki, E. L.; Hore, S.; Deshayes, K.; Piotrowiak, P., *J. Am. Chem. Soc.* **2004,** *126*, 9888-9889.

132. Porel, M.; Klimczak, A.; Freitag, M.; Galoppini, E.; Ramamurthy, V., *Langmuir* **2012,** *28* (7), 3355-3359.

133. Myahkostupov, M.; Pagba, C. V.; Gundlach, L.; Piotrowiak, P., *J. Phys. Chem. C* **2013,** *117* (40), 20485-20493.

134. Adams, S. R.; Tsien, R. Y., *Annu. Rev. Physiol.* **1993,** *55*, 755-784.

135. Ellis-Davies, G., *Nat. Methods* **2007,** *4*, 619-628.

136. Rai, P.; Mallidi, S.; Zheng, X.; Rahmanzadeh, R.; Mir, Y.; Elrington, S.; Khurshid, A.; Hasan, T., *Adv. Drug Deliv Rev.* **2010,** *62*, 1094-1124.

137. Riggsbee, C.; Deiters, A., *Trends Biotechnol.* **2010,** *28*, 468-475.

138. Shao, Q.; Xing, B., *Chem. Soc. Rev.* **2010,** *39*, 2835-2846.

139. Klan, P.; Solomek, T.; Bochet, C. G.; Blanc, A.; Givens, R.; Rubina, M.; Popik, V.; Kostikov, A.; Wirz, J., *Chem. Rev* **2013,** *113*, 119-191.

140. Jayaraj, N.; Jagadesan, P.; Samanta, S. R.; Da Silva, J. P.; Ramamurthy, V., *Org. Lett.* **2013,** *15* (17), 4374-4377.

141. Jagadesan, P.; Da Silva, J. P.; Givens, R.; Ramamurthy, V., *Org. Lett.* **2015,** *17*, 1276–1279.

142. Kamatham, N.; Mendes, D. C.; Da Silva, J. P.; Givens, R. S.; Ramamurthy, V., *Org. Lett.* **2016,** *18*, 5480-5483.

143. Kamatham, N.; Da Silva, J. P.; Givens, R. S.; Ramamurthy, V., M *Org. Lett.* **2017,** *19*, 3588-3591.

144. Il'ichev, Y. V.; Schworer, M. A.; Wirz, J.,. *J. Am. Chem. Soc.,* **2004,** *126*, 4581-4595.

145. Gaplovsky, M.; Il'ichev, Y. V.; Kamdzhilov, Y.; Kombarova, S. V.; Mac, M.; Schworer, M. A.; Wirz, J., *Photochem. Photobiol. Sci.,* **2005,** *4*, 33-42.

146. Hellrung, B.; Kamdzhilov, Y.; Schworer, M. A.; Wirz, J., *J. Am. Chem. Soc.,* **2005,** *127*, 8934-8935.